REPORT DOCUMENTATION PAGE

Form Approved
OMB NO. 0704-0188

1. AGENCY USE ONLY (Leave Blank)	2. REPORT DATE	3. REPORT TYPE AND DATES COVERED
	April 16, 2003	Final Report

4. TITLE AND SUBTITLE

Effect of Nitric Oxide and Other Diluents on Cold Starting, Combustion Instability and White Smoke Emissions in Diesel Engines.

5. FUNDING NUMBERS

DAAG55-98-1-0285
(06-01-98 to 11-30-02)

6. AUTHOR(S)

Naeim A. Henein

7. PERFORMING ORGANIZATION NAME(S) AND ADDRESS(ES)

Wayne State University, College of Engineering, Detroit , MI 48202

8. PERFORMING ORGANIZATION REPORT NUMBER

9. SPONSORING / MONITORING AGENCY NAME(S) AND ADDRESS(ES)

U. S. Army Research Office
P.O. Box 12211
Research Triangle Park, NC 27709-2211

10. SPONSORING / MONITORING AGENCY REPORT NUMBER

37730.1-E6

11. SUPPLEMENTARY NOTES

The views, opinions and/or findings contained in this report are those of the author(s) and should not be construed as an official Department of the Army position, policy or decision, unless so designated by other documentation.

12 a. DISTRIBUTION / AVAILABILITY STATEMENT

Approved for public release; distribution unlimited.

12 b. DISTRIBUTION CODE

13. ABSTRACT (Maximum 200 words)

This report covers an investigation aimed at developing electronic control strategies to improve the cold startability of diesel engines for military, dual-use and hybrid electric vehicles. The emphasis is on the analysis the processes that affect the cranking and acceleration modes during starting. The analysis indicated that NO present in the residual and recirculated gases has on effect on the order or the activation energy of the global autoignition reactions. The mathematical models developed for the two modes are able to determine the zones of misfiring, the number of cranking cycles and the causes of misfiring after firing, known as combustion instability. Further more, the research identified the strategy needed to reduce combustion instability. Also, the models developed in this work showed very clearly that the Cetane number is not a good indicator of the startability of the engine, and that fuel volatility plays a major part in the success of the autoignition process. In this regard JP8 proved to be a better fuel that DF2, as far as the number of cranking cycles. However, its combustion is unstable if compared with DF2. The results indicated that the problems with cold starting of diesel engines with JP8 are caused by the fuel injection strategy used in the commercial engines.

14. SUBJECT TERMS

Diesel engines, Cold Starting, Cranking Period, Misfiring, Autoignition, Cetane Number, Fuel Volatility, DF2 , JP8.

15. NUMBER OF PAGES

86

16. PRICE CODE

17. SECURITY CLASSIFICATION OR REPORT	18. SECURITY CLASSIFICATION ON THIS PAGE	19. SECURITY CLASSIFICATION OF ABSTRACT	20. LIMITATION OF ABSTRACT
UNCLASSIFIED	**UNCLASSIFIED**	**UNCLASSIFIED**	**UL**

NSN 7540-01-280-5500

Standard Form 298 (Rev.2-89)
Prescribed by ANSI Std. 239-18
298-102

Enclosure 1

FINAL REPORT

Contract: DAAG55-98-1-0285, (06-01-98 to 11-30-02)

PART I: Effect of Nitric Oxide and Other Diluents on Cold Starting, Combustion Instability, and White Smoke Emissions in Diesel Engines.
PART II: Autoignition, Combustion Instability and White Smoke Under Transient Conditions with JP-8.

By

N. A. Henein, Ph.D.
Professor of Mechanical Engineering
Director, Center for Automotive Research
Wayne State University
Engineering building
5050 Anthony Wayne Drive
Detroit, Michigan 48202
Tel. (313) 577 3887
Fax. (313) 577 878
Email: henein@wayne.edu

To
U. S. Army Research Office
Research Triangle Park, NC 27709-2211

April 16, 2003

Table of Contents **Page**

List of Illustrations

List of Appendixes

Appendix A : "Exploration of the Contribution of the Start/Stop Transients in HEV Operation and Emissions," Henein, N. A., Taraza, D., Chalhoub, N., Lai, M-C, Bryzik, W., SAE 2000-01-3086.

Appendix B: " Simulation of Diesel Engines Cold-Start," Lui, H, Henein, N. A. and Bryzik, W, SAE 2003-01-0080,(2003).

Appendix C: "Effect of EGR on Autoignition, Combustion, Regulated Emissions and Aldehydes in DI Diesel Engines," Nitu, B., Henein, N. A., Singh, I. P., Zhong, L., Badreshany, K. and Bryzik, W., SAE 2002-01-1153, SP-1698, pp 193-208, 2002.

Appendix D: "A New Ignition Delay Formulation with Predictions of Diesel Engine Cold Start Misfiring," Zhiping Han, Naeim A. Henein and Walter Bryzik, SAE 2000-01-1184, SP-1533, pp 175-184, 2000

Appendix E: "Diesel Engine Cold Start Combustion Instability and Control Strategy," Zhiping Han, Naeim A. Henein, Bogdan Nitu and Walter Bryzik, SAE . 2001-01-1237.

Contract: DAAG55-98-1-0285, (06-01-98 to 11-30-02)

FINAL REPORT

PART I: Effect of Nitric Oxide and Other Diluents on Cold Starting, Combustion Instability, and White Smoke Emissions in Diesel Engines.
PART II: Autoignition, Combustion Instability and White Smoke Under Transient Conditions with JP-8.

(1) Foreword

This report gives the results of an investigation aimed at developing more insight and a better understanding of the basic physical and chemical processes that affect the cold start of diesel engines. This would lead to the development electronic control strategies for the different engine operating parameters to improve the cold starting of military and dual use diesel engines and the hybrid electric vehicles. (Appendix A)

The cold start process consists of two modes of engine operation. The first is the cranking mode when the engine is motored while the fuel is injected into the cylinder. The second is engine acceleration after the start of combustion. Most of the previous studies concentrated on the length of time the engine takes to reach the steady idle speed. Some studies investigated the cranking period. Very few studies dealt with the acceleration mode. Work conducted at the Center for Automotive Research at Wayne State University indicated that after the engine fires, it might misfire once, twice or more, before it fires again and reaches a steady idling speed. This type of operation is referred to as combustion instability. Combustion instability causes engine hesitation, rough operation and long warm up periods before the engines reaches a steady idling speed. In the worst case, the engine may completely fail to start. Part of the fuel accumulated during the misfiring cycles evaporates during combustion in the next cycles and appears as white smoke in the exhaust.

The approach taken in this investigation is a combination of theoretical and experimental investigations. Mathematical models are developed for the cranking period and the transient engine dynamics during acceleration to the idle speed. The models are validated by comparing the predicted results with the experimental data.

The report consists of two integrated parts. Part I investigates the effect of the concentration of nitric oxide on the autoignition process of hydrocarbon fuels in general. Nitric oxide is the result of combustion in the previous cycle. The concentration of the nitric oxide in the charge was varied by controlling the percentage of the recirculated gases. Part II investigates the specific behavior of JP8 used in military vehicles under low temperature conditions. A comparison is made between the commercially used DF2 fuel and JP8 fuel during the starting process.

The experiments were conducted on two engines: (a) an air cooled, direct injection, single-cylinder research engine, and (b) a heavy-duty, multi-cylinder, water cooled, direct injection diesel engine. The tests covered a wide range of ambient temperatures in the cold room facility at Wayne State University.

Statement of problem studied

Cold start problems

The cold start problems in military and domestic diesel engines include hesitation, emission of large amounts of unburned fuel in the form of white smoke, and complete failure of the engine to start. In military applications, such problems affect the mobility and survivability in the field, in addition to penalties in fuel consumptions. Reduction of fuel consumption is a major goal in order to reduce the cost and mass of fuel transported in the field. To solve the cold start problems there is a need for a better understanding of the physical and chemical processes that affect the combustion process at low ambient temperatures. This is achieved in this investigation by developing mathematical models, validated with experimental data on engines under actual low temperature conditions.

Two factors contribute to the cold start problems:

A. Failure of the autoignition process.
B. Combustion instability.

A. Failure of the autoignition process:

The failure of the autoignition process causes an increase in the cranking period before the engine fires and is the result of the slow oxidation processes and the long ignition delay (ID) at the low temperatures. Many experimental investigations on the (ID) of hydrocarbon fuels were conducted in constant volume vessels, where the temperature, pressure and volume remain almost constant during the ID. This is not the case in engines because of the piston motion during the ID period.

To account for the effect of piston motion on the global autoignition reactions rate, a new formulation is developed for the ignition delay (ID) in diesel engines. A differentiation is made between the ID measured in engines and that measured in constant volume vessels. In addition, a method is presented to determine the coefficients of the ID_e correlation from actual engine experimental data. The new formulation for ID_e is applied to predict the misfiring cycles during the cold starting of diesel engines. The predictions are compared with experimental results obtained on a multi-cylinder heavy-duty diesel engine.. The details of this investigation are given in reference (2) and Appendix B.

A new mathematical model was developed, based on the fundamentals of heat and mass transfer between the fuel spray and air The model takes into consideration, for the first time, the effect of the engine dynamics, thermodynamics and combustion kinetics into consideration. The model is able to predict the number of engine rotation the engine takes before it fires for the first time. This led to the development of the "AUTO IGNITION INDEX" (AI), for each of the cranking cycles.

$$AI = \int_{t_{inj}}^{t_{end}} k_0[F]\exp(-\frac{E}{RT})dt$$

AI combines the effects of the global activation energy E that depends on the chemical structure of the fuel and its vapor concentration [F] that depends on its volatility. .k_o is a constant, R is the universal gas constant and t is time. The AI covers the period from the start of injection to the end of ID. AI increases with the number of cranking cycles because of the increase in [F] and temperature T. The engine fires when the AI reaches a specified value. The details of this study are given in reference (2) and Appendix B.

Prediction of the Cranking Period

The cranking period is predicted by calculating AI for the consecutive cycles after the engine is cranked by the electric motor. Autoignition occurs when AI reaches a critical value, determined from the cold start test at normal room temperature. AI is calculated for pure paraffin compounds having 7 to 19 carbon atoms considering their physical properties. The results, shown in Figure (1) indicate that the engine would start in the first cycle for paraffins having seven to nine carbon atoms. However, the cranking period would be longer in proportion to the number of carbon atoms for the larger molecules. It should be noted that longer chain paraffins have a higher Cetane Number, but lower volatility.

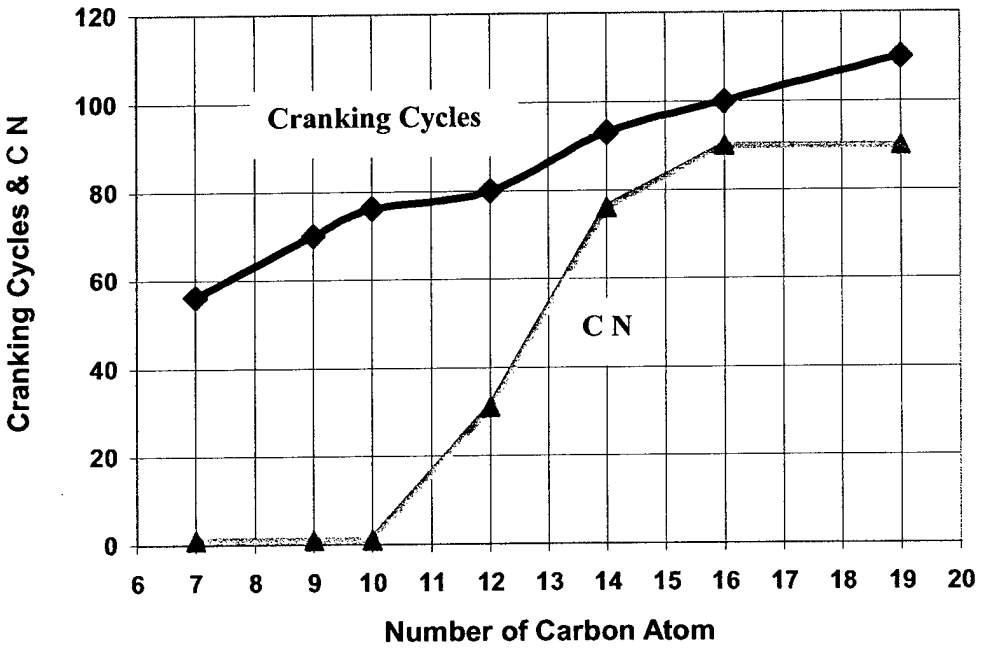

Fig.1. Effect of number of carbon atoms in the paraffin on Cetane Number and cranking cycles.

Comparison between the cranking periods for JP8 and DF2

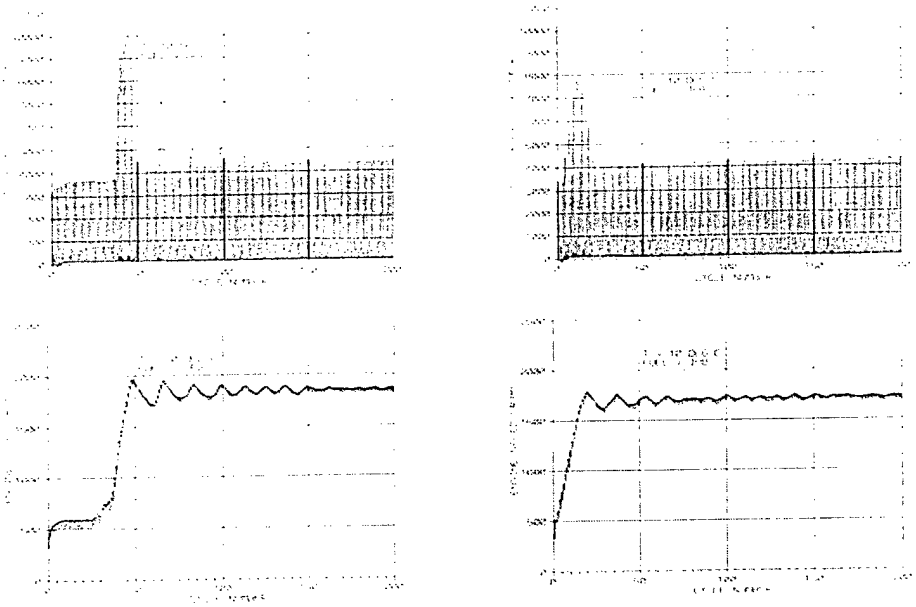

Fig. 2. Comparison between the pressure traces and instantaneous engine speed during the cold start of a single cylinder diesel engine on DF2 and JP8.

Figure 2. shows the engine to start on JP8 after cranking for a shorter period of time than that with DF2. This is in spite the fact that CN for JP8 is 37 while CN for DF2 is 45.

Gas Chromatic Analysis of DF2 and JP8

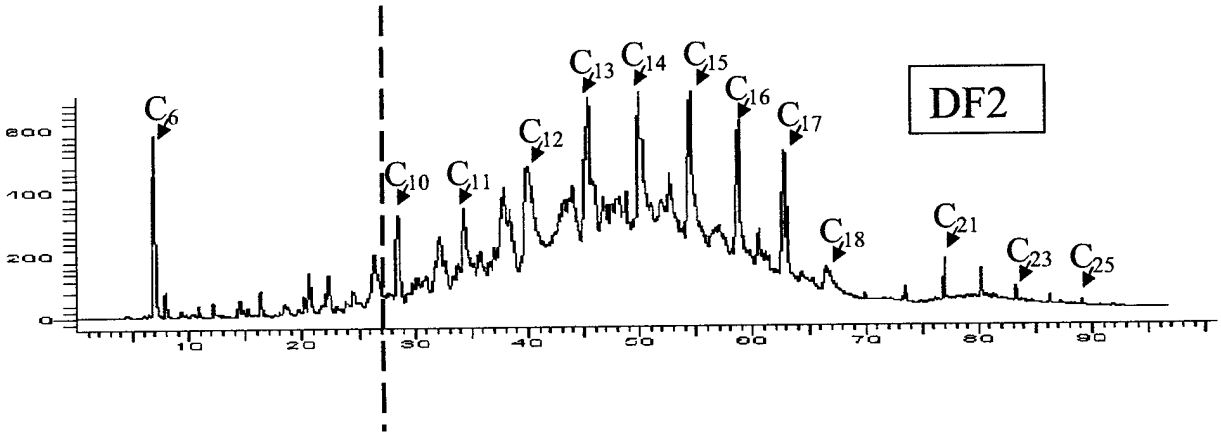

Figure 3. Gas Chromatic Analysis of DF2 Fuel

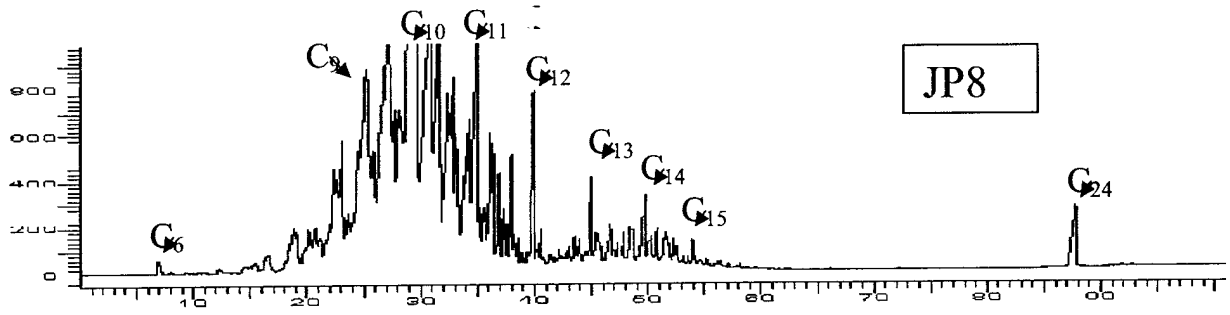

Figure 4. . Gas Chromatic Analysis of JP8 Fuel.

Figures 3 and 4 show the composition of DF2 and JP8 respectively. It is clear that JP8 has higher concentrations of the lighter paraffins than DF2. This explains why the cranking period with JP8 was shorter than that with DF2, as predicted by the model.

Cause of cold-start problems with JP 8

The first part of this investigation indicated that the cranking period with JP8 is shorter than that with DF2. Then why commercial diesel engines experience more difficulty in starting with JP8 than with DF2? This leads to the second part of this investigation that deals with combustion instability.

B. Combustion Instability

Early investigations at Wane State University indicated that combustion instability during cold start is repeatable, rather than random, is not specific to any engine or fuel, and increases with the drop in ambient temperature.(3) The parameters that affect combustion instability include the ambient temperature, cranking speed, injection timing and injection mode such as pilot and main injection. The effect of these parameters on combustion instability is investigated, both theoretically and experimentally, in this project.

Cold start experiments were conducted, using DF2 and JP8, on two engines at ambient temperatures ranging from normal room temperature on to -10°. The first engine is a single-cylinder, direct-injection, air-cooled four-stroke-cycle engine. The second was a heavy-duty, water-cooled, 4-cylinder, turbo-charged, inter-cooled, 4-stroke-cycle diesel engine. Cylinder gas pressures, exhaust gas temperature, needle lift, were measured in each cylinder. The instantaneous engine speed was recorded during motoring and acceleration over about 100 cycles, (200 revolutions).

Detailed cycle analysis indicated that misfiring occurs after a firing cycle. One of the reasons for this behavior was thought to be the presence of NO in the residual gases from the previous firing cycle. To clarify this point, experiments were conducted on a single cylinder diesel engine where the mole fraction of NO in the fresh charge was changed by controlling the EGR ratio. Detailed analysis of the data indicated that NO has no effect on the global activation energy of the autoignition reactions or on the global rate of the reactions. The only effect EGR has on the ignition

delay is to reduce the rates of the autoignition reactions because of the drop in oxygen concentration and the increase in its thermal capacity of the charge. The details of this work is given in reference (7) and Appendix C.

Cycle-to-cycle analysis of the data indicated that the number of misfiring cycles increases at lower ambient temperature. This investigation indicated that misfiring is caused by a mismatch between the injection parameters and the instantaneous engine speed. This became clear from the maps developed from the theoretical investigation for the injection timing and engine speed. The misfiring zone shown in the maps agreed fairly well with the experimental results.

Based on the above analysis, a new strategy for cold starting was developed to reduce combustion instability and white smoke emissions.

The details of this work are published in references (2 and 6) and given in Appendix D and Appendix E.

Summary of the most important results

1. Nitric oxide concentration in the charge at high EGR ratios has no effect on the global activation energy and the order of the autoignition reactions. EGR reduces the rates of the autoignition reactions, as indicated by the increase in the ignition delay, because of drop in oxygen concentration and the increase in its thermal capacity.
2. A first generation simulation model for the cold-start cranking-period is developed in this investigation. The model predictions agreed with the experimental on the following conclusions: (a) CN alone is not a good indicator of the number of cranking cycles and (b) Fuel volatility is as important as CN in controlling the cranking period at the low ambient temperatures.
3. A new auto-ignition index (AI) is developed to predict the cranking period. AI combines the effects of the physical and chemical properties of the fuel, and the concentration of the oxygen in the charge. This is the first time, a model is developed to show the dependence of the cranking period on both the cetane number and fuel volatility..
4. The model predictions indicated that the volatile paraffin components of the DF2 and JP8 are the initiators of the autoignition process at the end of cranking period. The model predictions agreed with the experimental results that showed shorter cranking periods with JP8 than with DF2 at the low ambient temperatures.
5. The reason for the difficulty in the cold starting of commercial diesel engines on JP8 is found to be a mismatch between the injection timing and the instantaneous engine speed. Maps developed in this investigation give the firing zones needed for the control of injection timing at different instantaneous engine speeds during the transient acceleration mode of the cold start process.

List of publications

1. "Exploration of the Contribution of the Start/Stop Transients in HEV Operation and Emissions," Henein, N. A., Taraza, D., Chalhoub, N., Lai, M-C, Bryzik, W., SAE paper number 2000-01-3086 (2000).
2. "A New Ignition Delay Formulation with Predictions of Diesel Engine Cold Start Misfiring," Zhiping Han, Naeim A. Henein and Walter Bryzik, SAE Paper No. 2000-01-1184, SP-1533, pp 175-184, (2000).
3. "Fundamental Cold Start Phenomena Within Advanced Military Diesel Engines," Walter Bryzik and Naeim Henein, Army Science Conference Proceedings, Vol. III, pp 1091-1099, (1994).
4. "Simulation of Diesel Engines Cold-Start," Lui, H, Henein, N. A. and Bryzik, W, SAE paper No. 2003-01-0080,(2003).
6. "Diesel Engine Cold Start Combustion Instability and Control Strategy," Zhiping Han, Naeim A. Henein, Bogdan Nitu and Walter Bryzik, SAE paper 2001-01-1237.2001
7. "Effect of EGR on Autoignition, Combustion, Regulated Emissions and Aldehydes in DI Diesel Engines," Nitu, B., Henein, N. A., Singh, I. P., Zhong, L., Badreshany, K. and Bryzik, W., SAE 2002-01-1153, SP-1698, pp 193-208, 2002.

Scientific personnel supported by this project

1. Dr. Yasu Itoh, Manager,
2. Dr. Zhiping Han, ...DDC
3. Dr. Hengqing Liu... GM
4. Bogdan Nitu, Ph.D. Candidate, Wayne State University.
5. Lurun Zhong, Ph.D. Candidate, Wayne State University
6. Inderpal Singh, Ph. D Applicant, Wyne State University
7. Naeim A. Henein, Professor and Director of Center for Automotive Research , WSU.

Report of Inventions

None

APPENDIX A

2000-01-3086

Exploration of the Contribution of the Start/Stop Transients in HEV Operation and Emissions

Naeim A. Henein, Dinu Taraza, Nabil Chalhoub and Ming-Chia Lai
Wayne State University

Walter Bryzik
U S Army TARDEC

Abstract

The effects of the start/stop (S/S) transients on the Hybrid Electric Vehicle (HEV) operation and emissions are explored in this study. The frequency with which the engine starts and stops during an urban driving cycle is estimated by using the NREL's Advanced Vehicle Simulator software (ADVISOR). Furthermore, several tests were conducted on single-cylinder and multi-cylinder direct injection diesel engines in order to measure the cycle-resolved mole fractions of the hydrocarbons and nitric oxide exhaust emissions under frequent start/stop mode of operation. The frictional losses in engine in its entirety as well as in its components are also determined. In addition, the dynamic behavior of different high pressure fuel injection systems are investigated under the start and stop mode of operation.

Background

The drive for better fuel economy and low emissions in automotive vehicles brought the HEV concept in the forefront of research. The auxiliary Power Unit (APU) can be a combustion engine or a fuel cell. Combustion engines, considered to power future HEVs, include the direct injection diesel engine, the direct injection gasoline engine, and the gas turbine. The engine might be required to start and stop many times depending on the driving cycle, the configuration of the powertrain and the control strategy.

The energy expenditure during starting consists of two parts. The first part provides the kinetic energy of the engine's moving parts. The second part aims at overcoming losses that are associated with the engine operation during the transient period of the start. The losses include the inefficiencies of combustion and the mechanical friction in the moving parts. Combustion inefficiencies depend on the design of the injection system and its performance under the transient S/S conditions.

Engine-out emissions during the start transient depend primarily on the engine temperature, as well as the fuel injection strategy. During the first start after a long shutdown period, the engine temperature will be the same as the ambient temperature. However, the engine temperature during subsequent starts will depend on the shutdown period.

The goal of this paper is to explore the effects of (S/S) transients on the fuel economy and emissions under urban driving conditions.

has been increased by fifty percent. It should be pointed out that in spite of the fact that ADVISOR may not be able to accurately predict the dynamic response of an HEV vehicle, its results do capture the general trend of vehicle response.

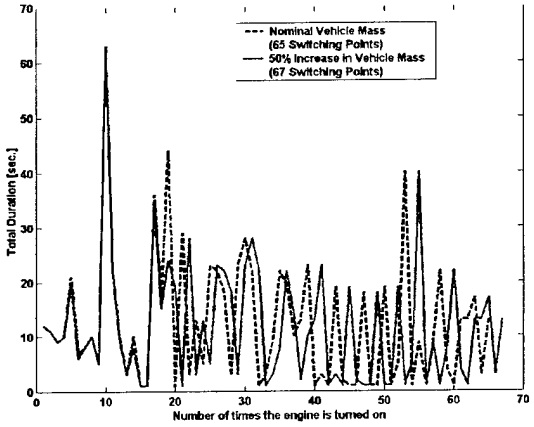

Fig. 3 Duration for each time the engine is turned on based on the FUDS drive cycle and a parallel HEV configuration

Engine-Out Emissions During a Start Transient

Experiments were conducted on a single-cylinder direct-injection, four-stroke-cycle, air-cooled diesel engine to determine the emissions under the cold and hot starts. The instrumentation includes a piezoelectric pressure transducer for the cylinder pressure, a needle lift sensor, a fuel line pressure sensor, a fast response NOx analyzer for both the intake and exhaust gases, a fast response FID analyzer for the exhaust gases, pressure transducers for both intake and exhaust manifolds, fast response thermocouples for measuring the exhaust temperature, a Bosch air flow meter for measuring the intake air flow rate, and a crankcase pressure sensor. The engine starts by its own electric starter with a fully charged battery. The cycle resolved mole fractions of the unburned hydrocarbons and nitric oxide were measured and recorded for the first 200 revolutions. All the experiments were conducted at 29°C. The AMOCO premium diesel fuel was used in all experiments.

Figure 4 shows the experimental data for the first 100 cycles that were obtained by starting the engine after it has been shut down for 20 minutes. The unburned hydrocarbons reached 1500 ppm, while the NO reached more than 5000 ppm.

Figure 5 shows the experimental data for the first twenty cycles of a cold start after soaking the engine at the ambient room temperature overnight. The hydrocarbons reached 2250 ppm, and NO reached 900 ppm, respectively.

The emission index in gm/ kg of fuel is given in Fig. 6 for different shutdown periods and for the first cold start. As expected, the first cold start produced negligible NO, but high HC. The emissions indexes for HC and NO vary with the length of the shutdown period. NO is strongly dependent on the charge temperature. The longer the shutdown period, the cooler the engine will be, and the lower is the NO formation. This is evident from the exhaust gas temperature, which dropped with the length of the shutdown period, as illustrated in Fig. 7.

It is clear that the reduction of engine-out emissions of HC and NO during the cold and hot start transients is critical for HEV to meet the future stringent standards. This is because the

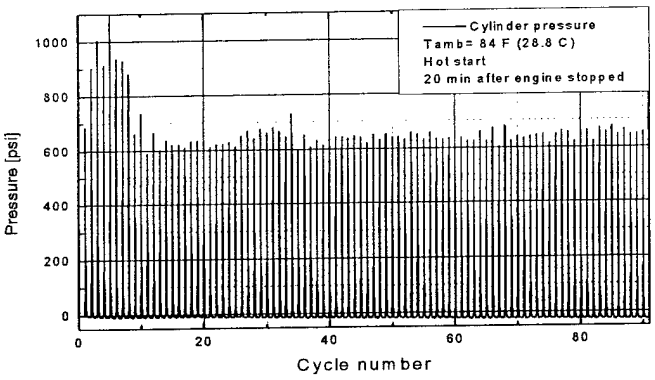

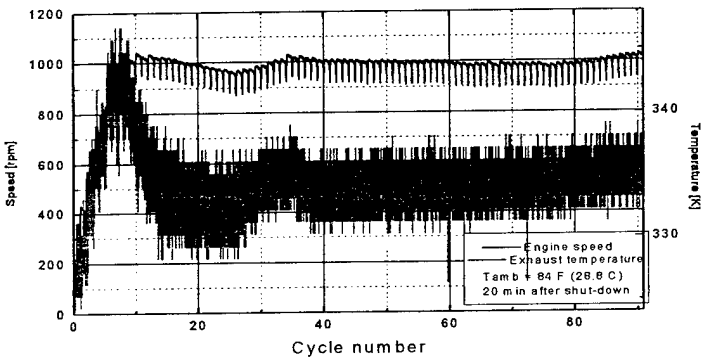

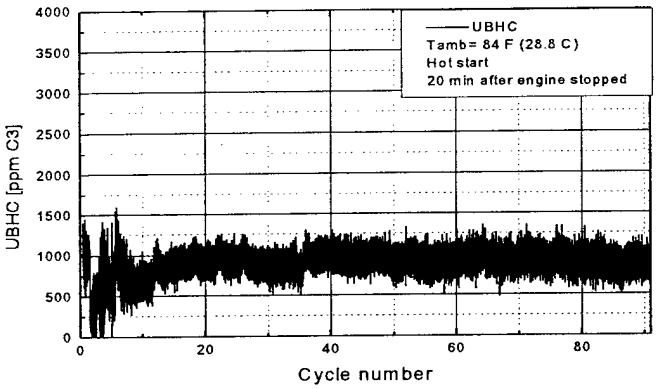

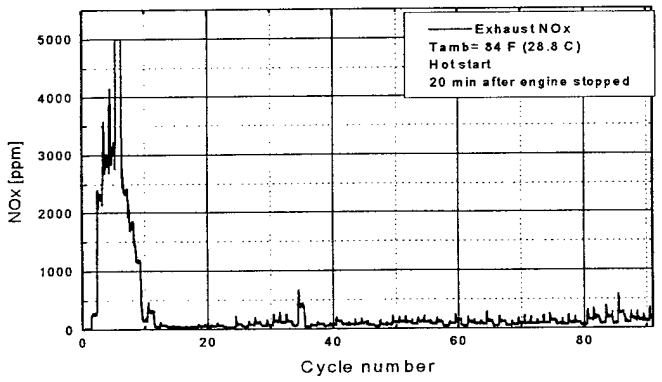

Fig. 4 Hot start after 20 minutes shutdown

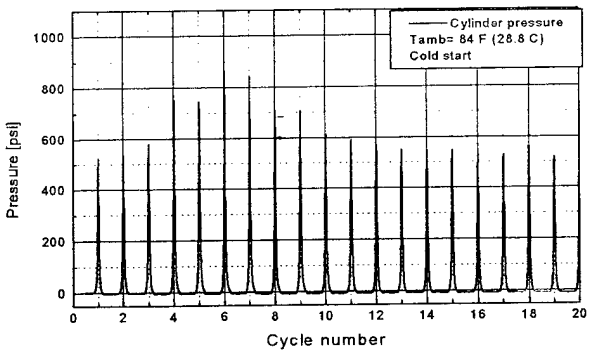

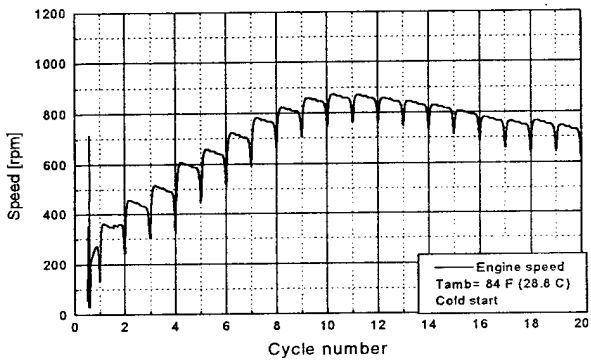

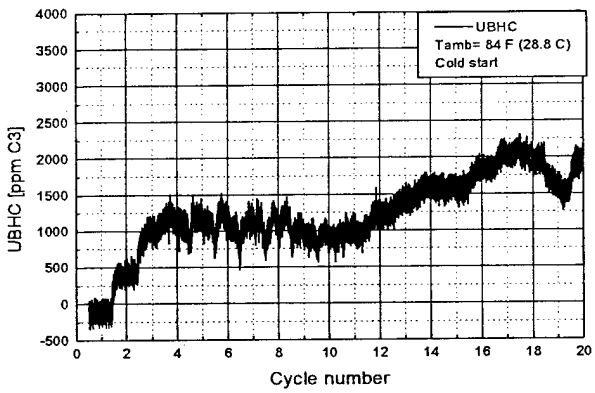

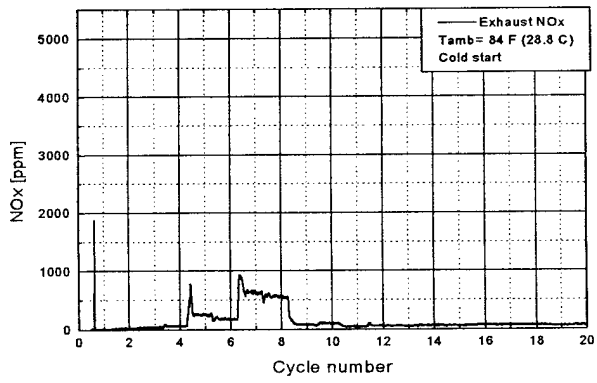

Fig. 5 Cold start after a long soak period

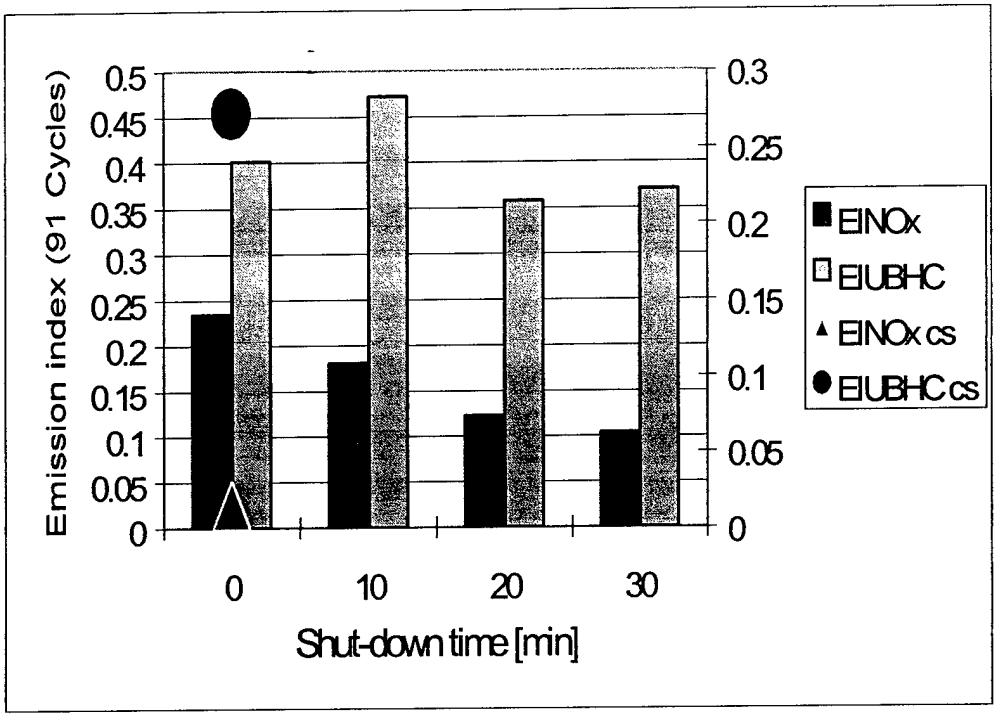

Fig. 6 Emission index for HC and NO for the cold and hot starts after different

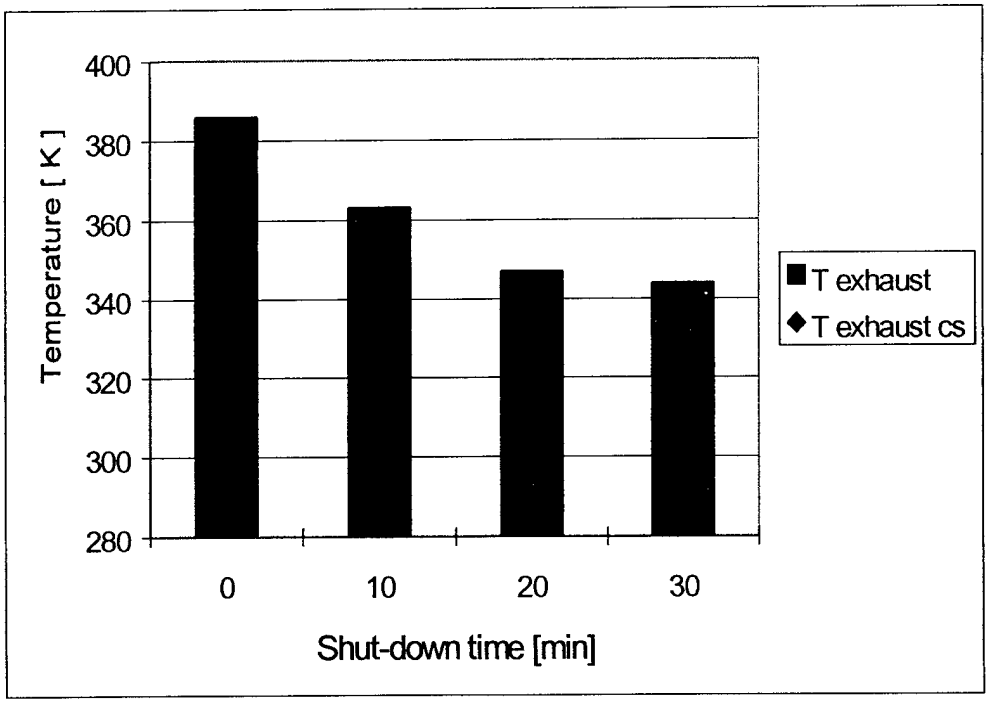

Fig. 7 Maximum exhaust gas temperature reached at different hot starts

after-treatment devices are not effective at the low exhaust gas temperatures existing during the cold and hot starts after a long shutdown period.

Minimum Warmup Periods

Engine cold start and operation at low temperatures allow some fuel to reach

the crank case, dilute the lubricating oil and reduce its viscosity. This results in poor lubrication and an increase in engine wear. The wear can be avoided, if the engine is warmed up to such a temperature where the fuel mixed with the oil is evaporated before the engine is shut down.

Limited Shut Down Periods

Long shut down periods allow the after treatment devices, such as a catalytic converter, to cool down. If the catalyst temperature drops below a certain level, electric energy might be needed to warm it up for a quick light off. Accordingly, the engine control strategy should take into consideration the length of the shut down to minimize the electric energy consumed to heat the catalyst.

Fuel Economy Under Frequent S/S Operating Conditions:

S/S transients adversely affect the fuel economy because they increase the frictional losses. The engine friction is highly dependent on the oil viscosity and the relative speed between the rubbing parts. The oil viscosity, in its turn, is a function of the thermal state of the engine. The latter, under HEV operation, is influenced by the time interval between the engine shut down and its subsequent engine start, as well as the speed of the vehicle. Thus long shutdown periods while the vehicle is moving at highway speeds will cause the oil temperature during the subsequent start to be considerably low.

Engine starts consume more power from the battery pack if the engine is cold and the oil viscosity is high. On the other hand, the kinetic energy of the running engine cannot be totally recovered when the engine stops. Before stopping, it is necessary to run the engine at a low load for a while in order to reduce the temperature of the hot spots on the cylinder wall and cylinder head. If the engine is suddenly stopped while operating at high load, the coolant may boil at the hot spots causing overheating of the piston top, piston rings and valves and damaging the oil present at these spots. This situation is especially critical for the top ring, where oil decomposition may increase carbon deposits in the rig grove blocking the motion of the ring and compromising cylinder sealing. Thus, every S/S sequence will cause energy losses and contribute to the increase in fuel consumption. In the control strategy it is important to consider also optimization of the frequency of the S/S events.

Because friction losses at engine start are important for the overall fuel economy, the contribution of each friction component during the starting event will be considered.

Piston ring assembly friction.

Piston ring assembly (PRA) friction is a transient process even under steady state operating conditions. The transient character is determined by the large variation of the piston speed during a piston stroke. Under normal operating conditions, for most of the piston stroke, the lubrication regime is hydrodynamic and the friction coefficient is strongly correlated to the duty parameter

$$S = \frac{\mu V_P}{F/L}$$

μ represents the dynamic viscosity of the oil, V_P the piston speed and F/L the load per unit length. In the vicinity of the dead centers, the piston speed approaches zero and the lubrication regime switches to mixed and even boundary at the firing top dead center (TDC). During engine start, the piston speed is low and the fraction of the stroke in which mixed lubrication occurs is larger. In the mixed lubrication regime, metallic contact occurs and friction and wear are higher. The average PRA frictional force, immediately after engine start, is presented in Fig. 8 showing an increase of about 10% during the first ten cycles.

If the engine would be motored at a higher speed before starting, the PRA frictional force may be reduced. However, more energy would be expended in motoring causing an overall loss in vehicle economy during starting.

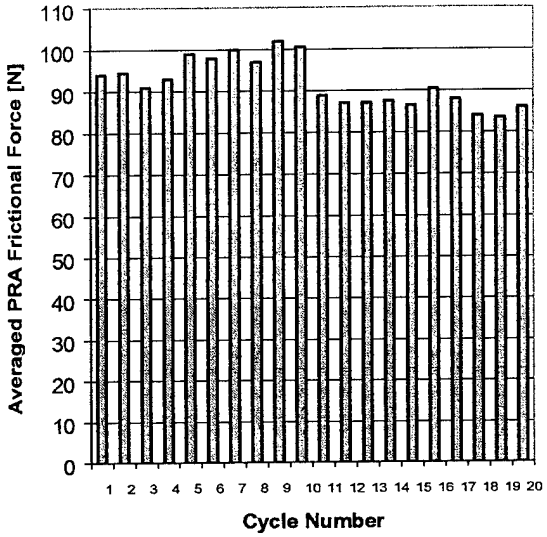

Fig. 8 Average PRA frictional force for the first 20 cycles after engine start

Bearing friction

Under normal operating conditions, the lubrication regime of the engine bearings is hydrodynamic. The bearings are subjected to a highly variable load, but the rather high relative velocity between the crankshaft's pins and the bearing bushings maintains a sufficient value of the duty parameter to assure hydrodynamic lubrication. At the same time, a higher engine speed increases the reciprocating inertia force, which acts against the gas-pressure force at the firing TDC, reducing the maximum load on the bearings. The polar diagram of the connecting rod bearing presented in Fig. 9 shows the bearing load under normal operating conditions of a diesel engine at 2000 rpm.

when the engine is started, usually more fuel is injected, meanwhile the ignition delay is long. the high peak pressures reached, and the resulting force produce a shock that might disrupt the oil film and produce metal to metal contact. This situation will contribute to the bearing wear. The difference between the maximum force acting in the connecting rod bearing at engine start Fig. 10 and under normal operating conditions could be seen by comparing the two polar diagrams in Fig. 9 and Fig. 10.

Increasing the motoring speed before starting a warm engine could significantly reduce the bearing load, providing, at the same time, the injection of a controlled amount of fuel at the

appropriate timing. For a cold engine, a very high motoring speed could hinder

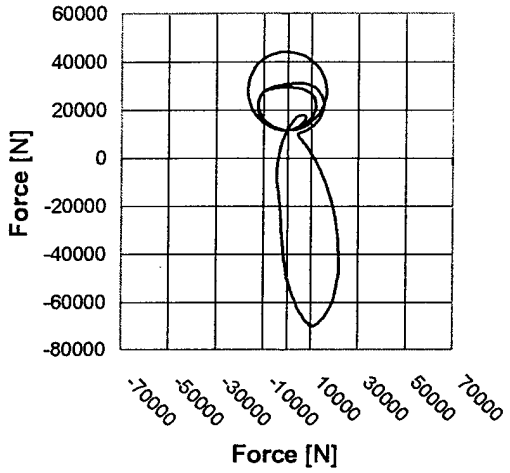

Fig. 9 Polar diagram of the connecting rod bearing;2000 rpm, IMEP = 0.85 MPa.

starting. This situation points again at the importance of optimizing the starting speed of the engine for HEV operation.

Valve train friction.

The friction between the cam and follower represents the most significant friction loss in the valve train. Due to the small contact area and large contact pressure, the lubrication regime is elastohydrodynamic (EHD). With increasing engine speed, the EHD oil film thickness increases and the friction force decreases. This situation is presented in fig. 11, where the torque required to drive the camshaft is

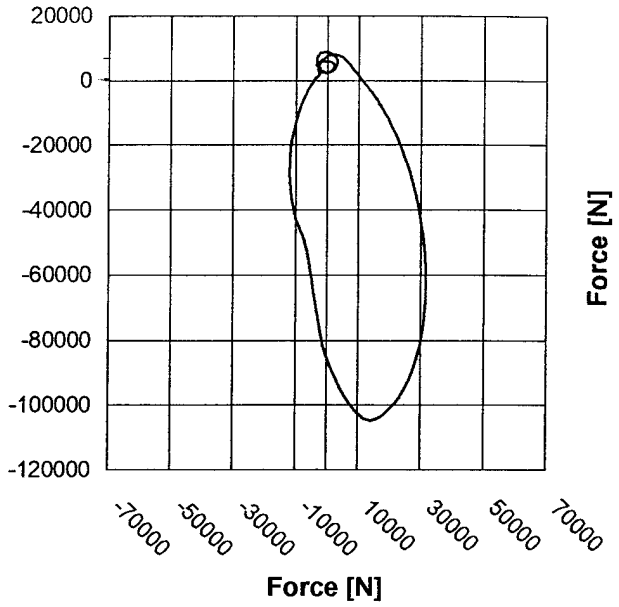

Fig. 10 Polar diagram of the connecting rod bearing;900rpm, fifth cycle after engine start.

given at different engine speeds. A strain gauge bridge applied on the camshaft of a single cylinder diesel engine measured the torque.

Under the starting conditions at low speed the friction losses in the valve train are larger than under the normal operating conditions. Increasing the motoring speed before starting will produce the same energy loss, this time supplied by the battery pack.

Total engine friction

The contribution of the three major friction components in a diesel engine: PRA, bearings and valve train will add together to yield the energy necessary to overcome friction at the engine start. In addition, the energy required to drive the engine auxiliaries

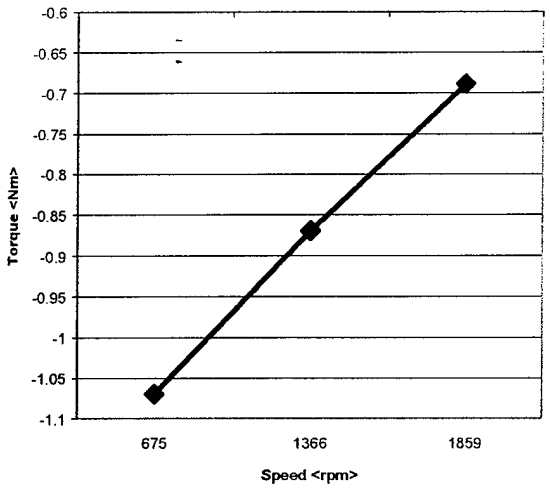

Fig. 11 Effect of engine speed on the camshaft driving torque.

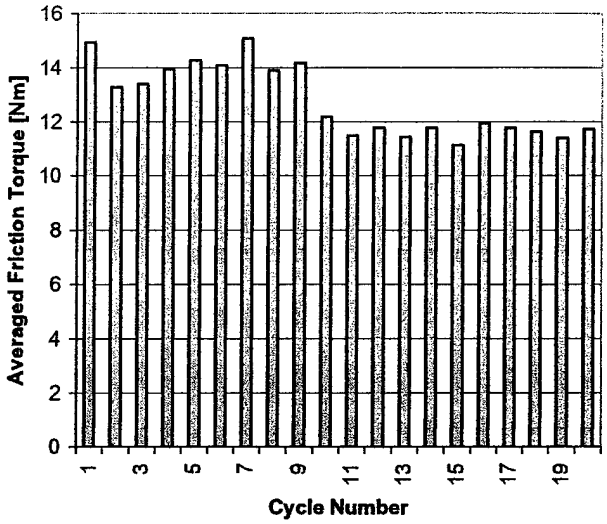

Fig. 12 Average friction torque for the first 20 cycles after engine start.

must be added to obtain the total mechanical losses for the start event. The energy required to start the engine will be provided by the battery pack and the losses in the starting motor, generator and battery should be accounted for.

The instantaneous Frictional Torque (IFT) is determined according to the p-ω method (Rezeka et al.1984). IFT is averaged over the hole cycle for a single cylinder diesel engine as shown in Fig. 12. The frictional losses in the first 10 cycles after engine start are about 16% larger than the losses in the following cycles.

Performance of Different Diesel Injection Systems Under the S/S HEV Transients

The development of the diesel engine as an Auxiliary Power Unit (APU) for the HEV will most likely follow the current state-of-the-art passenger car high-speed diesel engine technology. The concern for spray-wall interactions and their effects on combustion phasing and engine-out emissions is the same but needs to be optimized under the HEV S/S operation. Currently, there are three types of advanced high-pressure electronically controlled fuel injection systems continuously being developed.

1. Common Rail (CR) system, consists of a low pressure electrical fuel delivery pump submerged in the fuel tank, a high pressure fuel supply pump driven by a DC electric motor, a common rail, pressure regulator mounted on the fuel supply pump, an electronic-controlled

injector, and the ECU (Electronic Control unit). This system is used in Fiat 1.9-liter JTD.

2. Electrical Unit Injector (EUI) system consists of a low-pressure fuel supply pump, an overhead-cam-driven integrated solenoid injector. This system is used in VW 1.2-liter TDI (Pumpe-Düse-Einspritzung)

3. Hydraulic Electronic Unit Injector (HEUI) system, consists of a high-pressure lubricant oil pump, a common-rail type oil accumulator equipped with PWM (Pulse Width Modulation) pressure regulator, a low-pressure fuel supply pump, an intensifier, and a nozzle holder.

Table 1 and table 2 show the main system operating and design parameters that affect the injection characteristics.

In the following section, the effects of injection system and their operation on HEV fuel consumption, performance and emissions are discussed in terms of injection system start-and-stop transient, parasitic power consumption, injection rate, and spray performance at end-of-injection, since it directly affects the engine out emission.

Injection Characteristics	HEUI	EUI	CR
Response time	Response of solenoid valve, nozzle opening pressure, and length of rate-shaping pipe	Cam profile ,response of solenoid valve, and nozzle opening pressure	Response of solenoid valve, inlet and outlet throttles, and nozzle opening pressure
Peak Pressure	Intensifier ratio and length of rate-shaping pipe	Cam profile and plunger diameter	Pressure limit of high-pressure fuel line
Rate	Nozzle hole flow area	Nozzle hole flow area	Nozzle hole flow area
Rate shape	Nozzle seat flow area and length of rate-shaping pipe	Cam profile and nozzle seat flow area	Inlet and outlet throttles, and nozzle seat flow area

Table 1. Main system operating parametrs that affect the injection Chracteristics

Injection Characteristics	HEUI	EUI	CR
Response time	Rail pressure	Engine speed	Rail pressure (but insignificant)
Peak Pressure	Rail pressure and injection duration	Engine speed and injection duration	Rail pressure and injection duration
Rate	Rail pressure	Engine speed	Rail pressure
Rate shape	Rail pressure	Engine speed	Rail pressure

Table 2. Main system design and operating parameters that affect injection characteristics.

Injection System Startup Behavior

From Table 1, the dependency of injection pressure of the EUI system on engine speed, cam profile, and injection duration is obvious (Wang et al, 1999). As shown in Fig 13, a typical EUI with 1000-rpm engine speed, the pressure rising rate was 50 MPa per millisecond; with 25 crank angle injection duration, the peak injection pressure could reach 160 MPa. The injection pressure decreased as the speed of the camshaft decreased, as shown in Fig 14. The injector response time increased from 1.6 ms to 2.1 ms corresponding to the decrease in the camshaft speed from 600 rpm to 300 rpm. Therefore, for an EUI-equipped diesel APU, the speed and timing at which the injection starts is an important consideration. A low injection pressure usually results in poor spray and emission performance at the HEV starting transient. The parasitic power consumption EUI system is probably the best among the systems considered, since the fuel injection system is turned off as soon as the engine is turned off. EUI usually has the highest peak injection pressure and the best end-of-injection spray characteristics (Lai et al., 1998; Wang et al, 1999); the latter is because of the shorter and bulkier needle and larger needle cone angle. However, packaging into a small-bore cylinder head is an important consideration because of its size.

Figure 15 and 16 show a typical HEUI transient injection pressure and injection rate at system startup. With common-rail oil pressure maintained steadily at 380 bar, the injection system took 3 to 4 injections to build up the pressure in both the intensifier and high-pressure

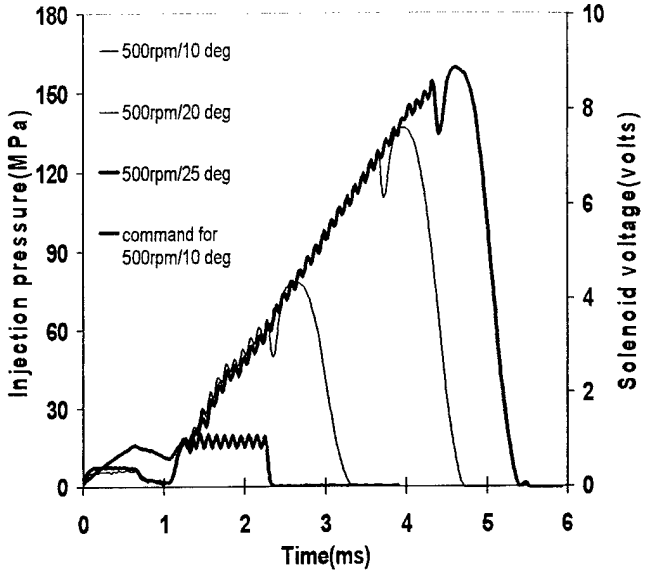

Fig.13 Injection pressure of EUI system, with various injection duration and 1000-rpm engine speed (500-rpm camshaft speed).

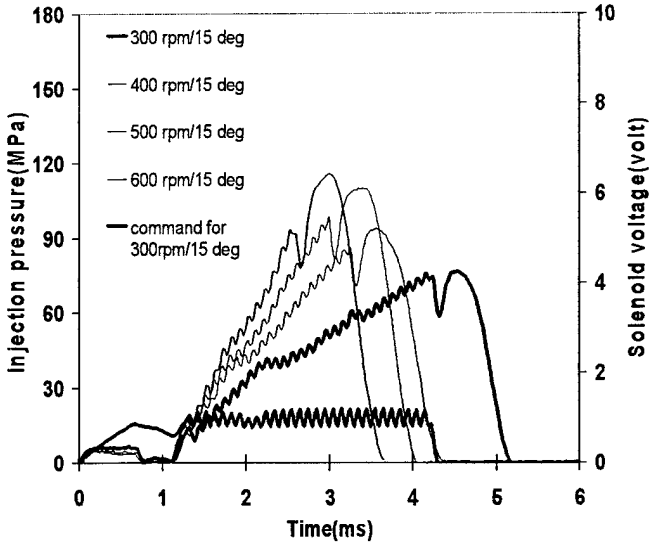

Fig. 14 Injection pressure of EUI system, with various camshaft speeds and 15-degree injection duration

line before a nominal injection was issued. The injection pressure, injection rate, and injection quantity became stable and repeatable after the 3rd injection was issued. The test results were summarized in Table 3. For the 1st injection, its pressure reached 56 percent of the nominal (140 MPa) and its quantity reached 71 percent of the nominal (101mg). The peak injection pressure is a function of the coupling between the two hydraulic systems; i.e., the low-pressure oil common rail and the high-pressure diesel fuel line upstream of the nozzle. Therefore, either the leakage tolerance of the entire injection system must be kept under tight control or the shut down duration cannot be too long, in order to insure the injection amount and spray quality of the first few injections during the HEV start transient. Integrating the hydraulic amplifier and solenoid unit with the injector reduces the high-pressure volume and system response. The parasitic power consumption HEUI system is most likely higher than that of EUI system, but comparable with or slightly higher than that of the CR system because of leakage concern. The oil pump may needs to be turned on intermittently in order to maintain a minimum pressure for unexpected HEV start transient.

The high-pressure common-rail (CR) injection system, with its independent pressure control and electronic injection-rate shaping capabilities, is an important enabling technology and is the first to be put into mass production for HSDI engine. The combined effect of nozzle geometry (e.g. mini-sac, VCO nozzles), needle and seat (single-guided/dual-guided, grove etc) design and multiple injection events on the spray dynamics of CR systems is quite complicated (Han et al.; 2000) and requires detailed optimization with HEV operation. The

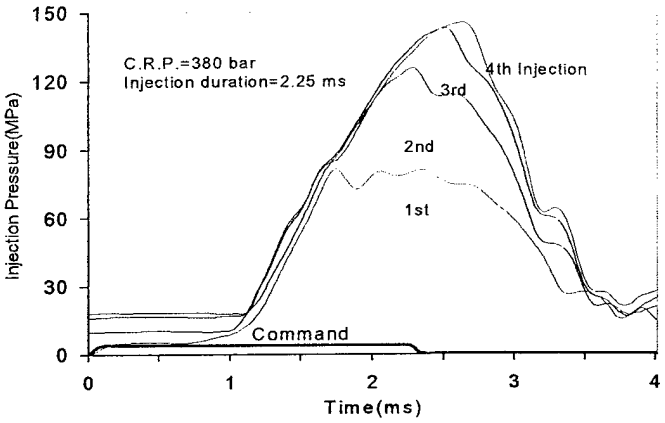

Fig. 15 Injection pressure transient at system start-up

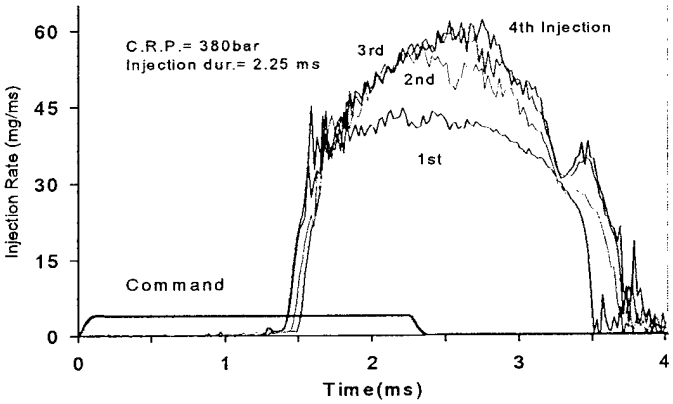

Fig. 16 Injection-rate transient at system start-up

Injection since engine start-up	Injector Response Time(ms)	Peak Injection Pressure(MPa)	Injection Quantity(mg)
1st	1.5	80	72
2nd	1.44	127	90
3rd	1.38	143	99
4th	1.4	145	101
5th	1.38	140	101

Table 3. HEUI startup characteristics.

concern for leakage of the common rail pressure is similar to that of HEUI. As a result, the parasitic power consumption of CR system is comparable with or slightly lower than that of the HEUI system because of the more efficient single-fluid high-pressure pump operation at the low flow rates.

Conclusion

1. Diesel engines used to power parallel HEV's have frequent hot starts after being shutdown.
2. While reducing fuel consumption by not operating the engine, some energy will be lost for both stopping and starting the engine.
3. The energy spent to start the engine increases with the drop in engine temperature, which can be significant for long shutdown periods.
4. Starting the engine at a higher motoring speed could be beneficial for engine wear. However, it will require more energy to be supplied by the starting motor, including the efficiencies of the motor, generator and battery pack.
5. Hot start transients produce NOx in addition to hydrocarbon emissions. Longer shutdown periods produce less NOx, but more HC emissions.
6. The control of engine-out emissions is critical during the cold and hot start transients, since the after treatment devices are not effective at low exhaust temperatures.
7. The strategy of stopping and starting the engine in HEV operation should be optimized, based on the engine thermal conditions before shut down, length of the shut down period and its effect on the temperature of the after treatment devices, battery charge status, overall fuel economy, and emissions.
8. High-pressure fuel injection systems behave in different ways under the S/S transients of the HEV. Some systems take a few cycles after starting to operate properly.

Acknowledgement

The authors acknowledge the technical and financial support of the US Army National Automotive Center and TARDEC to the ARC (A consortium of 8 universities directed by The University of Michigan), and the Army Research Office, Research Triangle Park, NC. The help and hard work of the graduate students in the Center for Automotive Research and the machine shop at Wayne State University is greatly appreciated.

References

1. Rezeka, S. and Henein, N. A. (1984) "A New Approach to Evaluate Instantaneous Friction and Its Components in Internal Combustion Engines", SAE 840179, SAE Transactions, Vol. 93, 1984.

2. Lai, M.-C., Wang, T.-C., Xie, X., Han, J., Henein, N. A., Schwarz, E., and Bryzik, W., (1998) "Microscopic characterization of Diesel Sprays at VCO Nozzle Exit" SAE 982542.

3. Han, J.-S., Wang, T. C., Lai, M.-C., Henein, N. A., Miles, P., and Harrington, D. L., (2000), "Dynamics of Multiple-Injection Fuel Sprays in a Small-Bore HSDI Diesel Engine," SAE 2000-01-1256, in SAE SP-1498, ***Advances in Diesel Fuel Injection and Sprays***, SAE Int'l Congress, Detroit, MI., March 6-9, 2000.

4. Wang, T. C., Han, J.-S., Lai, M.-C., Henein, N. A., Schwartz, and Bryzik, W., (2000) "Parametric Characterization of High-Pressure Diesel Fuel Unit Injection Systems," in ASME ICE Vol. 34-2 ***Fuel Injection, Combustion, and Engine Emissions***, pp. 113-130. ASME ICED Spring Technical Conference, San Antonio, April 9-12, 2000.

APPENDIX B

2003-01-0080

Simulation of Diesel Engines Cold-Start

Hengqing Liu
General Motors

N. A. Henein
Wayne State University

Walter Bryzik
US Army TARDEC

ABSTRACT

Diesel engine cold-start problems include long cranking periods, hesitation and white smoke emissions. A better understanding of these problems is essential to improve diesel engine cold-start. In this study computer simulation model is developed for the steady state and transient cold starting processes in a single-cylinder naturally aspirated direct injection diesel engine. The model is verified experimentally and utilized to determine the key parameters that affect the cranking period and combustion instability after the engine starts. The behavior of the fuel spray before and after it impinges on the combustion chamber walls was analyzed in each cycle during the cold-start operation. The analysis indicated that the accumulated fuel in combustion chamber has a major impact on engine cold starting through increasing engine compression pressure and temperature and increasing fuel vapor concentration in the combustion chamber during the ignition delay period. An "Autoignition Index" (AI) is introduced to determine the diesel engine first firing cycle. Also, diesel engine combustion instability is analyzed in details. The model indicated that misfiring after firing is caused by an imbalance between engine dynamic and combustion kinetics. The model predictions of the instantaneous engine speed variation during cold-start showed the same tend as the experimental results.

INTRODUCTION

The initiation of diesel fuel combustion is dependent on the compression temperature, compression pressure, fuel properties and fuel injection characteristic. During cranking, air temperature in cylinder is lower than those of during any other modes of engine operation. The low compression temperatures and pressures are caused partly by the low ambient temperature, and more importantly by the excessive heat losses and blow-by losses at low cranking speeds. Consequently, low compression temperatures and pressures result in poor startability of diesel engines. Diesel engine cold starting can be affected by any of the followings:

- fuel properties;
- intake air temperature and pressure;
- compression ratio;
- leakage or blow-by;
- cranking speed;
- fuel injection;
- combustion chamber design.

The residual gas affects diesel engine ignition delay. Liu and Karim [1] investigated the role of residual gas in a motored engine fueled with gaseous fuel. They found that residual gases have both positive and negative effect on ignition depending on the completeness of reactions which produce the residual gases. Residual gas which is the product of partial oxidation reaction has mainly kinetic effects which promotes ignition; on the other hand the product of more complete combustion has significant thermal, kinetic and diluting effects. All these effects are strong function of the equivalence ratio of the

such as piston, head and cylinder liner were warmed up sufficiently to influence combustion.

Austen and Lyn [6] found that an optimum timing for normal operation is generally too early for optimum cold starting, which lies between 10 and 20 BTDC by static timing. At extremely low engine speeds such as during cranking, the compression temperature is lower than that at higher engine speeds. Therefore the ignition delay time is longer at starting, but the required crank angle degrees for ignition delay become much less. Therefore retarded injection timing (compared to optimum injection timing for performance) results in good startability. With advanced injection timing, the fuel is injected into relatively lower density and lower temperature air. This causes longer ignition delay and thus strong penetration. Therefore more fuel impinges on the wall. With the progress of diesel fuel injection technology, some injection strategies were developed to improve diesel engine cold startability and exhaust emissions. Osuka et al. [8] investigated effect of split injection or pilot injection on diesel engine cold startability. Their results showed that with pilot injection, diesel engine startability was improved dramatically. The starting time was reduced to one third of conventional injection system, white smoke during starting was reduced more than half, and the duration of white smoke emission was reduced to one tenth of conventionally injected engine. They believed that pilot injection produce a cool flame reaction. Even though there is not much heat release in the cool flame, it does promote ignition of the main injection later on.

Ignition of CI engine relies on both high pressure and temperature. At higher compression ratios, engine compression temperature and pressure are higher, so are the wall temperatures. Higher compression temperatures and pressures lead to shorter ignition delay and remarkable reduction in fuel adhering to the walls [9]. Higher compression ratio helps engine cold start. For this reason a higher compression ratio is often chosen which is desirable for cold start but compromises optimum economy, power and exhaust emissions. Higher compression ratio engine requires higher power battery to maintain the desired cranking speed. In turbocharged diesel engines, compression ratio is often reduced to limit peak pressures. This obviously has a detrimental effect on engine starting performance.

Other things being equal, a direct injection engine should be an easier starter than an indirect injection engine. The difference in the starting performance of DI and IDI diesel engines have been reported in detail by Biddulph and Lyn [10]. They found that the increase in compression temperature once IDI diesel engines had started was much greater than the increase in compression temperature with DI diesel engines. Biddulph and Lyn concluded that this was a consequence of the higher level of heat transfer that occur in IDI diesel engines, and the greater time available for heat transfer at lower cranking speeds. They also pointed out that for self-ignition to occur in diesel engines, a combination of sufficient time and temperature is required. With IDI engines that have started firing on one cylinder, then the reduction in time available for ignition is more than compensated for by the rise in compression temperature. Thus once one cylinder fires, then all the rest cylinders should fire at the idle speed. Biddulph and Lyn found that this was not the case for DI diesel engines. The smaller increase in compression temperature did not necessarily compensate for the reduced time available for self-ignition, and it was possible under marginal starting conditions, for an engine to reach idling speeds with some cylinders misfiring, and for these cylinders not to fire until the engine coolant had warmed up. Such behavior is obviously undesirable, and is characterized by the emission of unburned fuel as white smoke. Tsunemoto, et al. [9] studied the influence of combustion chamber shape and depth on the adhering fuel to the chamber walls in a direct injection diesel engine. They

concluded that in shallow combustion chambers, the distance from injection nozzle to the combustion chamber walls with both bowl and square cavities is far, and fuel evaporates before impinging on the walls reducing the amount of remaining fuel. The work of Phatak and Nakamura [7] indicated that combustion chamber design and the resulting fuel air mixing process has a significant influence on the cold startability of DI diesel engine. To obtain both good cold startability and performance, the combustion chamber design should promote locally non-uniform air fuel ratios, but with well-organized spray pattern. Combustion chambers promoting high swirl and squish are not desirable for good startability. Further, they concluded that fuel impingement on chamber walls is not desirable for good cold startability. Regardless of the combustion chamber design, rate of injection and nozzle geometry, improved cold startability is obtained with retarded injection timing. Additional air does not have a beneficial effect on cold startability.

Starting diesel engines in cold conditions presents a serious problem. Many factors affect engine cold startability, such as fuel properties, ambient conditions, fuel injection, cranking speed, etc. For decades, researchers have worked on this problem intensively and tried to understand engine cold start and to find ways to improve engine cold startability. In the past, most works were done experimentally and great improvements were achieved. But there are still some questions left unanswered. For instance, why does the engine start after long cranking period under cold ambient conditions? Why does the engine misfire after firing?

In this study, a zero-dimensional diesel engine model is developed based on previous works [11,12]. The model is used to simulate the overall engine performance under cold start and fully warmed-up conditions and a fuel drop and fuel film evaporation model is developed for engine cold start analysis. The target engines are a naturally aspirated single cylinder direct injection diesel engine (DEUTZ). The filling and emptying approach is used to describe mass flow processes of the cylinder, blow-by, intake and exhaust manifolds. Optimization method was used to calibrate the engine models. For transient operation during cranking and starting, emphasis will be placed on factors that affect starting especially cold starting and engine cold start instability.

COLD STARTABILITY OF DIESEL ENGINES

Cold startability of diesel engines can be defined as the ability of an engine to quickly start and run with minimum assistance from the starting motor and to continue to run without faltering. Figure 1 and 2 show six typical traces for the instantaneous engine speed of Deutz engine using diesel fuel DF-2 during cold start at -15, -10, 0, 5, 10 and 30 ^{0}C. Figure 3 shows the engine cranking speed at different ambient temperatures. At –15 ^{0}C ambient temperature, the engine cranking at 280 rpm, the first engine firing was observed after 43 cycles. It indicated that the engine misfired in the next two cycles, fired again, followed by eight misfiring cycles, ran on a 16-stroke-cycle (cycles 56, 57, 58 and 59), a 20-stroke-cycle (cycles 60 to 65) and a 16-stroke-cycle again (cycles 66 to 69). No steady acceleration was observed till the end of data recording. At –10 ^{0}C ambient temperature, the engine cranking at 320 rpm, the first engine partial firing was observed after 30 cycles. Acceleration started at cycle 38. But there was repeated misfiring where the engine operated in some cases on a 12-stroke-cycle (cycles 54, 55 and 56), followed by many 8-stroke-cycles (cycles 57 and 58; 59 and 60; 61 and 62), and so on till cycle 70 when the data recording ended. At 0 ^{0}C ambient temperature, the engine cranking at 350 rpm and the first attempt for ignition and poor firing was observed after 14 cycles. The steady acceleration, without misfiring, started in cycle 56. At 5 ^{0}C ambient temperature, the first partial firing was observed in the twenty ninth cycle, after which the engine misfired three times, fired and misfired again. Because the heat release rate was very low, the

engine speed basically remained the cranking speed. After 46 cycles, the engine started to accelerate. At 10 ^{0}C ambient temperature, the first partial firing was observed in cycle number twenty one and followed by many partial firing cycles. Due to weak heat release from partial firing, engine speed increased slowly. Two misfiring cycle was observed in cycle 25 and 32. Sharp increase in engine speed started after cycle 45. The engine started immediately at 30 ^{0}C ambient temperature. No misfiring was observed.

Why does the diesel engine require long cranking periods before starting at low ambient temperature is unknown. Explanations have been made for the effect of cranking on engine startability. However, the author is not aware of any published model in the literature that would predict the effect of the ambient temperature and fuel properties on the number of cranking cycles before the first firing. The following will be investigated by using engine model:

- Effect of cranking period on combustion chamber wall temperature.
- Effect of cranking speed on ignition delay.
- Effect of accumulated fuel on the compression ratio.
- Effect of accumulated fuel on the fuel vapor concentration.
- Effect of fuel properties on cranking period.

At low ambient temperatures, the diesel engine goes through a long period of cranking before it starts. During cranking, hot compressed air heats up the cylinder wall gradually. This process is slow due to the high thermal inertia of engine cylinder wall and the relatively low cylinder gas temperatures reached in the engine under motoring compared with those reached under firing condition. Lower gas temperatures lead to lower heat transfer rates to cylinder walls. Figure 4 shows the simulated piston surface temperature for the Deutz engine during cold start motoring without fuel injection at 0 ^{0}C ambient temperature. After 50 cycles, the piston surface temperature increased by 6.9 ^{0}C.

Low cranking speeds produce low compression pressures and temperatures due to excessive heat transfer losses and blow-by losses. Higher cranking speeds increase the engine compression pressures and temperatures, which reduces instantaneous ignition delay at any given engine crank angle point. Instantaneous ignition delay is defined as ignition delay calculated by using equation:

$$ID = AP^{-n} \exp(\frac{E_a}{RT}) \qquad (1)$$

at a given pressure and temperature. But higher speeds leave less time for the autoignition reaction to proceed. There must be a cranking speed which balances the two aspects and leads to a minimum ignition delay time. Equation (2) is used to calculate ignition delay integral.

$$\int_{t_{inj}}^{t_{inj}+t_{id}} \frac{1}{\tau} dt = 1 \qquad (2)$$

where t_{inj} is time to start injection, t_{id} is ignition delay time, τ is instantaneous ignition delay calculated using equation (1). The integration is terminated at 390 crank angle degree after which combustion is considered to fail. The engine model is applied to calculate cylinder pressure, temperature, instantaneous engine speed and ignition delay integral. The fuel injection starts at 20 crank angle degrees before TDC. The results are shown in figure 5. The intersections of a unity line and the ignition delay integrals represent the ignition delay period in crank angle degrees. If the engine cranking speed is too low, the ignition integral never reaches one, which means misfiring. Although ignition delay in millisecond decreases as engine cranking speeds increase, ignition delay in crank angle degrees is not monotonically changing with cranking speed. At low engine cranking speeds, ignition delay in crank angle degrees decreases as cranking speed increases. After a certain point, increasing cranking speed causes ignition delay in crank angle degrees to increase as shown in figure 6. In this case at 300 rpm the minimum ignition delay in crank angle degrees is reached.

The accumulated fuel in the combustion chamber increases the actual compression ratio, hence it boosts the compression pressure and temperature. In practice, in order to start the diesel engine in cold weather, more fuel is delivered, usually more than full load fuel delivery. During this cranking period, fuel is injected into the combustion chamber. Figure 7 shows, at 0 ^{0}C ambient temperature, the Deutz engine with 60 mm^3 of fuel per cycle, the change of actual compression ratio. Figure 8 shows the impact of the accumulated fuel on engine peak compression pressure and temperature, and cylinder wall temperature. For comparison purposes, the wall temperature, peak pressure and temperature without fuel injection are also plotted on the figures. As expected, the actual engine compression ratio increased from 17 to 18.07 after 50 cycles. The peak compression pressure increased by 205 kPa, compared to 9.9 kPa without fuel injection; the peak compression temperature increased by 8.1 ^{0}C, compared to 3.0 ^{0}C without fuel injection; the piston surface temperature increased by 7.2 ^{0}C, compared to 6.9 ^{0}C without fuel injection. Please note that the sharp changes in peak pressure and temperature at cycle number two are due to low engine speed at first cycle, which causes lower compression pressure and temperature than normal cranking. The simulation results show that the accumulated fuel does have an impact on the gas pressure, gas temperature and cylinder wall temperature during cold start.

Another effect of the accumulated fuel in the combustion chamber on engine cold start is due to its evaporation during the ignition delay period. The evaporation of accumulated fuel increases the overall fuel vapor concentration, therefore increase the chance of fuel ignition. In order to analyze the accumulated fuel evaporation in details, fuel injection and spray behavior need to be analyzed first. Fuel evaporation can be from liquid droplets before they impinge on the wall and from the liquid film on the wall.

The evaporation of liquid droplet has been a subject of extensive research. Borman and Johnson's drop evaporation model [13] is adopted in this study. The assumptions made are briefly repeated here. 1) radiation heat transfer is neglected; 2) the liquid is assumed to be spherically symmetric and the boundary layer thickness around droplet is assumed to have a space averaged value given by the empirical correlation; 3) effects of curvature on the vapor pressure are neglected; 4) the liquid is assumed to have infinite conductivity because of the rapid circulation within the drop; 5) thermal diffusion is neglected; 6) the liquid is and remains a pure hydrocarbon (no cracking); 7) collision, breakup, and droplet vibrations are neglected during the calculations; 8) the effect of air turbulence on the boundary layer are assumed negligible; 9) chemical reactions in the boundary layer are neglected.

Fuel injection rate is calculated using following equation,

$$\frac{dm_f}{dt} = C_d A\sqrt{2\rho_f \Delta P} \qquad (3)$$

The high-pressure sprays encountered in diesel engine operation have a very short breakup distance, so that almost the entire spray may be treated from the viewpoint of single droplet behavior. The initial fuel droplet diameter was represented by the Sauter Mean Diameter (SMD) in microns. Tanasawa and Hiroyasu [14] measured droplet size distribution in diesel sprays. They made extensive measurements for various parameters which included the type of injector nozzle, rack position of the fuel pump and the its speed etc., under atomosphere conditions. Further work was reported by Hiroyasu and Kadota [15]. They published a Sauter Mean Diameter (SMD) correlation in terms of injection pressure, air density and amount of fuel injected,

$$D_0 = 23.9(\Delta P)^{-0.135}\rho_a^{\ 0.121}V_f^{\ 0.131} \qquad (4)$$

D_0 is SMD in micron, ΔP is the pressure drop in MPa, V_f is the fuel injected per cycle in mm^3. More experimental works were reported in recent years. Some controversial results were reported in the literature about the effect of

ambient gas pressure on drop size. In this study, Hiroyasu's correlation equation (4) is used.

The number of fuel droplets formed from the injected fuel,

$$N = \frac{6m_f}{\pi D_0^3 \rho_f} \tag{5}$$

fuel droplet evaporation rate (Borman and Johnson, 1962),

$$\frac{dm_{drop}}{dt} = -\pi D_j D_{ij} Sh \frac{P}{RT_{fs}} \ln\left(\frac{P - P_v}{P - P_{fs}}\right) \tag{6}$$

convective heat transfer (Borman and Johnson, 1962),

$$Q_c = \pi D_j k (T_g - T_l) Nu \frac{z}{e^z - 1} \tag{7}$$

$$z = \frac{C_{pv} \frac{dm_{drop}}{dt}}{\pi D_j k Nu} \tag{8}$$

Droplet mass,

$$m_{drop} = \frac{\pi}{6} D_j^3 \rho_f \tag{9}$$

Droplet temperature equation:

$$m_{drop} C_L \frac{dT_l}{dt} = Q_c - \Delta h_{ev} \frac{dm_{drop}}{dt} \tag{10}$$

In this study, Gupta's [16] penetration correlation is used.

$$S = 1.895 \times 10^{-3} \rho_a^{-0.29} \Delta P^{0.257} t^{0.733} \tag{11}$$

Droplet temperature history is calculated using equation (6) through (10). Some simulation results, shown in figure 9 and 10, are the cylinder gas temperature and droplet temperature history and the change in cylinder fuel air ratio due to droplet evaporation during cold start motoring at ambient temperature 0 ^{0}C. Droplet temperature increases quickly after injection and gets close to equilibrium about 1 ms after injection. The fuel air ratio shown in figure 10 is the overall value over the whole volume of the cylinder. After fuel injection, fuel starts to evaporate. The fuel air ratio is the result of total mass of fuel vapor inside cylinder divided by total air mass inside cylinder. As fuel droplets evaporation goes on, more fuel vapor is added in the cylinder air and fuel air ratio increases. After wall impingement, evaporation of fuel drop is terminated and the fuel air ratio due to the evaporation of fuel drop keeps constant.

Once the fuel droplets impinge on the combustion chamber surface, a fuel film is formed and starts evaporation. The key for calculating fuel film evaporation is the film surface temperature, which is not known. Consider the top layer of the liquid film of thickness as a control volume as shown in Figure 11, which is dotted line. Apply the energy and mass balance to compute fuel film surface temperature.

The complete form of the first law of thermodynamic,

$$\frac{dE_{cv}}{dt} = \frac{dQ_{cv}}{dt} - \frac{dW_{cv}}{dt} + \sum \frac{dm_i}{dt}\left(h_i + \frac{V_i^2}{2} + gZ_i\right) - \sum \frac{dm_e}{dt}\left(h_e + \frac{V_e^2}{2} + gZ_e\right) \tag{12}$$

For the control volume defined in Figure 11, there is only mass out, no mass in, no work done to the control volume, and neglecting kinetic and potential energies, we have,

$$\frac{dE_{cv}}{dt} = \frac{dQ_{cv}}{dt} - \frac{dm_{ev}}{dt} h_g \tag{13}$$

Mass conservation equation,

$$\frac{dm}{dt} = -\frac{dm_{ev}}{dt} \tag{14}$$

The internal energy of the control volume, $E_{cv} = mu$

$$\frac{dE_{cv}}{dt} = \frac{dmu}{dt} = u\frac{dm}{dt} + m\frac{du}{dt} = -u\frac{dm_{ev}}{dt} + \Delta x A \rho \frac{du}{dt} \tag{15}$$

The heat transfer across the control volume boundary,

$$\frac{dQ_{cv}}{dt} = \frac{dQ_g}{dt} - \frac{dQ_l}{dt} \tag{16}$$

combine equation (10), (11), (12), (13), yield,

$$\Delta x A \rho \frac{du}{dt} = \frac{dQ_g}{dt} - \frac{dQ_l}{dt} - \frac{dm_{ev}}{dt}(h_g - u) \tag{17}$$

when Δx approaches zero, equation (17) becomes,

$$\frac{dm_{ev}}{dt}(h_g - u) = \frac{dQ_g}{dt} - \frac{dQ_l}{dt} \tag{18}$$

$h_g - u = \Delta h_{ev}$ is the latent heat of fuel at fuel film surface temperature. Rearrange equation (16),

$$\frac{dQ_g}{dt} - \frac{dQ_l}{dt} = \Delta h_{ev} \frac{dm_{ev}}{dt} \tag{19}$$

The heat transfer from the gas to the fuel film surface,

$$\frac{dQ_g}{dt} = h_c (T_g - T_{ls}) \tag{20}$$

The heat transfer inside fuel film, assuming the heat transfer is only by conduction.

$$\frac{dQ_l}{dt} = -K_l \frac{dT_{ls}}{dx} \tag{21}$$

combining equation (17), (18), (19) yield,

$$\frac{dm_{ev}}{dt} = \frac{h_c (T_g - T_{ls}) + K_l \dfrac{dT_{ls}}{dx}}{\Delta h_{ev}} \tag{22}$$

consider forced convection mass transfer,

$$\frac{dm_{ev}}{dt} = h_m (C_{ls} - C_\infty) \tag{23}$$

use heat transfer to mass transfer analogy [17], we have,

$$\frac{h_c}{h_m} = \rho C_p Le^{\frac{2}{3}} \tag{24}$$

$$Le = \frac{Sc}{\Pr} = \frac{\alpha}{D_{ij}} \tag{25}$$

$$h_m = \frac{h_c}{\rho C_p Le^{\frac{2}{3}}} \tag{26}$$

apply ideal gas state equation, the density of fuel vapor at fuel film surface,

$$C_{ls} = \frac{P_{ls}}{R_f T_{ls}} \tag{27}$$

the density of fuel vapor at infinity,

$$C_\infty = \frac{P_f}{R_f T} \tag{28}$$

note, $P = P_a + P_f$, and fuel air ratio $FA = \dfrac{m_f}{m_a} = \dfrac{P_f}{P_a}\dfrac{W_f}{W_a}$, air fuel ratio AF = 1/FA, we have,

$$P_f = \frac{P}{1 + FA\dfrac{W_a}{W_f}} FA \frac{W_a}{W_f} = \frac{P}{1 + AF\dfrac{W_f}{W_a}} \tag{29}$$

The partial pressure of fuel vapor at infinity can be computed using equation (29). The fuel properties used in this study are from Borman and Johnson [13], Reid and Sherwood [18], Henein [19], Petris and Giglio [20]. Initially, the wetted area is calculated assuming average fuel film thickness is 25 μm based on Stanton's [21] experimental work. As the number of motoring cycles goes up, the wetted area gradually reaches the whole combustion chamber area. The effect of wetted area on fuel vapor concentration is shown in figure 12. To find out the effect of wetted area on fuel evaporation, three cases are considered in one engine cycle. Assume the same amount of fuel impinged on combustion chamber in the three cases, the wetted areas or the fuel film thickness are different as shown in figure 12. More wetted area means thinner fuel film, which results in lower fuel surface temperature. The evaporation rate of fuel film is a function of fuel film surface temperature. Higher surface temperature results in higher evaporation rate. The amount of fuel evaporation is the product of evaporation rate and wetted area. This explains that more wetted area doesn't mean more fuel evaporated. The simulation shows that thicker fuel film (less wetted area) evaporates more fuel vapor. The change of fuel film thickness from 25 μm to 20 μm results in 2% fuel air ratio reduction. The change of fuel film thickness from 25 μm to 30 μm results in 3% fuel air ratio increase. As cycle number increases, fuel film covers more and more area. Eventually (roughly 3 to 5 cycles depending on the amount of fuel injected), the whole bottom of combustion chamber will be wetted.

Figure 13 through 15 show the results of fuel drop and fuel film evaporation simulation results. Figure 13 shows fuel film thickness changes with cycle number. The fuel film thickness gradually increases as more fuel added to the combustion chamber. Figure 14 shows fuel film surface temperature in cycle 10, 30 and 50. Fuel film surface temperatures keep going up as

cycle number increases. Figure 15 shows average fuel vapor concentration during ignition delay period changes with cycle number. From Figure 16 we can see that the majority of fuel film evaporation occurs in a short period of time around TDC during the whole engine cycle. Initially the fuel film surface temperature is high (droplet temperature). Because the fuel film is very thin, it cools down quickly as it losses energy to the cylinder wall. As fuel film thickness increases, the heat transfer through the fuel film become slower and the time during which the fuel film surface temperature stays at high level gets longer. Since fuel film surface temperature determines the rate of evaporation, that means more fuel will evaporate as the fuel film become thicker and thicker. As discussed in a previous section, the accumulated fuel also increases compression pressure and temperature. The compound effects of temperature increase and thicker fuel film increase fuel concentration quickly after cycle number 25 as shown in Figure 15. The rapid increase in fuel air ratio after cycle 25 mainly due to fuel film surface temperature stays at high level longer thus fuel concentration at fuel film surface stays at high level longer too, which is the driving force for fuel evaporation.

Diesel fuel auto-ignition involves many chemical processes. So far it is still too complicated to fully understand. Generally the chemical reaction rate for diesel fuel can be written as following,

$$r = k_0[F]\exp(-\frac{E}{RT}) \qquad (30)$$

where, r is the chemical reaction rate, k_0 is a constant, [F] is fuel concentration, E is the activation energy of the fuel, R is gas constant and T is the temperature of air fuel mixture.

From the chain reaction theory, when radical concentration reaches a certain value, ignition will occur. Integration of equation (30) can be considered as the radical concentration as shown in the following equation.

$$AI = \int_{t_{inj}}^{t_{end}} k_0[F]\exp(-\frac{E}{RT})dt \qquad (31)$$

We introduce the AI in equation (31) as autoignition index. If the AI at any given conditions is greater than an arbitrary reference point, autoignition is considered to occur. Figure 17 shows the AI at different ambient conditions. Now we will set the conditions in the third cranking cycle at an ambient temperature of 10 ^{0}C as a reference. The reference AI is shown as a dotted line in figure 17. The values used in the calculation of the AI are: k_0 is the specific chemical reaction constant, for simplicity considered equal to unity, $\frac{E}{R} = 4350$ K represents the activation energy of the fuel, [F] is fuel vapor concentration during ignition delay period calculated for consecutive cycles. The AI for the engine at four different ambient temperatures is plotted on the same figure. The points of intersection with the reference AI line indicate the end of cranking and the start of ignition, combustion and engine acceleration. For example, at an ambient temperature 278 K, cranking would end after 15 cycles. As the ambient temperature drops to 273 K and 268 K, cranking would end in cycles 32 and 36 consecutively. The model predicts the same trend as the engine experimental data shown in figure 18.

COMBUSTION INSTABILITY DURING COLD STARTING

It is common that at low ambient temperatures onset of the first firing cycle doesn't mean that the engine will fire next cycle and accelerate smoothly. Figure 1 shows a trace of the instantaneous engine speed during cold start at -15, -10 and 0 ^{0}C, using diesel fuel DF2 (fuel properties are listed in table 1). At –10 ^{0}C, the engine was cranked for 29 cycles, after which it fired in cycle 30. After cycle 30 it misfired in next two cycles, cycle 31 and 32. Then it fired again in cycle 33. This kind of process went on and on. Figure 19 and 20 also show traces of the instantaneous engine speed during cold start at -5 ^{0}C using the diesel fuel A and at 0 ^{0}C using the fuel B (fuel properties are listed in table 2). Similar engine operation was

observed. This means that combustion instability is not fuel specific. Engine fired or partially fired every other cycle or every third or fourth cycle. This mode of operation can be called to 8-stroke-cycle, 12-stroke-cycle and 16-stroke-cycle operation. This type of diesel engine operation is repeatable and referred to as combustion instability [22,23,24]. The 8-stroke-cycle, 12-stroke-cycle and 16-stroke-cycle operation is undesirable, because it causes engine hesitation and vibration. The unburned fuel accumulated in combustion chamber in misfired cycle is the major source of white smoke emission.

To analyze diesel engine combustion instability, a criterion for ignition must be established to quantitatively analyze engine cold start. Due to the complexity of diesel combustion, a full understanding of the processes is not reached yet. Based on a large number of experimental observations and scientific reasoning, researchers usually use ignition delay to predict first ignition. Unfortunately, there is no well-accepted criterion for ignition in cold start, due to the complexity of ignition processes and uncontrolled physical and chemical conditions. The method given in next the section is a rough estimate of the onset of ignition. At marginal conditions the prediction may not be correct. Here the focus is on the physical conditions during cold start and its effect on cold start.

It has been established that the criterion for ignition to occur in a diesel engine is that compression temperature and pressure should be high enough to reduce ignition delay to the time available between injection and some point around TDC during the compression process [25]. Biddulph [10] found that for a given mean cranking speed and injection condition, ignition would occur near or just after TDC. If the ignition delay ends close to TDC, combustion will take place. If the ignition delay ends way after TDC, while the expansion rate is high, the oxidation reactions may slow down and misfiring may occur [26,27]. Many experimental data in our laboratory showed also the same trend. Figure 21 shows experimental engine cylinder pressure traces in the first 30 cycles during cold start at ambient temperatures of $-5\ ^0$C and $5\ ^0$C respectively. From the figures we can see that the majority of combustion started roughly before 30 crank angle degree after TDC. The length of the ignition delay can be calculated by Arrhenius type equation, see equation (1). Usually the Arrhenius type of ignition delay is derived from combustion bombs, rapid compression machines or steady flow rigs. However, widely differing values for the parameters in equation (1) were found in the literature. The differences can be as large as several orders of magnitude. Not surprisingly, the ignition delay values predicted for engines also vary widely. In cold start, the compression pressure and temperature are usually in the lower bound of the test data range or even below the test data range; and both the gas mixture temperature and pressure keep changing during ignition delay period. In order to account for the changing conditions in the real engine, the integral in equation (2) is often used as a criterion for ignition. Obviously, equation (2) does not give an upper limit of integration. As observed in figure 21, if combustion did not start before a certain point in the expansion stroke, the engine misfired. After that point, the integration of equation (2) will be terminated, and the cycle is considered a misfiring cycle. In this study this point is set to be at 30 crank angle degrees after TDC. Some other workers reached similar conclusions [10,25,26].

Once autoignition takes place, the combustion reactions accelerate, resulting in a rapid rate of pressure rise. Both the rate and extent of the pressure rise depend on the amount of fuel that has had time to evaporate and mix with the air during the ignition delay period. Since the ignition is considered to only occur between the injection point and certain crank angle degree, let's say 30 degree after TDC, the time available for the ignition delay to lapse is therefore governed by the cranking speed. In other words, this available time represents the maximum allowable time for the delay period if ignition is to occur. The higher the cranking

speed, the shorter is the available time for ignition to occur. Conversely, the lower the cranking speed, the longer is the available time for ignition to occur. On the other hand, higher cranking speeds result in higher compression temperatures and pressures which are in favor of ignition, due to the reduced heat transfer losses and blow-by losses.

Since there is no well-accepted ignition delay correlation for diesel engines, especially for engine cold start, the focus here is on the relative changes in ignition delay during cold start rather than the absolute values. The following will discuss the integral in equation (2) at different ambient temperatures and the effect of the firing cycle on the integration.

From figure 22, we can see that equation (1), the constants are A=0.854, n=1.31, $\frac{E_a}{R} = T_0 = 4350$ K [28], gives the correct trend for the ignition delay. At lower ambient temperatures, the ignition delay calculated by using the pressures and temperatures at various crank angle degrees decrease as approaching TDC, reaches a minimum before TDC, after which it increases again. The ignition delay increases rapidly after 370 crank angle degree. Figure 23 shows that the integral in equation (2) reaches unity after different intervals at different ambient temperatures. From figure 23, we can see the integral increase at a fast rate before TDC at all the three different ambient temperatures. After 370 crank angle degree, the increase in the rates approaches zero. That explains why ignition is most likely to occur before 390 crank angle degree.

The first ignition that occurs in the combustion chamber does not necessarily mean that the engine will start smoothly. Marginal conditions in the combustion chamber may result in partial ignition or even misfire, which may prevent the engine from starting. Figure 1, 19 and 20 show the engine operating on the 8-stroke-cycle, 12-stroke-cycle and 16-stroke-cycle during cold start. What causes firing-misfiring cycles is really unknown, which involves complex chemical and physical processes. We do know that firing increases engine speed and heats up the cylinder walls. The increased wall temperature and engine speed due to firing will increase compression pressure and temperature for the following cycles. As the engine slows down in the second misfiring cycle, the time allowed for ignition gets longer, the integral increases and so the chances for successful firing improve. If the engine misfires again, the engine will slow down even more and the chances for successful firing get better.

As the unstable combustion continues, the engine gets warmer and both the compression temperature and pressure increase with time. When the engine gets warm enough, the combined effect of the increase in speed and the drop in heat transfer losses would raise the compression temperature and pressure and speed up the reaction rate of the autoignition processes. The engine might shift from running on a 16-stroke-cycle to a 12-stroke-cycle as the engine gets warmer. Eventually, the engine would shift to an 8-stroke-cycle, followed by the regular 4-stroke-cycle. The results of a continuous engine cycle simulation for the Deutz engine cold start at 0 and 5 ^{0}C ambient temperature with 60 and 48 mm^3 fuel injection per cycle, are shown in figure 29 and 30. In the simulation, the engine is assumed to fire in cycle number ten at 0 ^{0}C and cycle number 5 at 5 ^{0}C. By using the ignition integral in the first firing cycle as ignition threshold, the engine was found to fire and misfire in following cycles. Figure 24 and 25 show the predicted instantaneous engine speed at ambient temperatures 0 and 5 ^{0}C respectively.

The predicted instantaneous engine speeds follow the same trend as the engine experimental data shown in figure 1, 19 and 20. Figure 29 shows some of the trends observed in the experimental data for combustion instability. After the engine fired in cycles 16 and 22, it misfired three times (16-stroke-cycle). After cycles 27 and 33 the engine misfired two times (12-stroke-cycle). Figure 30 shows similar trends in combustion instability as those shown in figure 29. The number of firing cycles (before

a misfire) increase as the engine gets warmer. Comparing between the predicted and experimental results, it is noticed that the pattern of predicted instantaneous engine speed is more regular than that of the experimental data. This is expected because the conditions in the simulation are well controlled and many simplifying assumptions are made. There are many unknown parameters which affect engine cold start in the real engine. For example the effect of the drop in the ambient temperature on the injection system and spray formation have not been considered in this investigation. In addition, the detailed kinetics of the autoignition processes are not included in the model because they are not well understood yet. Further more, the correlations available in the literature for the heat transfer in the engine are based on experimental under warmed up conditions, which is not the case for cold starting. Those parameters are very difficult to be covered by the simulation models.

CONCLUSIONS

The major conclusions are the followings:

1. The length of the cranking period depends on a combination of physical and chemical parameters. The physical parameters contribute to the formation of a stoichiometric or slightly rich mixture of fuel-vapor and air. Fuel vapor concentration depends on fuel volatility, gas temperature and pressure, the rates of heat transfer to the liquid and mass transfer to the gas, degree of spray atomization, liquid film thickness on the wall and time allowed for evaporation. The chemical parameters affect the rate of the autoignition reactions, which are very sensitive to mixture temperature, global activation energy E (or fuel Cetane number) and fuel-vapor concentration.
2. The rise in mixture temperature during cranking is due to reduced heat transfer from the hot gas to the walls and reduced blow-by during compression and expansion. Fuel accumulation in the combustion chamber during cranking increases the effective compression ratio, and reduces ignition delay; and reduces the heat transfer losses to the walls, thus increases the film surface temperature and the rate of evaporation. Cranking at a higher speed reduces ignition delay period due to the higher compression temperatures and pressures; but, reduces the time available for autoignition reactions to be completed near TDC. Accordingly, there is a speed beyond which the ignition delay, in crank angle degrees, increases and cranking period becomes longer.
3. An Autoignition index (AI) is introduced to combine the physical and chemical parameters.

$$AI = \int_{t_{inj}}^{t_{end}} k_0[F]\exp(-\frac{E}{RT})dt$$

Cranking would continue till the autoignition index is reached.

4. The misfiring after firing is caused by an imbalance between engine dynamic and combustion kinetics. The high rate of acceleration after a firing cycle that reduces the time available for the physical and chemical processes to be completed near TDC, where the compressed air temperature and pressure are at their peak levels. There is a point in the expansion stroke after which the gas temperature drops at a rate that hinders the progress in combustion. After a misfiring cycle the engine decelerates for one or more cycles. As the engine speed is reduced, more time becomes available at TDC for the combustion reactions to proceed and produce firing. As the engine continues to fire and misfire, engine walls get warmer and the charge temperature increases. This enhances the combustion process, reduces the time needed near TDC, and the number of misfiring cycles drops.
5. The simulation model is able to predict the operation of the engine on a 16-stroke-cycle and its shifting to a fewer number of strokes per cycle. This phenomenon has been observed in previous experimental

investigations on different engines and fuels in our laboratories.

ACKNOWLEDGMENT

The authors wish to thank US Army TARDEC and ARO for the technical and financial support of this project.

Table 1 Fuel properties of DF2

Specific Gravity	0.8547
Kinematic Viscocity (40 ^{0}C)	2.7050
Flash Point (^{0}C)	58.33
Cetane No.	45
Calorific Value (kcal/kg)	10701.5
Sulfur Content, wt %	0.262
Distillation (^{0}C)	
5%	201.0
15%	217.5
25%	228.0
35%	239.5
45%	251.0
55%	262.0
65%	274.0
75%	286.0
85%	302.0
95%	336.0

Table 2 Fuel properties of Japanese fuel

Fuel	A	B
Cetane No.	49.2	38.7
Density at 15 ^{0}C (g/cm^3)	0.8066	0.8227
Viscosity at 30 ^{0}C (mm^2/s)	1.916	1.653
Sulfur (mass %)	0.014	0.012
Flash Point (^{0}C)	48.0	50.0
Distillation (^{0}C)		
5%	163.5	167.5
10%	170.0	173.0
20%	179.5	180.5
30%	191.0	187.5
40%	205.5	195.5
50%	221.0	205.0
60%	238.0	217.5
70%	257.0	236.0
80%	280.0	265.5
90%	313.5	304.5
95%	336.5	331.5

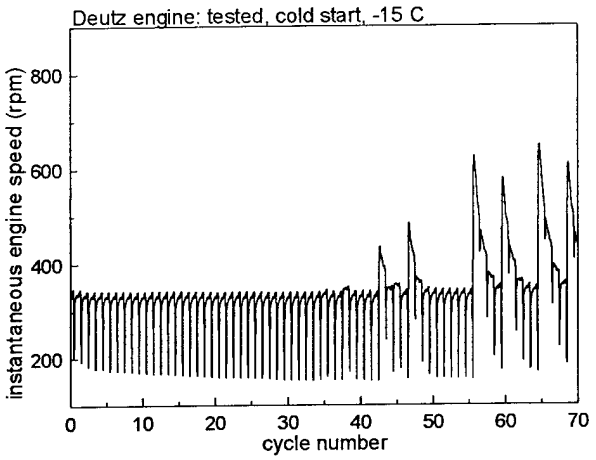

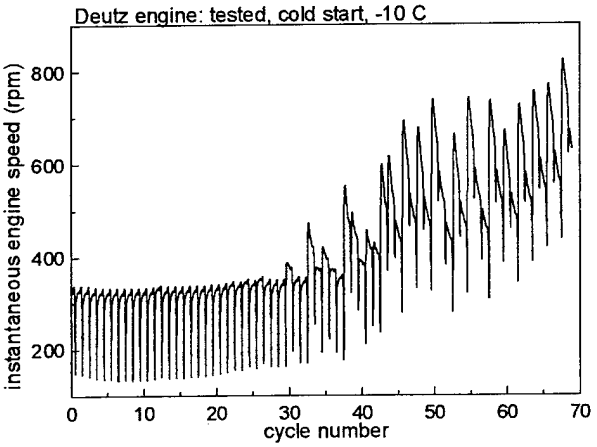

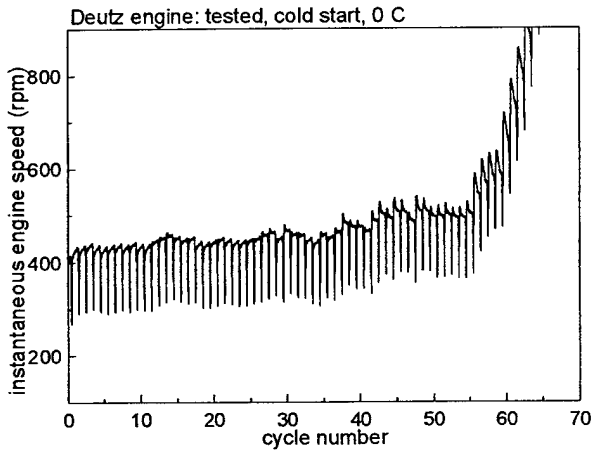

Figure 1 The experimental instantaneous engine speed from cycle#1 to 70, Deutz engine, cold start, DF2, at –15, -10 and 0 ^{0}C respectively.

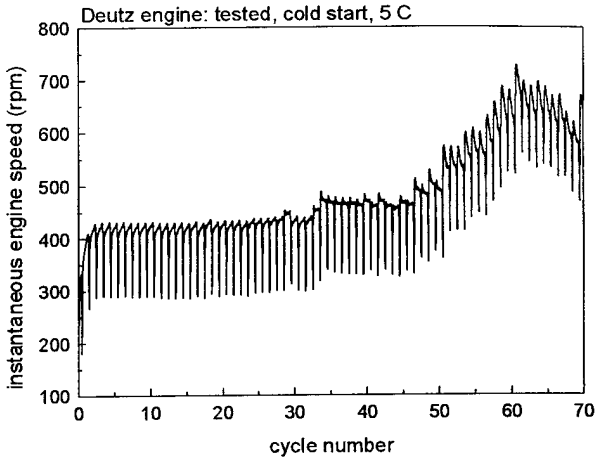

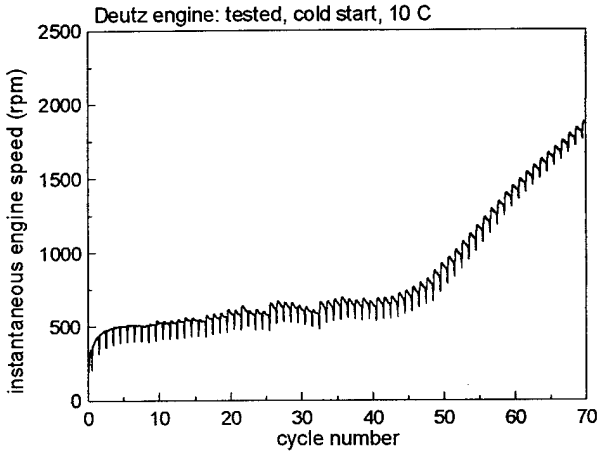

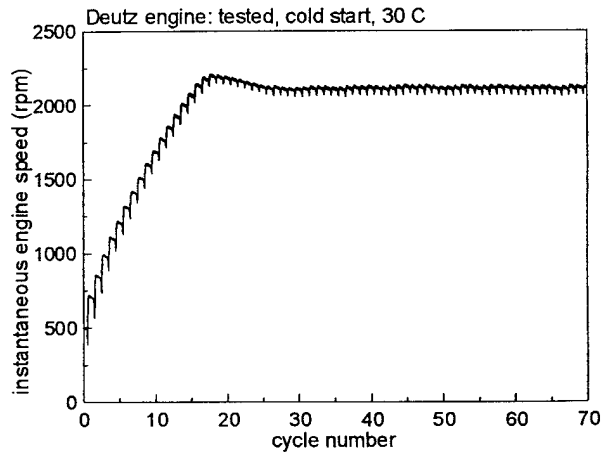

Figure 2 The experimental instantaneous engine speed from cycle#1 to 70, Deutz engine, cold start, DF2, at 5, 10 and 30 ^{0}C respectively.

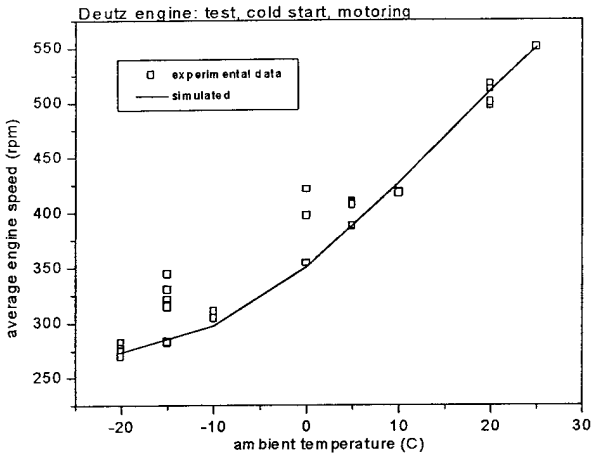

Figure 3 Engine cranking speed at different ambient conditions, Deutz engine, cold start motoring.

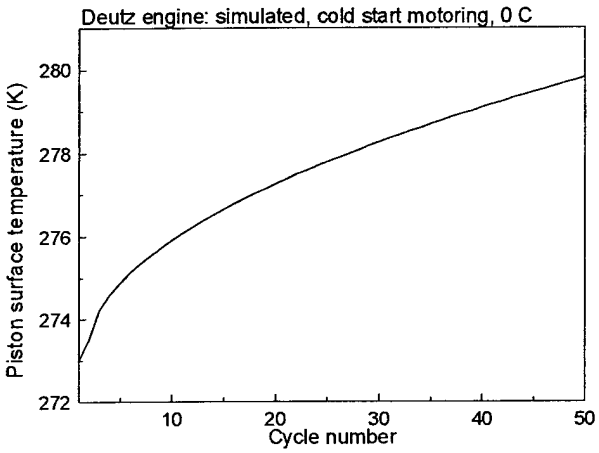

Figure 4 Simulated engine cylinder wall temperature warm-up history, Deutz engine, cold start motoring, no fuel injection, 0 ^{0}C.

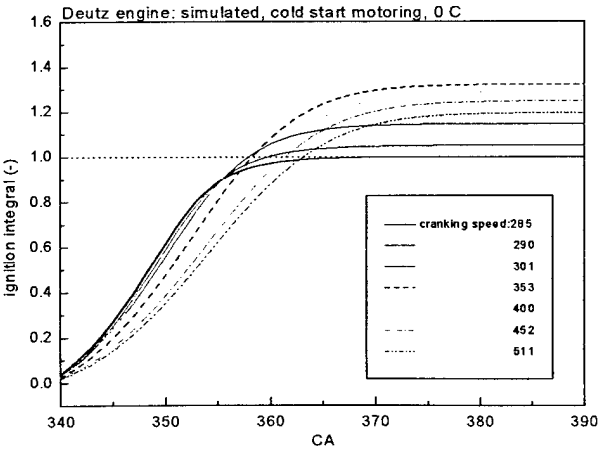

Figure 5 Simulated ignition delay integratal vs. engine cranking speed, Deutz engine, cold start motoring, 0 ^{0}C.

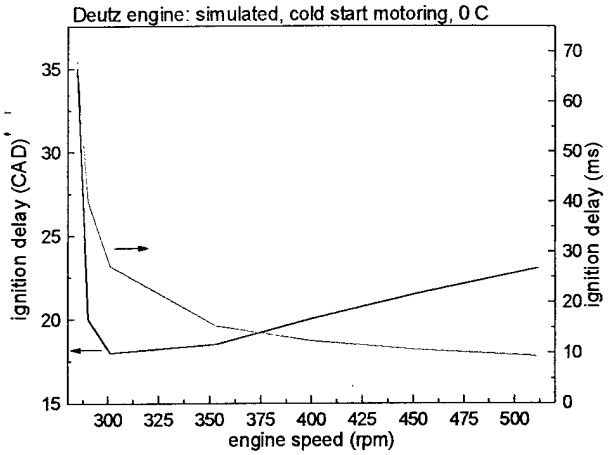

Figure 6 Simulated effect of engine cranking speed on ignition delay, Deutz engine, 0 ^{0}C.

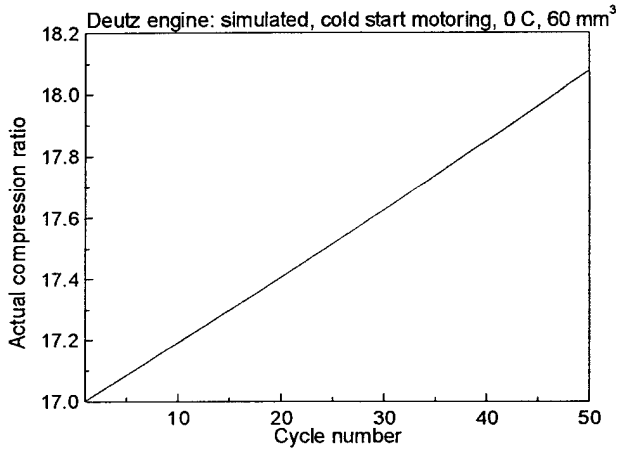

Figure 7 Effect of accumulated fuel on actual engine compression ratio, (Deutz engine, cold motoring, 0 ^{0}C, with 60 mm^3 fuel injection).

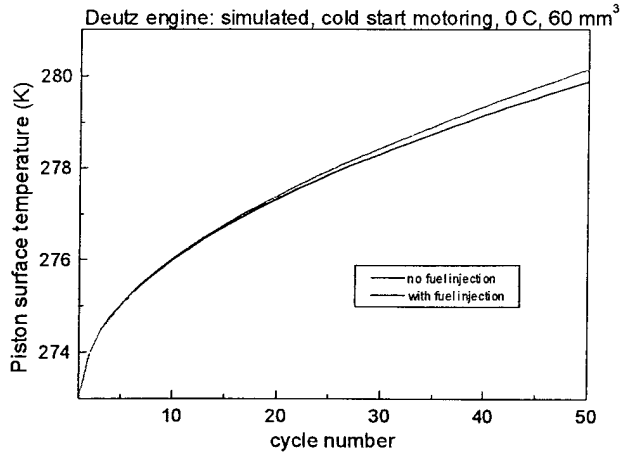

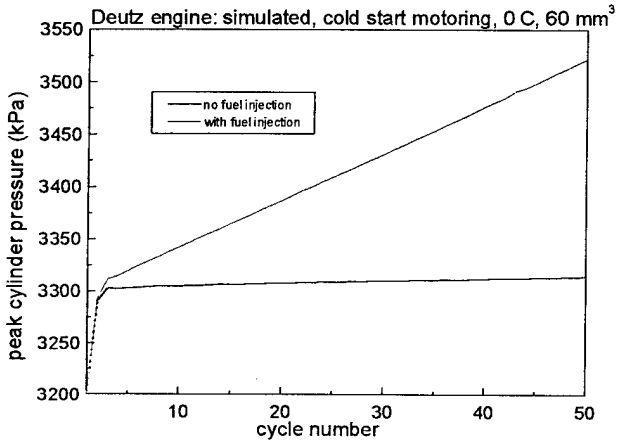

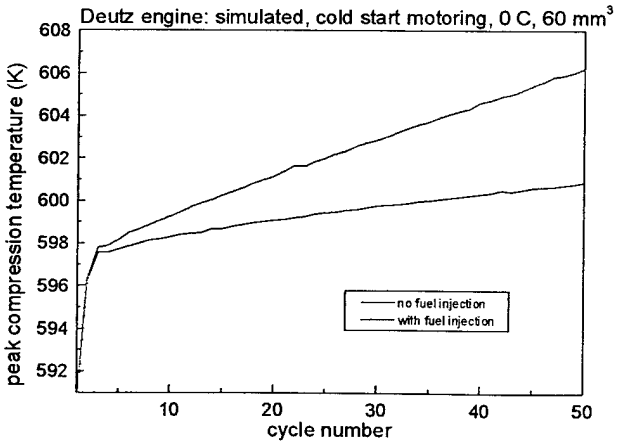

Figure 8 Simulated effect of accumulated fuel on piston surface temperature, peak cylinder compression temperature and peak cylinder pressure (Deutz engine, cold motoring, 0 ^{0}C, with 60 mm^3 fuel injection and without fuel injection).

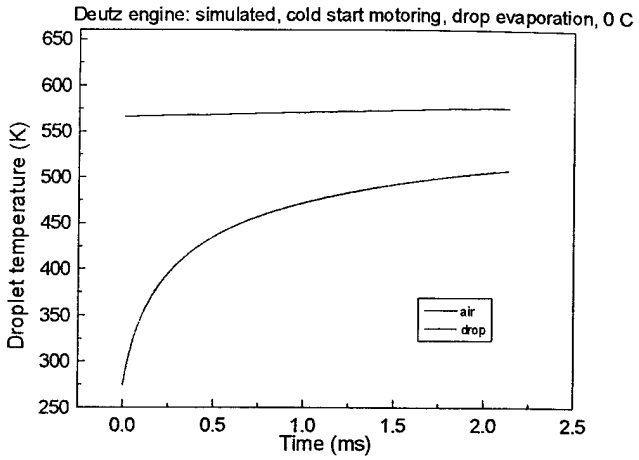

Figure 9 Simulated droplet temperature history, Deutz engine, cold start motoring, 0 ^{0}C.

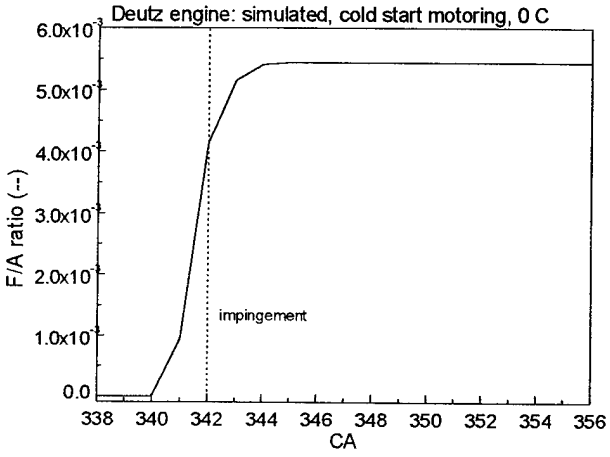

Figure 10 Simulated in cylinder fuel air ratio due to droplet evaporation, Deutz engine, cold start motoring, 0 ^{0}C.

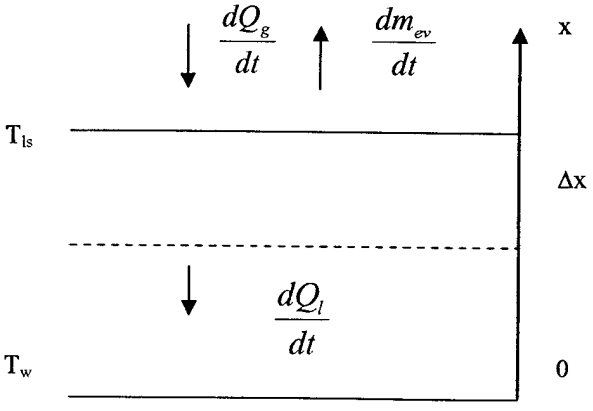

Figure 11 Diagram of fuel film evaporation model control volume.

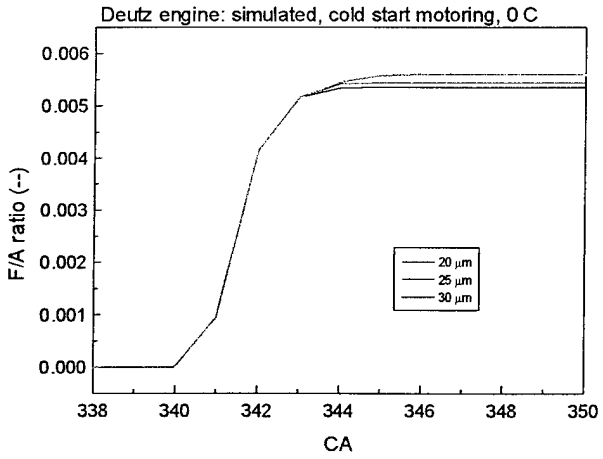

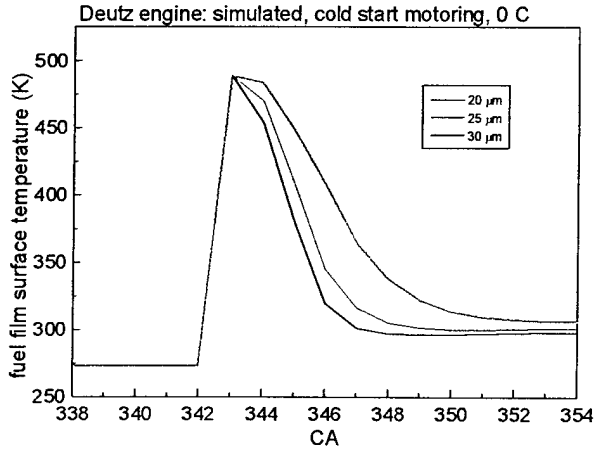

Figure 12 Simulated effect of fuel film thickness on fuel film evaporation: fuel air ratio and fuel film surface temperature, Deutz engine, cold start motoring, 0 ^{0}C.

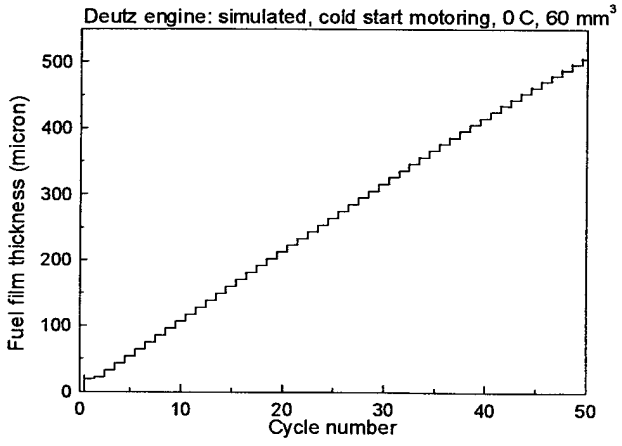

Figure 13 Simulated fuel film thickness, Deutz engine, 0 ^{0}C, 60 mm^{3}.

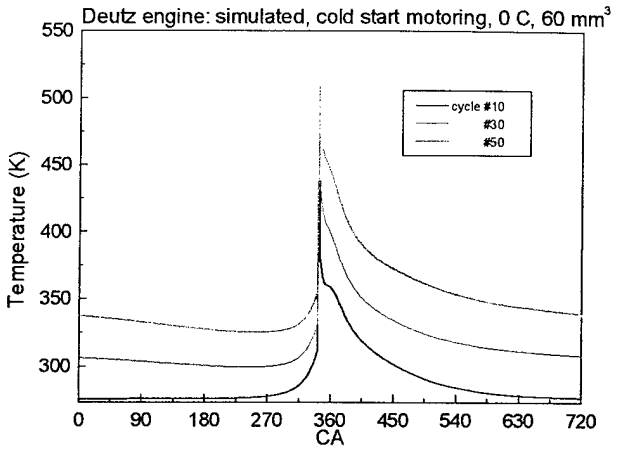

Figure 14 Simulated fuel film surface temperature, Deutz engine, 0 ^{0}C, 60 mm^{3}.

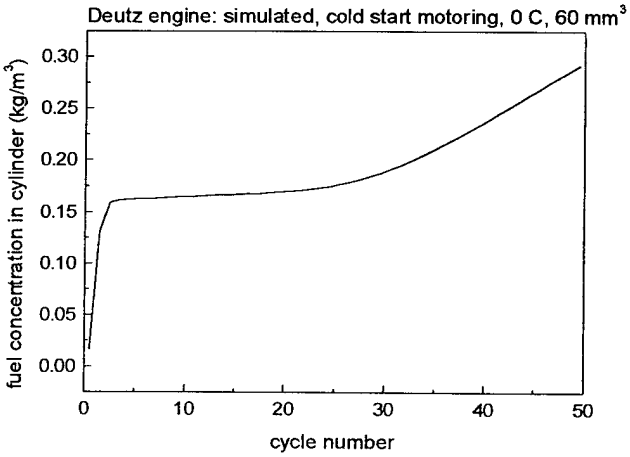

Figure 15 Simulated average fuel vapor concentration far away from fuel film surface during ignition delay period, Deutz engine, cold start motoring, 0 ^{0}C, 60 mm^{3}.

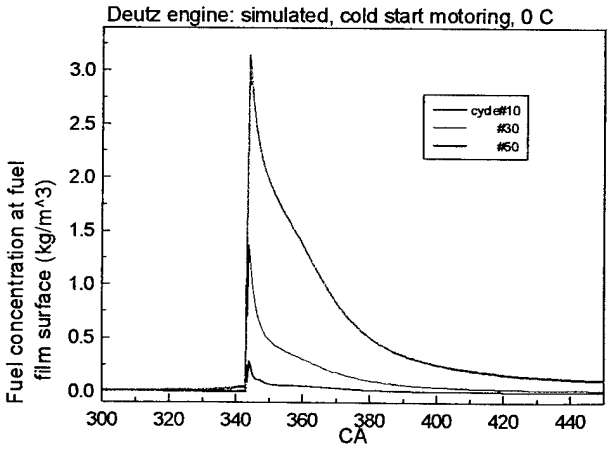

Figure 16 Simulated fuel concentration at fuel film surface, Deutz engine, cold start motoring, 0 ^{0}C, 60 mm^{3}.

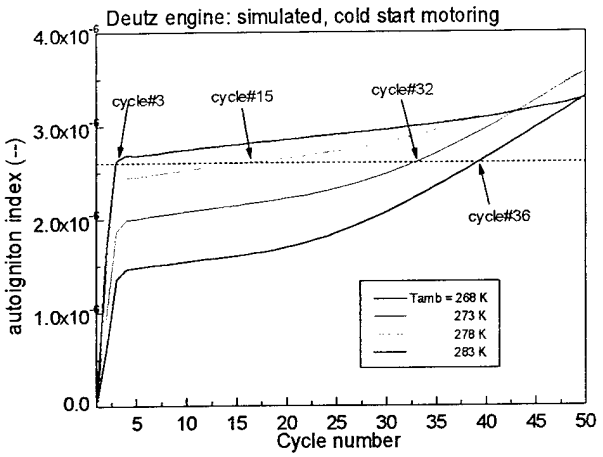

Figure 17 Simulated engine autoignition index at different ambient temperature, Deutz engine, cold start motoring.

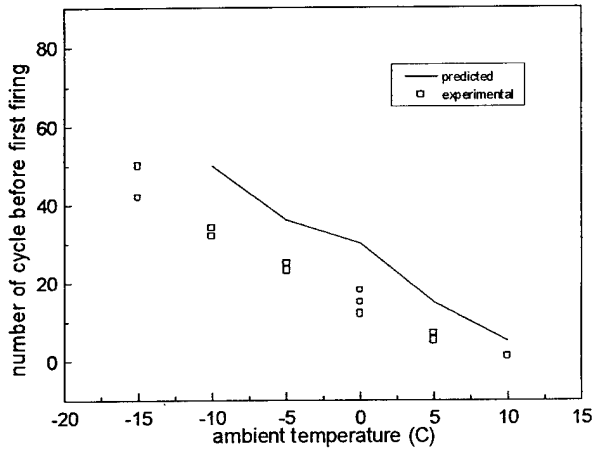

Figure 18 Comparison between predicted and experimental data of number of cranking cycle before first firing. Deutz engine.

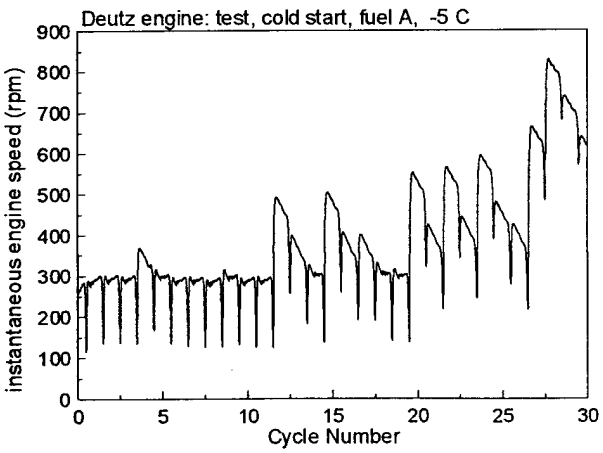

Figure 19 Experimental instantaneous engine speed cycle#1 to 30, Deutz engine, cold start, fuel A, -5 ^{0}C.

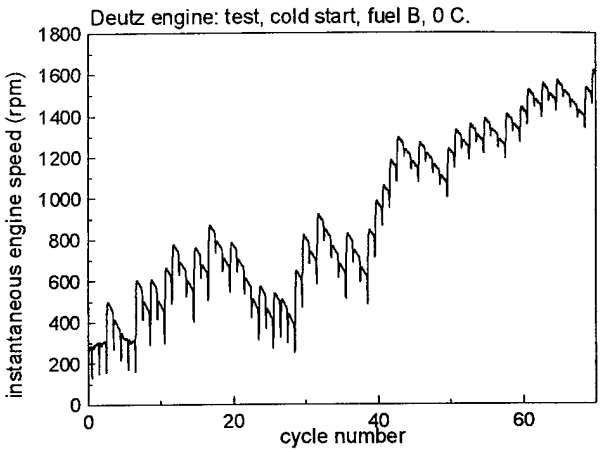

Figure 20 Experimental instantaneous engine speed cycle#1 to 70, Deutz engine, cold start, fuel B, 0 ^{0}C.

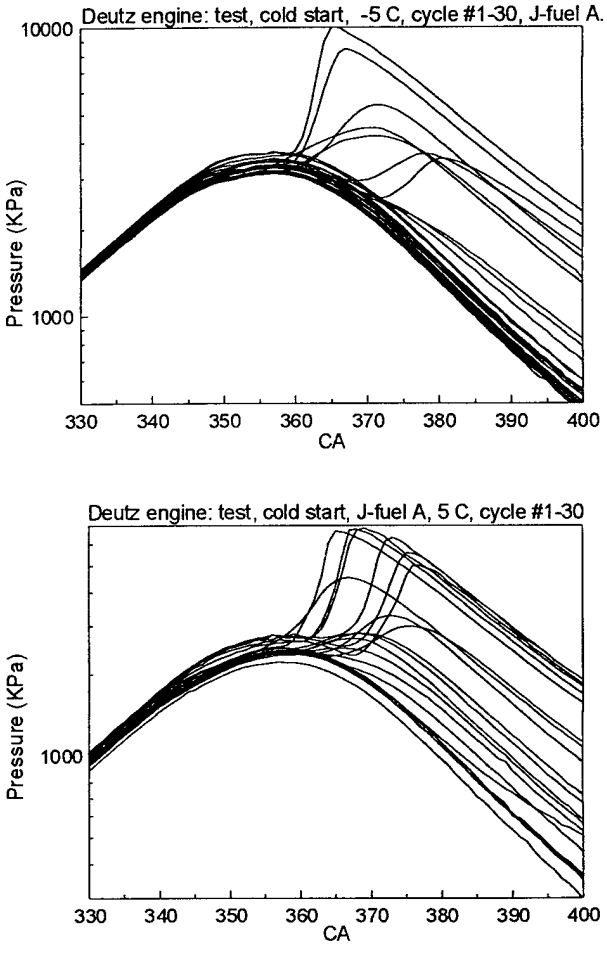

Figure 21 Experimental engine cylinder pressure in first 30 cycles, Deutz engine, cold start at –5 and 5 ^{0}C, fuel A.

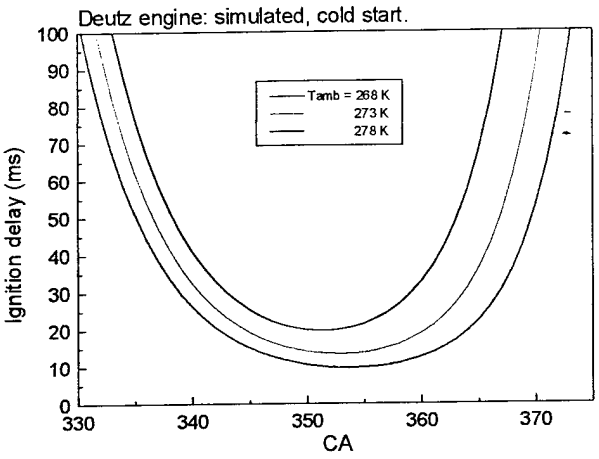

Figure 22 Ignition delay calculated at instanteous pressure and temperature, –5, 0 and 5 ^{0}C, Deutz engine, cold start motoring.

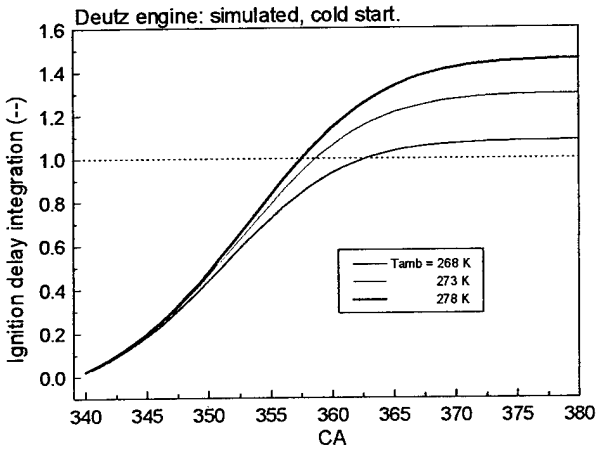

Figure 23 Simulated ignition delay integration at –5, 0 and 5 ^{0}C, Deutz engine cold start motoring.

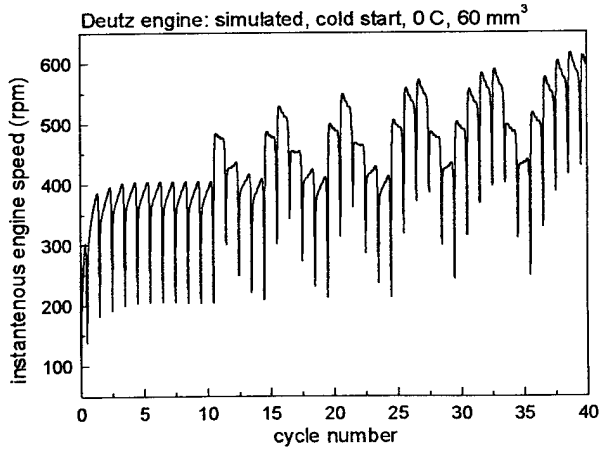

Figure 24 Simulated instantaneous engine speed during engine cold start, Deutz engine, cold start, 0 ^{0}C, 60 mm^3 fuel injected.

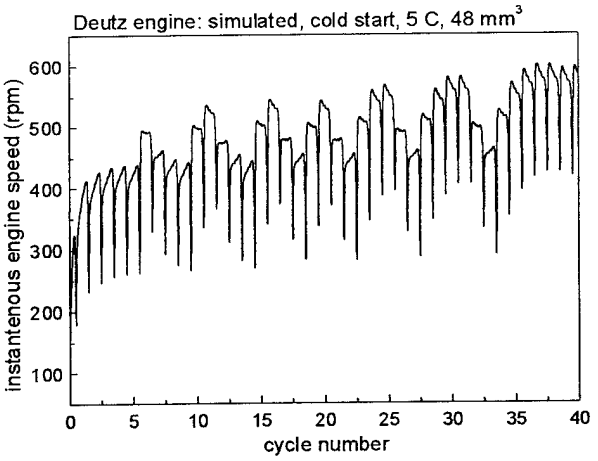

Figure 25 Simulated instantaneous engine speed during engine cold start, Deutz engine, cold start, 5^{0}C, 48 mm^3 fuel injected.

NOMENCLATURE

A	area, m^2
C_d	discharge coefficient, --
C_L	heat capacity of liquid fuel, J/kg·K
C_{ls}	concentration of fuel vapor at fuel film surface, kg/m^3
C_∞	concentration of fuel vapor at distance, kg/m^3
D_{ij}	diffusivity of fuel in air, m^2/s
D_j	fuel droplet diameter, m
E	activation energy, kJ/kg
h_c	heat transfer coefficient, $w/m^2 \cdot K$
h_m	mass transfer coefficient, m/s
ID	ignition delay, ms
K	thermal conductivity, w/m·K
Le	Lewis number, --
m_{drop}	mass of a fuel droplet, kg
m_f	mass of fuel injected, kg
Nu	Nusselt number, --
P	pressure, or total pressure, kPa
P_{fs}	partial pressure at droplet surface, kPa
P_v	fuel vapor pressure, kPa
Pr	Prandtl number, --
Q_c	convective heat transfer, J/m^2
R	gas constant, kJ/kg·K
rpm	revolutions per minute
S	spray penetration, m
Sc	Schmidt number, --
Sh	Sherwood number, --
SMD	Sauter Mean Diameter, micron
T_{fs}	temperature at fuel surface, K
T_g	cylinder gas temperature, K
T_l	temperature of liquid fuel, K
TDC	top dead center, --
V_f	fuel injected per cycle, mm^3
W_a	molecular weight of air, g/mol
W_f	molecular weight of fuel, g/mol
α	thermal diffusivity, m^2/s
ρ_a	density of gas, kg/m^3
ρ_f	density of fuel, kg/m^3
Δh_{ev}	latent heat of fuel, J/kg
ΔP	pressure difference cross the fuel injector nozzle, kPa

REFERENCE

[1] Liu, Z. and Karim, G. A., "An examination of the role of residual gases in the combustion processes of motored engines fuelled with gaseous fuels", SAE Paper 961087, 1996.

[2] Kwon, S. and Aral, M., "Ignition delay of a diesel spray injected into a residual gas mixtures", SAE Paper 911841, 1991.

[3] Hardenberg, H. O. and Hase, F. W., "An Empirical Formula for Computing the Pressure Rise Delay of a Fuel From its Cetane Number and from Relevant Parameters of Direct-Injection Diesel Engines", SAE Paper 790493, 1979.

[4] Clerc, J. C., "Cetane number requirements of light-duty diesel engines at low temperatures", SAE Paper 861525, 1986.

[5] Hara, H., Itoh, Y., Henein, N. A. and Bryzik, W., "effect of cetane number with and without additive on cold startability and white smoke emissions in a diesel engine", SAE Paper 1999-01-1476, 1999.

[6] Austen, W. and Lyn, W. T., "Some investigations on cold starting phenomena in diesel engines", SAE Paper no. 5, 1959-60.

[7] Phatak, R. E. and Nakamura, T., " Cold startability of open-chamber direct-injection diesel engines – part I Measurement technique and effects of compression ratio", SAE Paper 831335, 1983.

[8] Osuka, I. and Nishimura, M., "Benefits of new fuel injection system technology on cold startability of diesel engines – improvement of cold startability and white smoke reduction by means of multi injection with common rail fuel system (ECD-U2)", SAE Paper 940586, 1994.

[9] Tsunemoto, H., Yamada, T. and Ishitani, H., "Behavior of adhering fuel on cold combustion chamber wall in direct injection diesel engines", SAE Paper 861235, 1986.

[10] Biddulph, T. W. Lyn, W. T., "Unaided starting of diesel engines", Proc. Inst. Mech. Engrs. , Vol. 181, 1966-67.

[11] Gardner, T. P., "Optimization of compression ratio in compression ignition engines", Ph.D. dissertation, 1986.

[12] Liu, Hengqing, Chalhoub, N. and Henein, N. A., "Simulation of a single cylinder diesel engine under cold start conditions using Simulink", Advanced Engine Simulations vol. 1, ICE-Vol. 28-1, 1997.

[13] Borman, G. L. and Johnson, J. H., "Unsteady vaporization histories and trajectories of fuel drops injected into swirling air", SAE Paper 598C, 1962.

[14] Tanasawa, Y. and Hiroyasu, H., "On the drop size analyzer for liquid spray by sedimentation", Tech. Rep. Of Tohoku University, 27-1, 1962, 67.

[15] Hiroyasu, H. and Kadota, T., "Fuel droplet size distribution in diesel combustion chamber", SAE Paper 740715, 1974.

[16] Gupta, S., Poola, R. and Sekar, R., "Effect of injection parameters on diesel spray characteristics", SAE Paper 2000-01-1600, 2000.

[17] Incropera, F. P. and Dewett, D. P., "Fundamentals of heat and mass transfer", 3rd edition, 1990, pp356.

[18] Reid and Sherwood, "The properties of gases and liquids", 2nd edition, 1966.

[19] Henein, N. A., "Performance of diesel injection systems with alternative fuels Part 1: physical properties", Technical Report, 1987.

[20] Petris, C. D., Giglio, V. and Police, G., " A mathematical model of the evaporation of the oil film deposed on the cylinder surface of IC engines", SAE paper 972920, 1997.

[21] Stanton, D. W., Rutland, C., J., "Multi-dimensional modeling of heat and mass transfer of fuel films resulting from impinging sprays", SAE Paper 980132, 1998.

[22] Zahdeh, A. R., Henein, N. A. and Bryzik, W., "Diesel cold starting: actual cycle analysis under border-line conditions", SAE Paper 900441, 1990.

[23] Henein, N. A. and Bryzik, W., " Diesel engine cold starting: combustion instability", SAE Paper 920005, 1992.

[24] Bryzik, W. and Henein, N. A., "Fundamental cold start phenomena within advanced military diesel engines", Army Science conference proceedings, vol. III, 1994.

[25] Meyer, W. E. and Decarolis, J. J., "Compression Temperatures in Diesel Engines under Starting Conditionsn, SAE Trans., 1962, pp.163-174.

[26] Henein, N. A. "Starting of diesel engines: Uncontrolled fuel injection problems", SAE Paper 860253, 1986.

[27] Han, Zhiping, Henein, N. A. and Bryzik, W., "A New Ignition Delay Correlation with Predictions of Diesel Engine Cold Start Misfiring" SAE Paper, 2000-01-1184, 2000.

[28] Igura, S., Kadota, T., and Hirozasu, H., "Spontaneous Ignition Delay of Fuel Sprays in High Pressure Gaseous Environment," Jap. Soc. Mech. Engrs., Vol. 41, No. 345, p.1559, 1975.

APPENDIX C

2002-01-1153

Effect of EGR on Autoignition, Combustion, Regulated Emissions and Aldehydes in DI Diesel Engines

Bogdan Nitu, Inderpal Singh, Lurun Zhong, Kamal Badreshany, Naeim A. Henein
Wayne State University
and
Walter Bryzik
TARDEC

Abstract

In view of the new regulations for diesel engine emissions, EGR is used to reduce the NOx emissions. Diluting the charge with EGR affects the autoignition, combustion as well as the regulated and unregulated emissions of diesel engines, under different operating conditions. This paper presents the results of an investigation on the effect of EGR on the global activation energy and order of the autoignition reactions, premixed and mixing-controlled combustion fractions, the regulated (unburned hydrocarbons, NOx, CO and particulates), aldehydes, CO_2 and HC speciation. The experiments were conducted on two different direct injection, four-stroke-cycle, single-cylinder diesel engines over a wide range of operating conditions and EGR ratios.

Introduction

EGR is widely used in many types of combustion systems to reduce nitrogen oxides (NOx) emissions. Its main effect is to reduce the oxygen concentration in the charge and the temperature of the combustion products. In diesel engines, EGR affects the autoignition and combustion processes and other engine-out emissions [1-21]. This paper investigates the effects of EGR on the autoignition and combustion processes, cool flame, and the engine-out emissions of (CO), aldehydes (RCHO), acetone (CH3COCH3) and particulate matter (PM).

Experimental Setup

Two single-cylinder, direct-injection, four-stroke-cycle, diesel engines were used in this investigation. Engines' specifications are given in Appendix A. Both engines were instrumented to measure the needle lift and cylinder gas pressure using flush-mounted, water-cooled piezo-quartz pressure transducers. Since engine emissions are affected by fuel properties, it is important to note that AMOCO Premium diesel fuel was used in all the experiments. The fuel properties and its GC analysis are given in appendix B.

One engine was water-cooled and the tests simulated turbocharged diesel engines, with loads and speeds typical to the conditions in a hybrid diesel-electric medium size vehicle. The engine is equipped with an electronically controlled high-pressure common rail fuel injection system. The tests covered a wide range of fuel injection pressures and EGR ratios. The details of the engine and instrumentation are given in reference [9].

The second engine was naturally aspirated, air-cooled and ran under no load and different speeds. The engine is equipped with a pump-line-injector system. The details of the engine and instrumentation are given in reference [43].

The effect of the average charge temperature (during ignition delay) on the ID is plotted in Fig.5. At the same charge temperature, the rates of the physical processes are not affected by the presence of EGR. Accordingly, the increase in ID is mainly due to the drop in oxygen concentration at the higher EGR ratios.

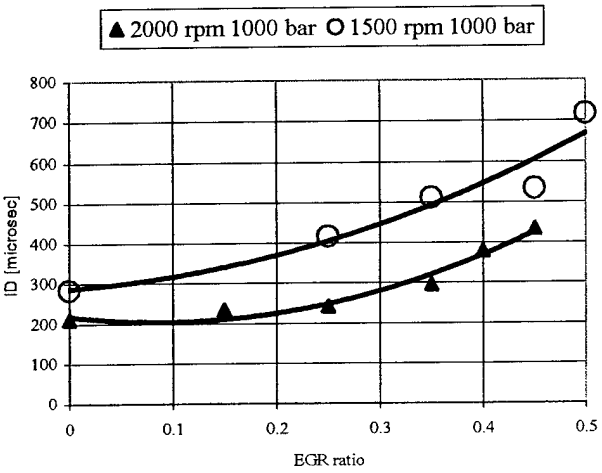

Figure 3. Effect of EGR on ID (Test conditions for Engine 1 are given in the appendix A)

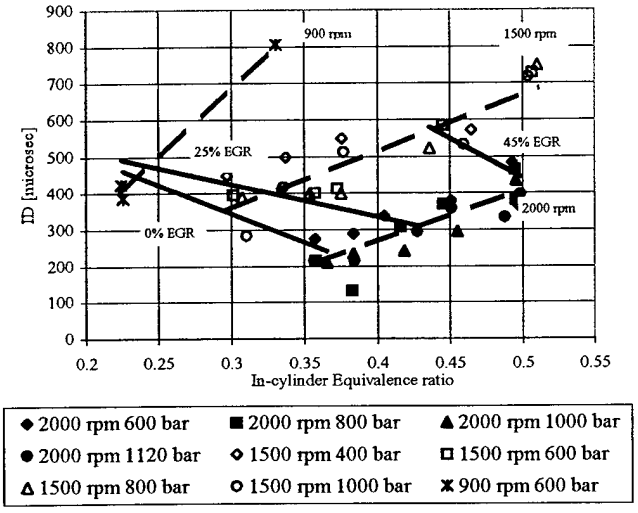

Constant EGR: continuous line; Constant Pressure: dotted line

Figure 4. Effect of in-cylinder equivalence ratio on ID, Engine 1

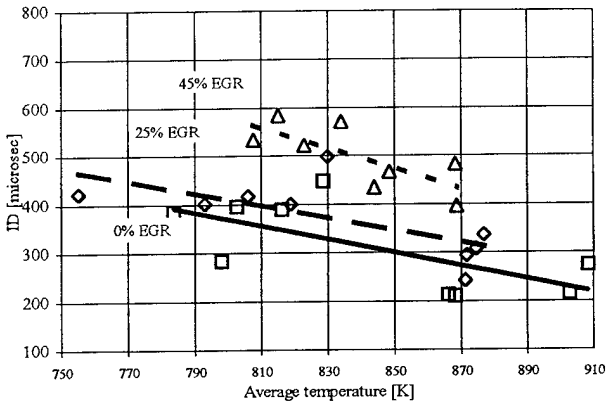

Figure 5 Influence of charge average temperature on ID, Engine 1

Effect of EGR concentration on the global rate of the autoignition reactions

The pre-ignition processes include the spray development and formation of droplets, heat and mass transfer between the gas phase and liquid phase and the formation of an auto-ignitable mixture, endothermic reactions leading to the formation of radicals at a critical concentrations in some parts of the spray, local exothermic reactions leading to the formation of auto-ignition nuclei and the start of flame propagation into the combustible charge in the spray. The details of these processes, in particular the chemical reactions, are not well understood. The auto-ignition reactions of some single compound light hydrocarbons appear in the literature. These reactions become more complicated and numerous as the number of carbon atoms in the molecule increases. The problem is much more difficult for distillate fuels that are composed of a large number of hydrocarbons of different molecular structure and number of carbon atoms. This justifies the use of the global approach for the auto-ignition reactions.

Since the inlet temperature and pressure are kept constant in all the runs, it is reasonable to consider that the physical processes are the same as explained earlier, and the autoignition reactions are the controlling process, at all EGR ratios.

The global chemical reaction rate between the fuel and air oxygen can be given by

$$r = A \exp[-E / (RT)] [F]^a [O_2]^b \qquad (1)$$

And the ID can be correlated to the oxygen concentration and temperature during ID, by

$$ID = k p^{-n} \exp [E / (RT)] \qquad (2)$$

The effect of EGR on the autoignition reactions can be determined, if we find its effect on E and n.

Effect of EGR on global activation energy E

EGR contains nitrogen oxides, aldehydes and other incomplete combustion products. Previous studies indicated that the addition of small amounts of NO in air significantly reduces the ignition temperature of hydrocarbon fuels [39]. Since the concentration of NO in the intake increases with EGR ratio, it is interesting to find out if increasing EGR has any effect on the mechanisms of autoignition, that would show in the variation in the activation energy E.
An extensive analysis was made to find out the change in E with EGR, using different variation functions and different reaction orders. It was finally concluded that EGR has a minor effect on E and amounted to an increase of only 2% at 65% EGR. Accordingly, the data for all the EGR ratios are used to determine the global activation energy.

A plot of the logarithm of the ID versus the reciprocal of the absolute average charge temperature during ID is given in Fig. 6.

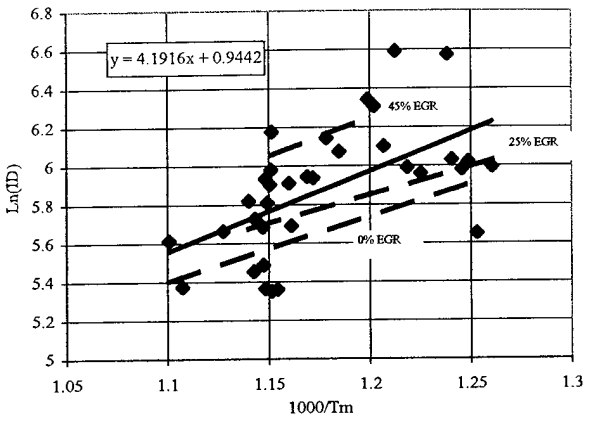

Figure 6. Ln ID versus the reciprocal of the absolute mean gas temperature (1/Tm) during ID.(Test conditions for Engine 1 are given in the appendix A)

The relationship is linear, and the equation of the best fitting line is

$$Y = 4191.6x + 0.9442 \qquad (3)$$

The slope of the line in Fig. (6) is the global activation energy divided by the universal gas constant R. The global activation energy is, therefore

E = 34,850 J.

Previous investigators developed correlations for ID, and reported different values for E. According to Ayoub and Reitz [4] E=618840/(CN+25). The CN for AMOCO Premium is 50,thus E = 34,515 J; according to Wolfer [41] E = 38,660 J; according to Sitkei [37] E = 32,653 J; according to Henein and Bolt [10] E = 31188 J, according to Stringer [38] E=45502.522 J, according to Pederson [30] E = 42,812 J and according to Hiroyasu [12] E=60,525.

The differences in the values of E are due to the variety of test equipment; the methods used in determine the end of ID and the properties of the diesel fuel used in the investigations. The equipment used includes constant volume vessels, and different engine designs. The methods used to detect the end of ID include the pressure trace, heat

release calculations and the luminosity of the flame. The fuels used include diesel fuels of different distillation ranges, cetane numbers. Some investigators used a blend of primary reference fuels. Han [9], in a recent study in our laboratories, conducted experiments on a heavy-duty diesel engine using DF-2 and reported E = 38,785 J. This is slightly higher than the value of E of the current study in which AMOCO Premium was used.

Effect of EGR on the order of the global reactions

The global order of the autoignition reactions obtained from the slope of the best straight line in the plot of ln (ID) versus ln $[O_2]$ is n = 1.97. The values for n given in the literature are: Wolfer n=1.19; Sitkei n=1.8; Stringer n=1; Hiroyasu n=1.23 and Han n=1.899..

Effect of EGR on cool flames

Cool flames can be detected from the cylinder gas pressure, or the apparent rate of energy (heat) release traces.

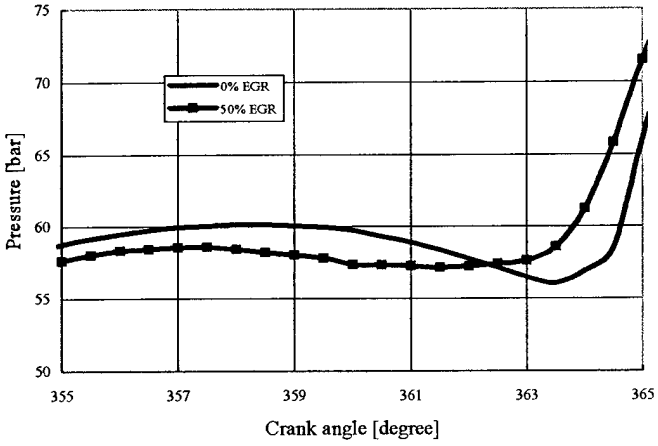

Figure 7. Pressure traces for 0 and 50% EGR (rpm: 1500, inj. pressure: 800 bar)

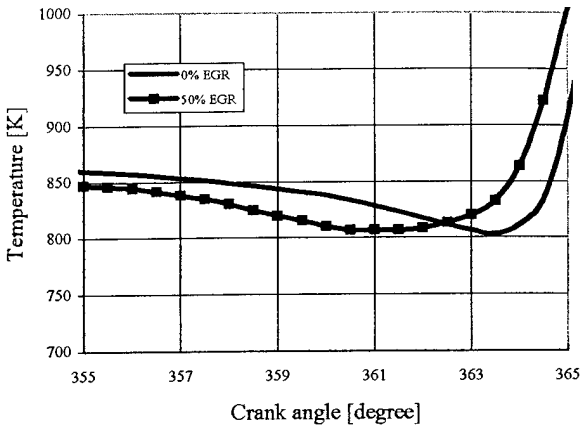

Figure 8. Cylinder gas temperature for 0% and 50 % EGR. (rpm: 1500, inj. pressure: 800 bar).

Figure (7) shows that for 0% EGR, the cylinder gas pressure dropped by 4 bar due to fuel evaporation, endothermic reactions, heat transfer to the walls and piston motion. The corresponding drop for 50% EGR is 1.5 bar. Similarly, Fig. 8 shows that the drop in cylinder gas temperature amounted to 60°C and 45°C for 0% and 50% EGR respectively

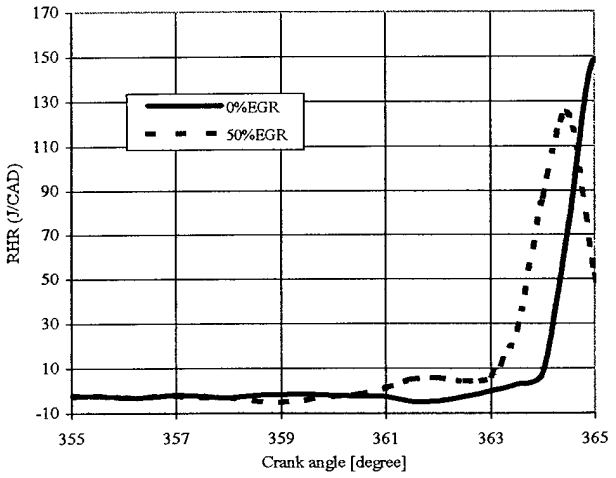

Figure 9. Apparent rate of energy release for 0% and 50% EGR (rpm: 1500, inj. pressure: 800 bar).

The difference in the energy released in the two cases is clear in Fig. 9. For 0% EGR no energy

was released before the start of the main combustion event. For 50% EGR, the energy released due to cool flames reached 11J / CAD.

Effect of EGR on combustion

In diesel engines, combustion is considered to take place in two modes: premixed combustion and mixing-controlled combustion. The two fractions, determined from the apparent energy (heat) release rate, are plotted at different EGR ratios in Fig. (10). The increase in the premixed combustion fraction with EGR is caused, mainly, by the increase in the ID. As explained earlier, dilution of the fresh charge with EGR reduces the oxygen concentration and rate of the auto-ignition reactions. The longer ID periods allow more fuel to be evaporated and mixed with the air and burn in a premixed mode.

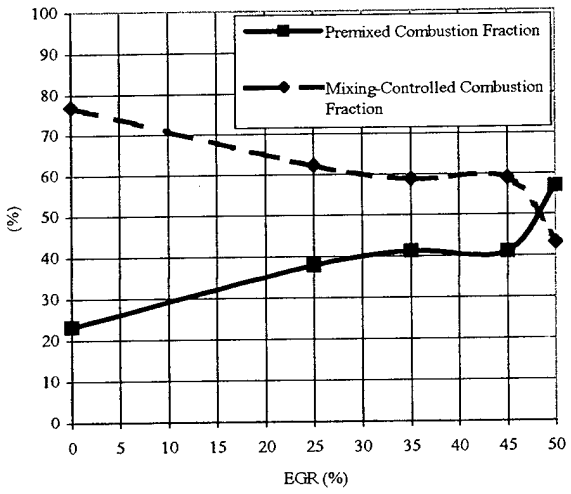

Figure 10. Effect of EGR on the premixed and mixing-controlled combustion fractions.(Engine 1, rpm: 1500, inj. pressure: 400 bar)

Effect of EGR on engine-out emissions

Effect on regulated incomplete combustion products

The effect of EGR on unburned hydrocarbons, carbon monoxide and soot are shown in figures (11 to 13). It is clear that the reduction in the oxygen concentration is the main cause of the increase in all the incomplete combustion products.

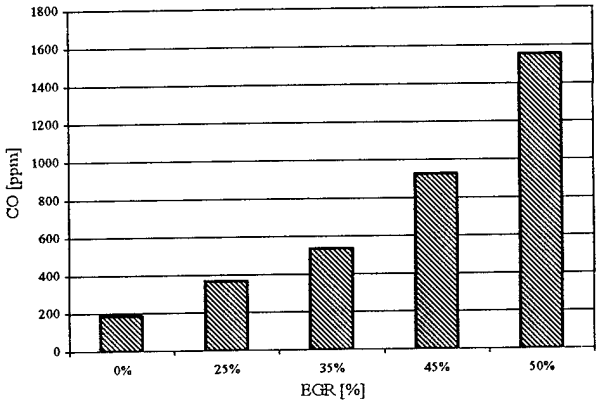

Fig. 11. Effect of EGR on carbon monoxide. (Engine 1, 1500 rpm, 800 bar inj. pressure).

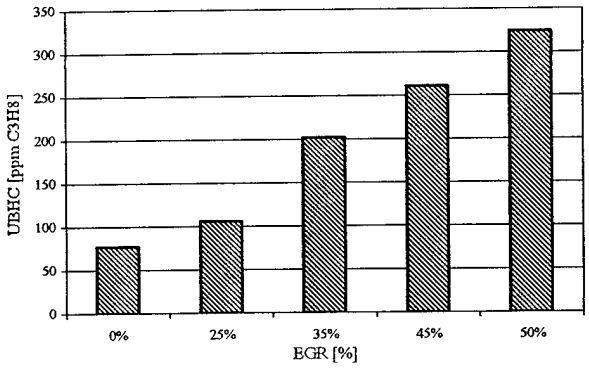

Figure 12. Effect of EGR on unburned hydrocarbons (Engine 1, rpm: 1500, inj. pressure: 800 bar).

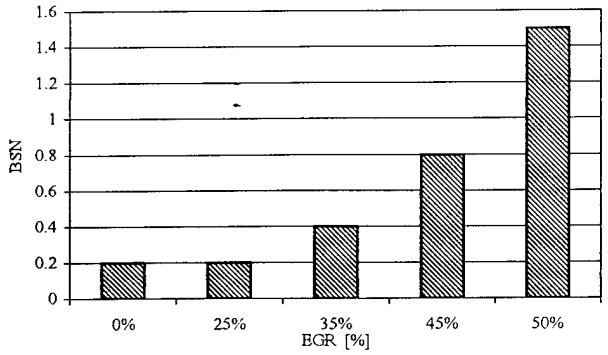

Figure 13. Effect of EGR on smoke emission (Engine 1, rpm: 1500, inj. pressure: 800 bar)

Effect of EGR on NO_x

Figure (14) shows that EGR has a strong impact on reducing NOx concentration. The drop in NO_x is linear at a sharp rate up to 40% EGR, and at a lower rate at higher EGR ratios. EGR reduces the oxygen concentration in the charge and reduces the temperature of the combustion products.

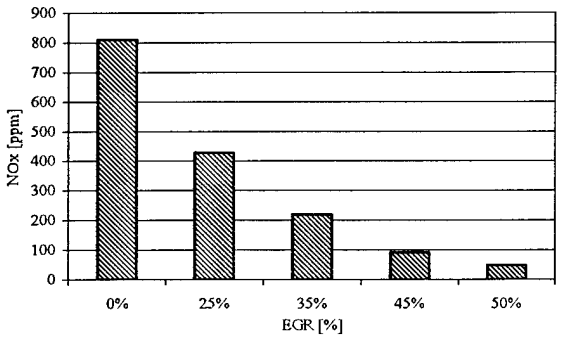

Figure 14. Effect of EGR on NO_x emissions (Engine 1, rpm: 1500, inj. pressure: 800 bar)

Effect of EGR on aldehydes

High Pressure Liquid Chromatography is used in measuring the exhaust aldehyde emissions.
Figure (15) shows a sample of the traces for different aldehydes at 0% EGR and 45% EGR ratios. In both cases, formaldehyde (HCHO) has the highest concentration; followed by acetaldehyde (CH3CHO). Acetone (CH3COCH3), acrolein (C3H4O) and propionaldehyde (CH3CH2CHO) have much lower concentrations.

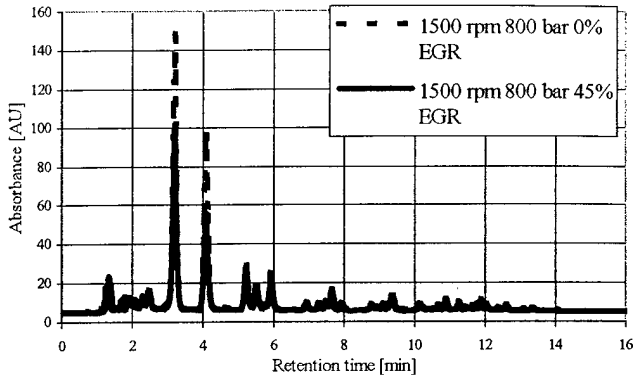

Figure 15. Comparison between the aldehyde HPLC traces with 0% and 45% EGR.(Engine 1, rpm: 1500, inj. pressure: 800 bar)

Figure (16) shows that all the aldehydes dropped as EGR increased up to 25%, but a further increase increases the concentrations, although the values remain lower than those for 0% EGR.

Aldehydes are known to be the result of low temperature partial oxidation reactions. These occur in the spray regions where the mixture is too lean or too rich and where combustion temperatures are relatively lower than in other areas of the spray. With EGR, these zones expand and cause an increase in aldehydes. This explains the rise in aldehydes with EGR above 25%.

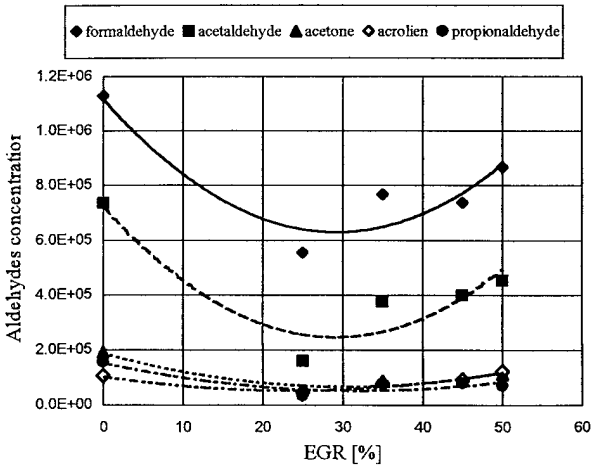

Figure 16. Effect of EGR on the aldehyde emissions (Engine 1, rpm: 1500, inj. pressure: 800 bar).

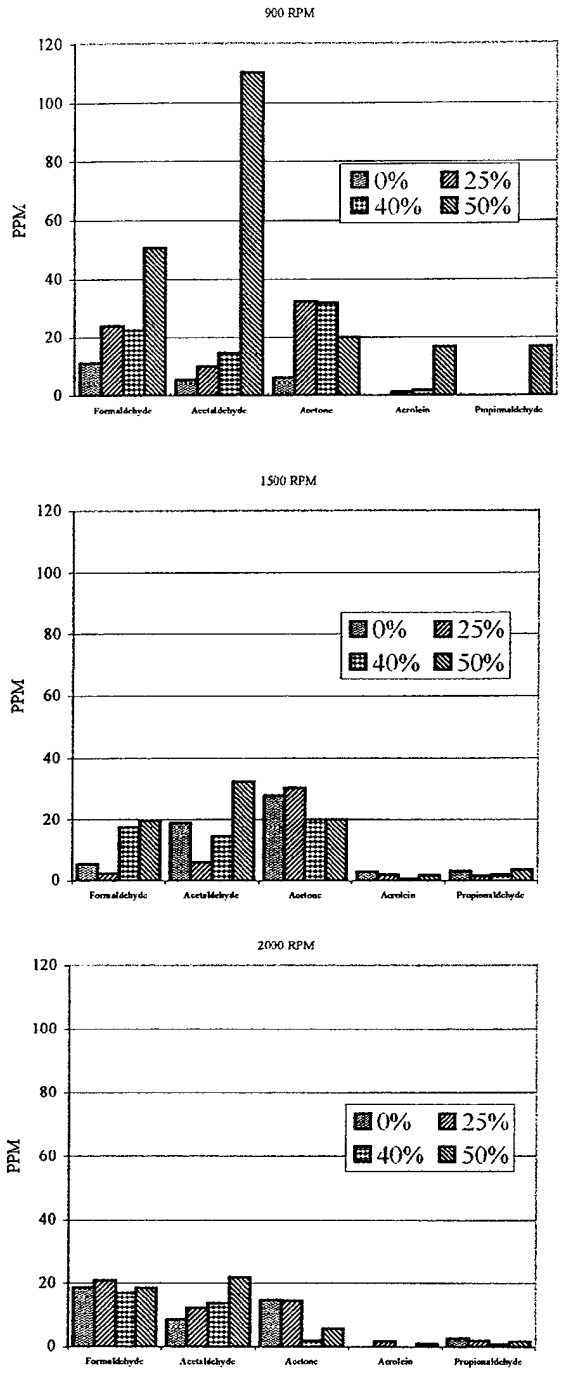

Figure 17. Effect of EGR (idling at various speeds) on aldehydes – Engine 2

It can be clearly seen that the acetone concentration decreases with the increase in EGR.

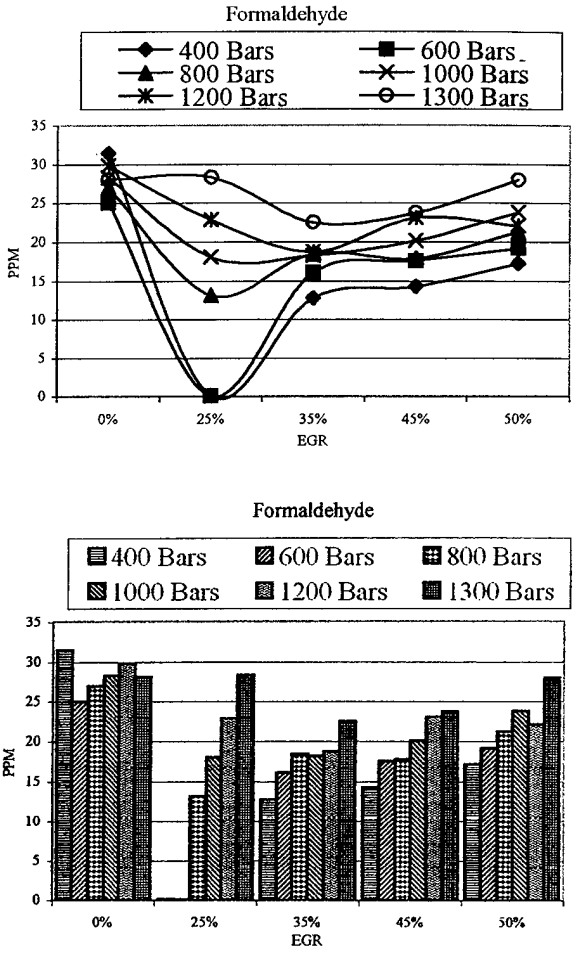

Figure 18. Effect of EGR on formaldehyde – (Engine 1, rpm: 1500, inj. pressure: 800 bar)

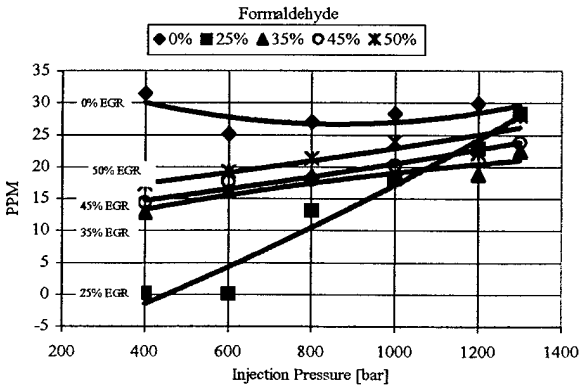

Figure 19. Effect of injection pressure on formaldehyde – (Engine 1, rpm: 1500, inj. pressure: 800 bar)

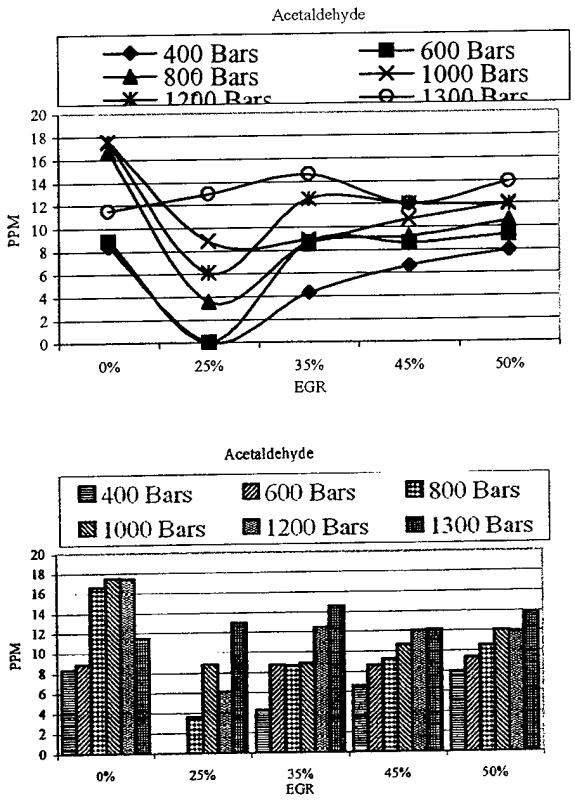

Figure 20. Effect of EGR on acetaldehyde – (Engine 1, rpm: 1500, inj. pressure: 800 bar)

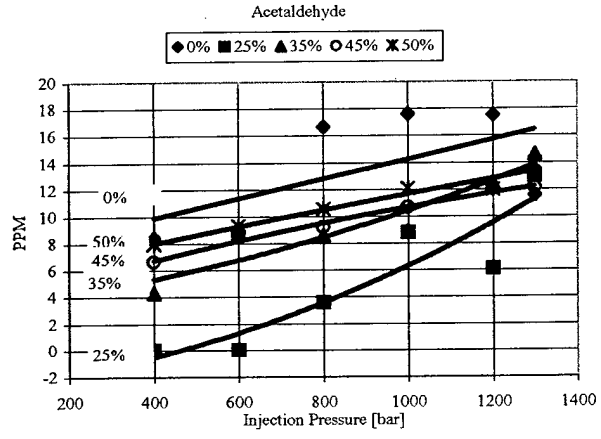

Figure 21. Effect of injection pressure on acetaldehyde – (Engine 1, rpm: 1500, inj. pressure: 800 bar)

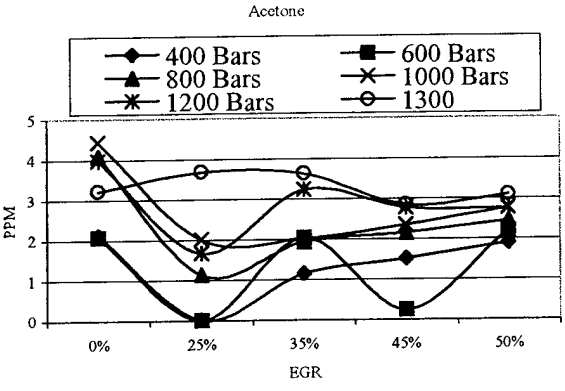

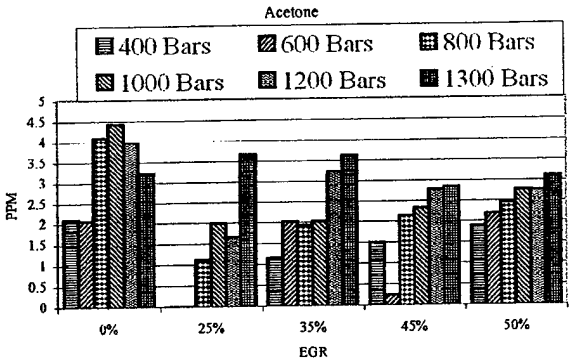

Figure 22. Effect of EGR on acetone – (Engine 1, rpm: 1500, inj. pressure: 800 bar)

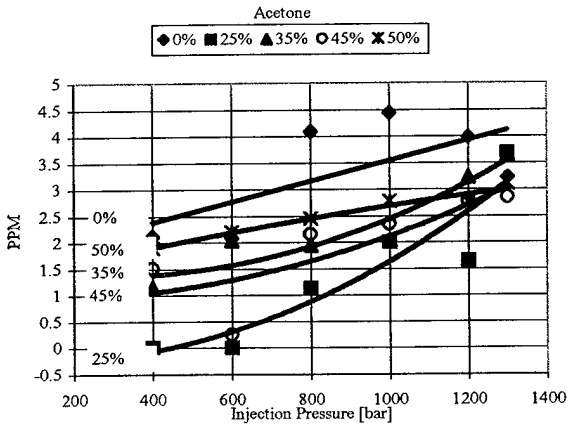

Figure 23. Effect of injection pressure on acetone – (Engine 1, rpm: 1500, inj. pressure: 800 bar)

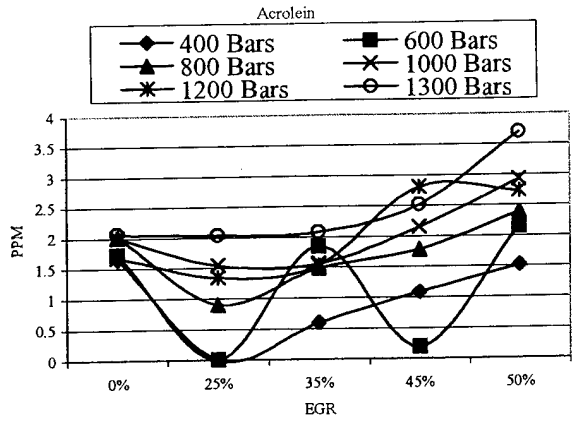

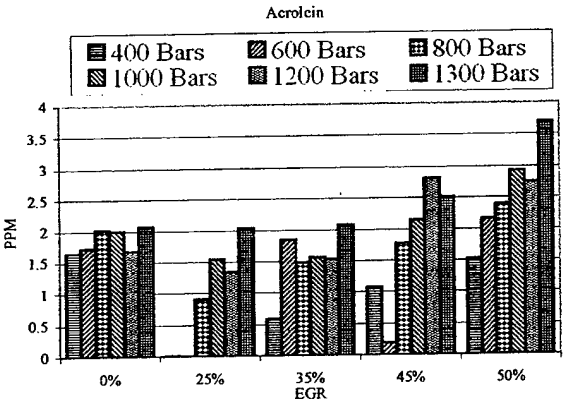

Figure 24. Effect of EGR on acrolein – (Engine 1, rpm: 1500, inj. pressure: 800 bar)

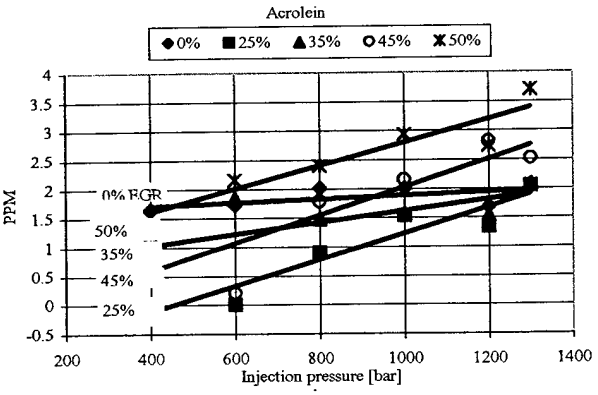

Figure 25. Effect of injection pressure on acrolein – (Engine 1, rpm: 1500, inj. pressure: 800 bar)

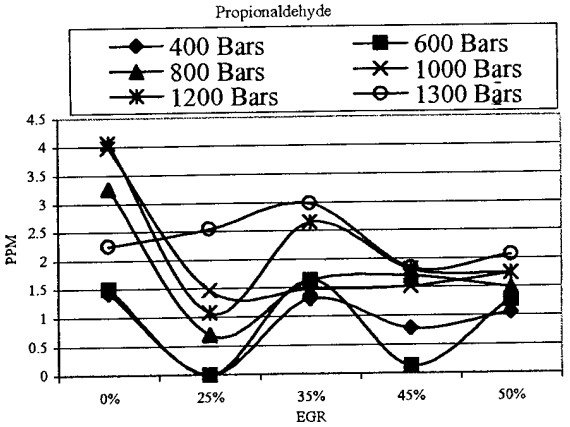

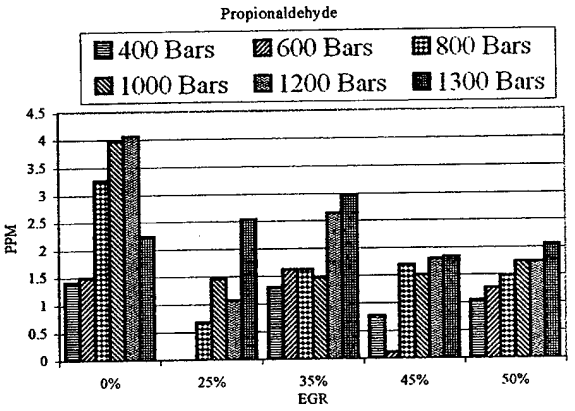

Figure 26. Effect of EGR on propionaldehyde – (Engine 1, rpm: 1500, inj. pressure: 800 bar)

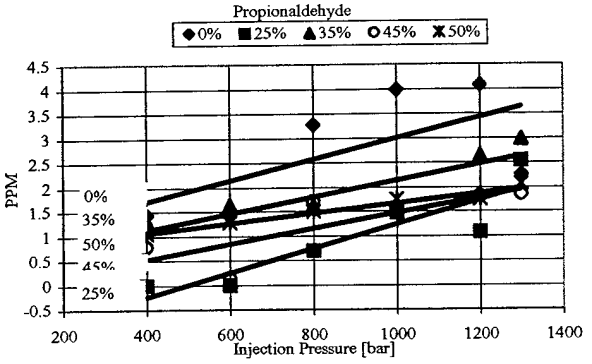

Figure 27. Effect of injection pressure on propionaldehyde – (Engine 1, rpm: 1500, inj. pressure: 800 bar)

Effect of EGR on hydrocarbons speciation

Speciation of unburned hydrocarbon exhaust emissions is of interest in the study of the sources of diesel order (Roy 2000). Most of the hydrocarbon species in diesel exhaust has been found to have up to 12 or 13 carbon atoms (Otsuki 1995, Clark 1996). Speciation covered hydrocarbons from C_6 to C_{18}. The chromatogram traces in figures (28 and 29) indicate that their concentrations reached higher peaks as EGR ratios increased. This agrees with the data in Fig 12, which indicates that the concentration of the total hydrocarbons increases at higher EGR ratios.

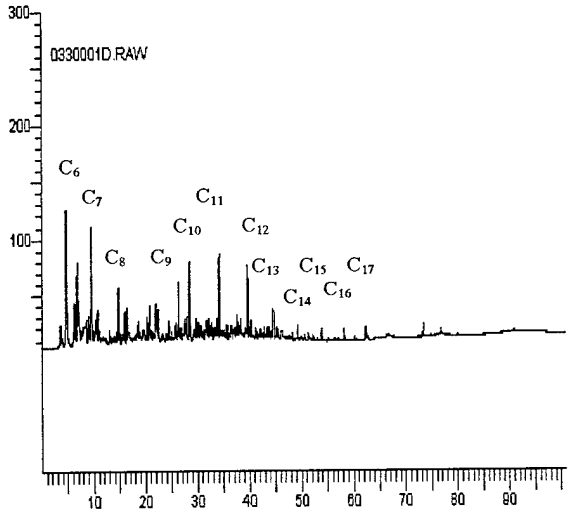

Figure 28. Gas chromatogram for unburned hydrocarbons with 0% EGR.(Engine 1, rpm: 1500, inj. pressure: 800 bar)

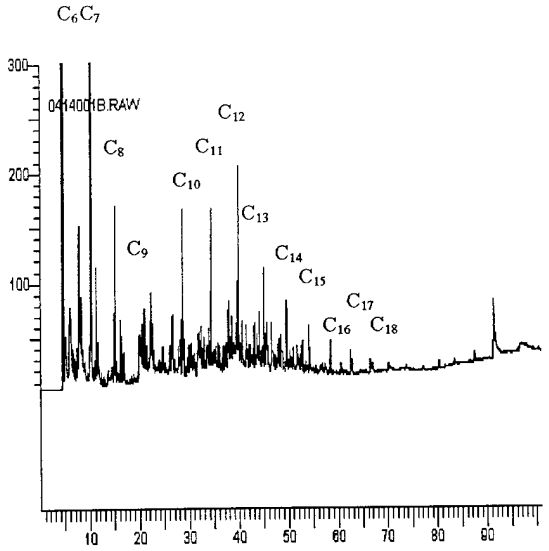

Figure 29. Gas chromatogram for unburned hydrocarbons with 50% EGR.(Engine 1, rpm: 1500, inj. pressure: 800 bar)

Conclusions

The following conclusions are based on an experimental investigation on two single cylinder; four-stroke-cycle, direct-injection research diesel engines. One engine is water cooled, has a common rail electronically controlled fuel injection system. The engine ran under simulated warmed up turbocharged conditions. The injection timing was adjusted to keep the peak pressure location at 6°-7° after TDC. The second engine was naturally aspirated, air cooled, and has a conventional pump-line-injector fuel system. The fuel used in both engines is AMOCO premium diesel fuel.

1. EGR reduces the rates of the autoignition reactions, as indicated by the increase in ignition delay period. EGR was found to have no effect on the activation energy and the order of the global autoignition reactions. Its main effect is to reduce oxygen concentration.
2. Cool flames are observed and their intensity increased at higher EGR ratios.

3. The premixed combustion fraction increased with EGR, because of the larger amount of fuel injected during the longer ignition delay period.

4. While EGR was very effective in reducing NO_x, it increased all the incomplete combustion products, such as unburned hydrocarbons, carbon monoxide, and soot.

5. The main aldehydes emitted in the exhaust were in the form of formaldehyde and acetaldehyde. Acetone, acrolein and propionaldehyde had much lower concentrations. The general trend for the aldehydes under the loaded conditions is to decrease in concentration with the addition of EGR and reached a minimum at about 25%.

6. Hydrocarbon's speciation traces showed an increase in all the species with EGR.

Acknowledgement

The U S Department of Energy, Office of Transportation Technologies, Office of Advanced Automotive Technologies, support this program. This is a part of the PNGV program, conducted under the technical sponsorship of Sandia National Laboratories. The continuous technical support and help of Dr. Paul Miles, in running this program and supplying engine parts and instruments is gratefully acknowledged and appreciated.

Also, the support of the U.S. Army TARDEC, NAC, ARO and ARC is acknowledged. The cooperation and help of Lydia Nedeltcheva, other members of the Center for Automotive Research and the machine shop at Wayne State University is appreciated.

List of abbreviations

ATDC – After Top Dead Center
BTDC – Before Top Dead Center
CAD – Crank angle degree
E – Activation Energy
EGR – Exhaust Gas Re-circulation
F – Fuel
GC – Gas Chromatograph
ID – Ignition Delay
inj. - injection
R – Universal Gas Constant
T – Temperature
TDC – Top Dead Center
Tm – Average charge temperature during ID

References:

1. Al-Rubale, M.A.R., Griffiths, J.F., Sheppard, C.G.W. – Some Observation on the Effectiveness of Additives for Reducing the Ignition Delay Period of Diesel Engines – SAE 912333, 1991
2. Arcoumanis, C., Bae, C., Nagwaney, A., Whitelaw, J.H., - Effect of EGR on combustion in a 1.9L DI Diesel optical engine- SAE 950850, 1995
3. Arcoumanis, C., Nagwaney, A., Hentschel, W., Ropke, S., - Effect of EGR on spray development, combustion and emissions in a 1.9L direct-injection Diesel engine – SAE 952356, 1995
4. Ayoub, N.S., Reitz, R.D. – Multidimesional Modeling of Fuel Composition Effects on Combustion and Cold-Starting in Diesel Engines – SAE 952425, 1995
5. Clark, N. N., Atkinson, C. M., McKain, D. L., Nine, R. D., El-Gazzar L. – Speciation of Hydrocarbon Emissions from a Medium Duty Diesel Engine - SAE 960322, 1996
6. Desantes, J. M., Arregle, J., Molina, S.A., Lejeune, M. - Influence of the EGR rate, oxygen concentration and equivalent fuel/air ratio on the combustion behavior and pollutant emissions of a heavy-duty Diesel engine - SAE 2000-01-1813, 2000

7. Gautam, M., Kelly, B., Gupta, D., Clark, N., Atkinson, R., El-Gazzar, L., Lyons, D.W. – Sampling Strategies for Characterization of the Reactive Components of Heavy Duty Diesel Exhaust Emission – SAE 942262, 1994
8. Gerini, A. Montagne, X. – Automotive Direct Injection Diesel Engine Sensitivity to Diesel Fuel Characteristics – SAE 972963, 1997
9. Han, Z., Henein, N.A., Nitu, B., Bryzik, W. – Diesel Engine Cold Start Combustion Instability and Control Strategy – SAE 2001-01-1237, 2001
10. Henein, N.A. and Bolt, J.A. – Correlation of air charge temperature and ignition delay for several fuels in a Diesel engine – SAE 690262, 1969
11. Henein,N.A., Lai, M.C.,Singh, I.P. Wang D. and Liu, L. - Emissions Trade-Off and Combustion Characteristics of a High-Speed Direct Injection Diesel Engine – SAE 2001-01-0197
12. Hiroyasu, H. and Kadota, T. – Evaporation and spontaneous ignition delay of a fuel droplet and spray in high pressure gaseous environments – Report III-2, Department of Mechanical Engineering, Hiroshima University, Hiroshima, Japan, February (1977)
13. Hupperich, P., Dürnholz, M. - Exhaust Emissions of Diesel, Gasoline and Natural Gas Fuelled Vehicles - SAE 960857, 1996
14. Khalil, N., Levendis, Y.A., Abrams, R.F., - Reducing diesel particulate and NOx emissions via filtration and particle-free exhaust gas recirculation – SAE 950736, 1995
15. Kouremenos, D.A., Hountalas, D.T., Binder, K.B., Raab, A., Schnabel, M.H. – Using advanced injection timing and EGR to improve DI Diesel engine efficiency at acceptable NO and soot levels – SAE 2001-01-0199, 2001
16. Kouremenos, D.A., Hountalas, D.T., Binder, K.B. – The effect of EGR on performance and pollutant emissions of heavy-duty Diesel engines using constant and variable AFR – SAE 2001-01-0198, 2001
17. Kreso, A. M., Johnson, J. H., Gratz, L. D., Bagley, S. T., Leddy, D. G. - A study of the effects of EGR on heavy-duty Diesel engine emissions - SAE 981422, 1998
18. Ladommatos, N., Balian, R., Horrocks, R., Cooper, L. - The effect of Exhaust Gas Recirculation on Combustion and NOx Emissions in High-Speed Direct injection Diesel Engines - SAE 960840, 1996
19. Ladommatos, N., Abdelhalim, S.M., Zhao, H., Hu, Z. – The dilution, chemical and thermal effects of EGR on Diesel engine emissions-part 1: effect of reducing inlet charge oxygen – SAE 961165, 1996
20. Ladommatos, N., Abdelhalim, S.M., Zhao, H., Hu, Z. – The dilution, chemical and thermal effects of EGR on Diesel engine emissions-part 2: effect of carbon dioxide – SAE 961167, 1996
21. Lapuerta, M., Salavert, J.M., Domenech, C. –Modelling and experimental study about the effect of EGR on Diesel engine combustion and emissions – SAE 950216, 1995
22. Lenvendis, Y.A., Pavlatos, I., Abrams, R.F. –Control of Diesel soot, hydrocarbon and NOx emissions with a particulate trap and EGR – SAE 940460, 1994
23. Lundqvist, U., Smedler G., Stalhammar, P., - A comparison between different EGR systems for HS diesel Engines and their effect on performance, fuel consumption and emissions - SAE 2000-01-0226, 2000
24. Martin, B. Aakko, P., Beckman, D., Del Giacomo, N., Giavazzi, F. - Influence of Future Fuel Formulations on Diesel Engine Emissions-A Joint European Study - SAE 972966, 1996
25. Mitchell, D.L., Pinson, J.A., Litzinger, T.A. – The effects of simulated EGR via intake air dilution on combustion in a

optically accessible DI Diesel engine – SAE 932798, 1993
26. Murayama, T., Zheng, M., Chikahisa, T., Oh, Y-T., Fujiwara, Y., Tosaka, S., Yamashita, M., Yoshitake, H. - Simultaneous reductions of smoke and NOx from a DI Diesel engine with EGR and dimethyl carbonate – SAE 952518, 1995
27. Narusawa, K., Odaka, M., Koike, N., Tsukamoto, Y., Yoshida, K. – An EGR control method for heavy-duty Diesel engines under transient operations – SAE 900444, 1990
28. Ogawa, T., Araga, T., Okada, M., Fujimoto, Y. - Fuel effects on particulate emissions from D.I. engine-chemical analysis and characterization of Diesel fuel - SAE 952351, 1995
29. Otsuki, S., Oie, T., Ishida, K. - Hydrocarbons speciation of automotive emissions using high speed gas chromatography - SAE 950513, 1995
30. Pederson, P.S. and Quale, B. – A model for the physical part of the ignition delay in a Diesel engine – SAE 740716, 1974
31. Pierpont, D.A., Montgomery, D.T., Reitz, R.D. – Reducing particulate and NOx using multiple injections and EGR in a DI Diesel – SAE 950217, 1995
32. Roy, M. M., Tsunemoto, H., Ishitani, H., Akiyama, J., Minami, T., Noguchi, M. - Influence of aldehyde and hydrocarbon components in the exhaust on exhaust odor in DI Diesel engines SAE 2000-01-2820, 2000
33. Sato, Y., Noda, A., Sakamoto, T. - Effect of EGR on NOx and thermal efficiency improvement in a DI methanol engine for light duty vehicles – SAE 930758, 1993
34. Schulz, H., De Melo, G.B., Ousmanov, F. – Volatile Components of Diesel Engine Exhaust Gas – Combustion and Flame, 1999
35. Shiga, S., Ehara, H., Karasawa, T., Kurabayashi, T. – Effect of EGR on Diesel knock intensity and its mechanism – Combustion and flame 72, 1988
36. Shiozaki, T., Nakajima, H., Kudo, Y., Miyashita, A., Aoyagi, Y. The analysis of combustion flame under EGR conditions in a DI Diesel engine – SAE 960323, 1996
37. Sitkei, G. – On the ignition lag in Diesel engines – MTZ 24, No. 6 190-194, June (1963)
38. Stringer, et al. – Spontaneous ignition of hydrocarbon fuels in a flowing system – Paper presented to Symp. On Diesel Combustion held by Inst. Of Mechanical Engineers, London, April (1970).
39. Tan, Y, Fotache, C. G. and Law, C. K.," Effects of NO on the Ignition of Hydrogen and Hydrocarbons by Heated Counterflowing Air," Combustion and Flame, The Combustion Institute, 119:346-355 (1999)
40. Tsao, K.C., Meyers, P.S. and Uyehara, O.A. – Gas temperature during compression in motored and fired Diesel engines – Trans. SAE 70, 136-145 (1962)
41. Wolfer, H.H. – Ignition lag in the Diesel engine – VCI-Forschungscheft, No 392 (1938). Trans. By Royal Aircraft Establishment, Farnborough Library, No. 358, UDC No. 621-436047, August (1959)
42. Wong, Y.K., Karim, G.A. – An analytical examination of the effects of EGR on the compression ignition process of engines fuelled with gaseous fuels – SAE 961936, 1996
43. Yassine, M.K., Tagomori,M. K., Henein, N. A. and Bryzik, W,"White Smoke Emissions under Cold Starting of Diesel Engines," SAE 960249, SP 1161, pp89-109, 1996.
44. Yokota, H. - A New concept for Low Emission Diesel Combustion - SAE 981933, 1998

Appendix A

Engines specification

Engine 1

* 4-S DI Diesel engine
* Single cylinder
* Supercharged
* Water-cooled
* Electronically controlled common rail injection
* 400,600,800, 1000,1120 bar injection pressure
* Variable timing

Engine 2

* 4-S DI Diesel engine
* Single cylinder
* Naturally aspirated
* Air-cooled
* Mechanically controlled injection
* 250 bar injector opening pressure
* Fixed timing

Test matrix for engine 1

Speed [rpm]	900	1500	2000
IMEP [kPa]	180	300	500
Intake press. [bar]	1	1.2	1.4
Back press. [bar]	1.1	1.5	1.8
Intake temp. [K]	350	350	350
Water temp. [K]	355	355	355

Running conditions for engine 1

			0 % EGR	15 % EGR	25 % EGR	35% EGR	40% EGR	45% EGR	50% EGR	55% EGR
low load	900 rpm	600 b inj press	X		X					X
light load	1500 rpm	400 b inj press	X		X	X		X	X	
light load	1500 rpm	600b inj press	X		X	X		X	X	
light load	1500 rpm	800b inj press	X		X	X		X	X	
light load	1500 rpm	1000b inj press	X		X	X		X	X	
half-load	2000 rpm	600b inj press	X	X	X	X	X			
half-load	2000 rpm	800b inj press	X	X	X	X	X			
half-load	2000 rpm	1000b inj press	X	X	X	X	X			
half-load	2000 rpm	1120b inj press	X	X	X	X	X			

Test matrix for engine 2

	900 rpm	1500 rpm	2000 rpm
No load	X	X	X
Inj opening pressure	250 bar	250 bar	250 bar
0% EGR	X	X	X
5% EGR	X	X	X
10% EGR	X	X	X
15% EGR	X	X	X
20% EGR	X	X	X
25% EGR	X	X	X
30% EGR	X	X	X
35% EGR	X	X	X
40% EGR	X	X	X
45% EGR		X	X
50% EGR		X	X
55% EGR		X	X
60% EGR		X	X
65% EGR		X	X

Appendix B

Fuel properties

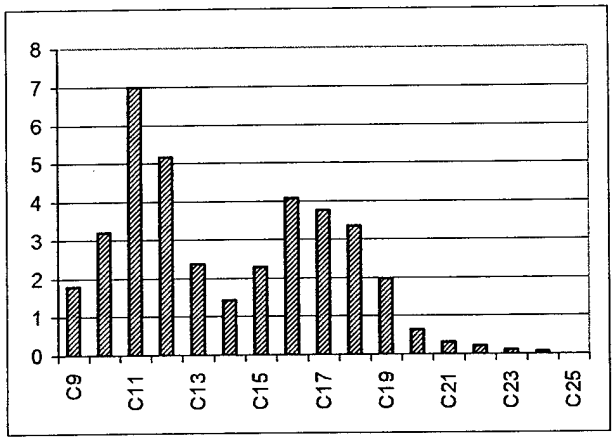

Figure B-1. Amoco Premium composition

Figure (B-1) represents the Amoco Premium fuel composition in terms of carbon numbers as measured at Wayne State University by using the gas chromatograph.

Other characteristics:

SPGR 60: 0.8438 (specific weight)

LHV : 42.78 mJ/kg (lower heating value)

H/C : 1.819 (hydrogen to carbon ratio)

APPENDIX E

2001-01-1237

Diesel Engine Cold Start Combustion Instability and Control Strategy

Zhiping Han, Naeim Henein and Bogdan Nitu
Wayne State University

Walter Bryzik
U. S. Army TARDEC

ABSTRACT

Combustion instability and white smoke emissions are serious problems during cold starting of diesel engines. In this investigation, a model has been applied to predict misfiring based on an analysis of autoignition process. The effect of injection timing on combustion instability during the cold start transient, at different ambient temperatures is investigated, both theoretically and experimentally. Maps have been developed to show the zones where misfiring would occur. The experimental work was conducted on a direct injection heavy-duty diesel engine in a cold room. The room temperature covered a range from 21 ° C to -10 ° C. The cycle-by-cycle data analysis was made and results plotted on the developed maps. The experimental results correlated fairly well with the model prediction. Based on the analysis, a new strategy for cold starting can be developed to reduce combustion instability and white smoke emissions.

INTRODUCTION

Diesel cold starting is influenced by many design and operating parameters, which affect the air temperature and pressure near the end of the compression stroke. Such parameters include the ambient temperature (1-4, 12,13); cranking speed (5, 9,15, 16, 18); injection parameters and fuel properties particularly cetane number and volatility (4). Many investigations have been conducted on diesel cold starting, and concentrated on the length of the cranking period. Very few studies dealt with the engine performance after it starts to fire. Work conducted at the Center for Automotive Research at Wayne State University indicated that misfiring may occur once, twice or more, before the engine fires again and reach a steady idling speed. This type of operation is referred to as combustion instability. Combustion instability causes engine hesitation, rough operation and long periods of time before it reaches a steady idling speed. In the worst case, the engine may suffer complete starting failure. Part of the fuel accumulated during the misfiring cycles is emitted in the next firing cycle and appears as white smoke.

Diesel engine combustion instability has been found to be repeatable, rather than random, during cold start; not engine or fuel specific, and increases with the drop in ambient temperature (1-4). Other investigators make similar observations (10, 14, 20, 21).

In this investigation, experimental and analytical studies are made and aimed at developing a new diesel engine cold start strategy to reduce or eliminate combustion instability and white smoke emissions.

Diesel Autoignition and ID Reformulation

The autoignition process, often represented by the ignition delay period (ID), plays an important role in diesel combustion process. The ID includes physical and chemical delays. Misfiring is the result of autoignition failure. The dependence of ID of the gas pressure and temperature is often expressed as:

$$\tau_{id} = Ap^{-n} \exp\left(\frac{E_A}{\tilde{R}T}\right) \qquad (1)$$

where

τ_{id}	the ignition delay period
p	pressure
E_A	apparent activation energy
$\tilde{R}$	universal gas constant
T	absolute temperature

To account for the variation in the air pressure and temperature during ID in engines the following integral is used to calculate ID.

$$\int_{t_{si}}^{t_{si}+\tau_{id}} \left(\frac{1}{\tau}\right) dt = 1 \qquad (2)$$

where

t_{si} the time at start of injection
τ_{id} the ignition delay period
τ the ignition delay calculated from Eq. 1

A recent study showed that Eq. 2 does not account for the effect of piston motion on ID computations (26). The error in the ID calculations grows rapidly when the injection timing is retarded, which is often the case during cold starting. Equation (3) has been developed to account for the change in cylinder volume caused by piston motion.

$$\frac{dX}{dt} = 0.876 p^{1.899} e^{-\frac{4665}{T}} - \frac{X}{V}\frac{dV}{dt} \qquad (3)$$

where

X a parameter that reaches unity at the end of ID.
p cylinder pressure (Bar)
T cylinder temperature (K)
V volume
t time

Equation (3) is a first order differential equation with an initial condition, X = 0, at the start of fuel injection.

EXPERIMENT SET UP

A heavy-duty, four-stroke-cycle, 4-cylinder, direct injection, turbocharged diesel engine was used in this investigation. Table 1 is a list of the engine specifications. The inter-cooler was removed considering that it will not have any substantial effect on the intake process during cold starting. A coolant tower was connected to the engine to keep the coolant temperature at the ambient temperature throughout the cold starting test. Diesel fuel was used in all the experiments.

Table 1. Engine Specifications

Firing order	1 - 3 - 4 - 2
Compression ratio	15 : 1
Bore	130 mm
Stroke	160 mm
Displacement	8.5 Liter

The engine was installed in a cold room where the ambient temperature can be controlled from -40 °C to 32 °C. Its own electric starter and 12 volt batteries cranked the engine. The batteries were put in the cold room but connected in parallel with an out of room booster to ensure enough and repeatable cranking power. Before a test, the engine with the fuel tank, and batteries were soaked in the cold room for at least 8 hours under the required ambient temperature.

An optical shaft encoder was installed on the flywheel side of the crankshaft to measure the instantaneous angular velocity and determine the position of top dead center (TDC). The TDC signal was aligned with cylinder # 4 which is the closest to the flywheel.

Each of the four cylinders was instrumented with a quartz crystal pressure transducer to measure the gas pressure, a high response thermocouple in the exhaust manifold close to the port, and a strain gauged rocker arm to measure the start and duration of injection of the unit injector (EUI). The output of the strain gauge is proportional to the force on the plunger, and hence the fuel pressure. A special fuel injection test rig was built to calibrate the strain gauge of each of the four rocker arms and determine the fuel delivery per cycle at different speeds and loads. A description of the method developed to utilize the strain gauge signal to determine the injection events is given in the appendix.

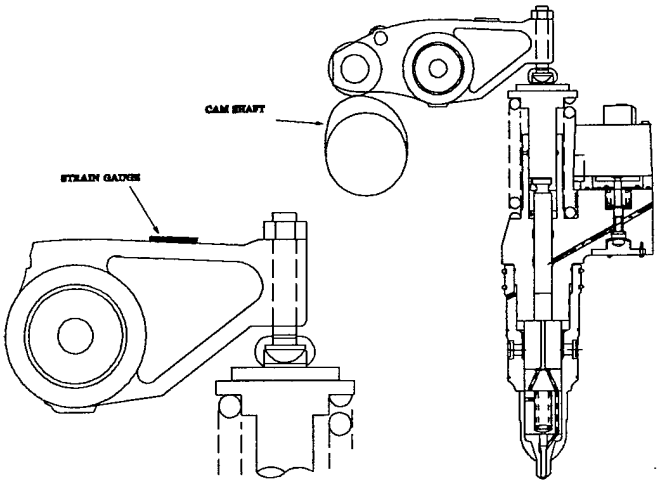

Figure 1. Strain gauge installation on the rocker arm of the Unit Injector.

EXPERIMENTAL RESULTS AND DISCUSSIONS

Tests were conducted at 5 different ambient temperatures: 21°C, 5 °C, 0 °C, -5 °C, and -10 °C. Figure 2 shows the instantaneous engine speed trace during the cold start transient at an ambient temperature of 21°C. It should be reminded that TDC is aligned with cylinder # 4. Figures 3 to 5 are for the cylinder gas pressure, fuel injector rocker arm strain gauge signal, and exhaust temperature of cylinder # 4 respectively. Figure (2) shows that the engine was cranked for two revolutions, after which one of the cylinders fired, followed by the other firing cylinders. This caused the engine to accelerate and reach 900 rpm, after which the speed fluctuated several times. The engine eventually stabilized at an idling speed of about 800 rpm. The engine speed traces at other ambient temperatures are shown in figure 6,8, 10 and 12 . It can be seen from these figures, that the engine

experienced more speed fluctuations and took longer time to reach the stable idling speed. This is caused by the increase in the number of misfiring cycles at lower ambient temperatures. This is evident on the cylinder pressure trace of cylinder #4, given in figures 7, 9, 11 and 13. The pressure traces of the other cylinders, not given in this paper, show a similar behavior to cylinder # 4.

Misfiring can be detected from dynamic, thermal or thermodynamic indicators. When a cycle misfires, the instantaneous engine speed after the expansion stroke is lower than that before compression stroke. Under steady state, these two speeds should be the same. The thermal indicators include the exhaust gas temperature after the exhaust valve open (EVO). The thermodynamic indicators include the cylinder gas pressure or IMEP, and the amplitude of the pressure pulse in the exhaust port after EVO.

Typical traces for different types of cycles during cold starting process are shown in figures 14 through 19. Figure 14 is a normal firing cycle during engine starting at a room temperature of 21°C, with a single injection. The engine gained 250 rpm after this cycle. Figure 15 is a misfiring cycle during engine starting at 21°C, with pilot and main injections. For this cycle, the pilot injection failed to deliver any fuel, because the pulse width for the pilot injection was too short for the fuel pressure to reach the opening pressure of the needle. (Refer to the appendix). Notice that the engine decelerated after this cycle, and the exhaust temperature showed no evidence of combustion. Figure 16 is a firing cycle during engine starting at 21°C with pilot and main injections. Figure 17 is for a cycle during engine starting at 5 °C, without fuel injection during engine deceleration. Figure 18 is a misfiring cycle during engine starting at 5 °C, with a single injection. Figure 19 is for a cycle during engine starting at -10 °C, with as single injection. Here, combustion started very late in the expansion stroke.

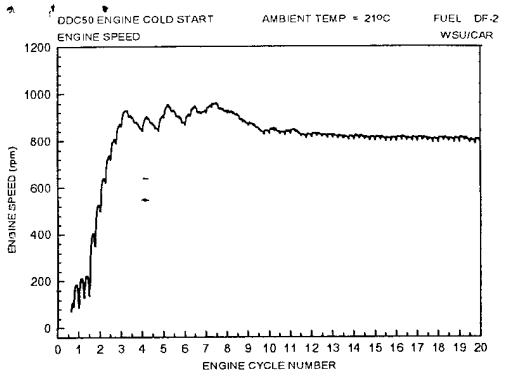

Figure 2. Instantaneous engine speed at 21 °C

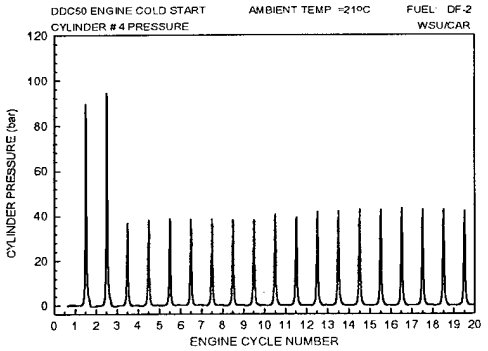

Figure 3. Cylinder # 4 pressure trace at 21 °C

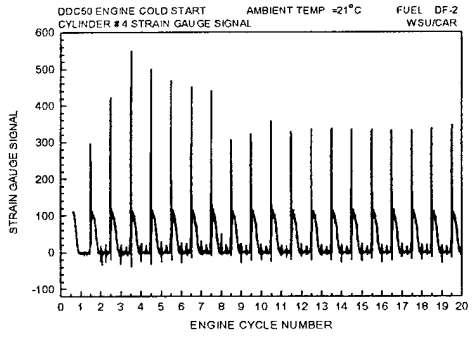

Figure 4. Cylinder # 4 strain gauge signal at 21 °C

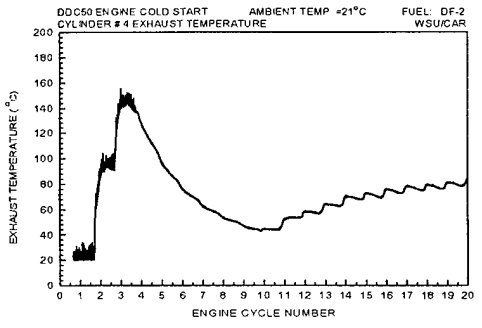

Figure 5. Cylinder # 4 exhaust temperature at 21 °C

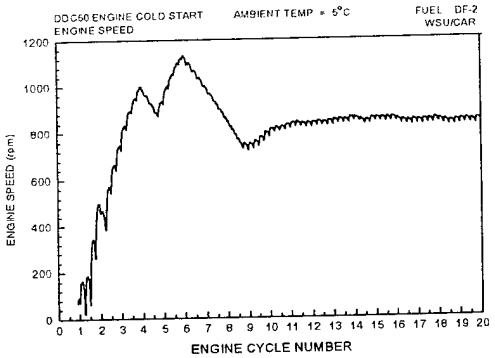

Figure 6. Instantaneous engine speed at 5 °C

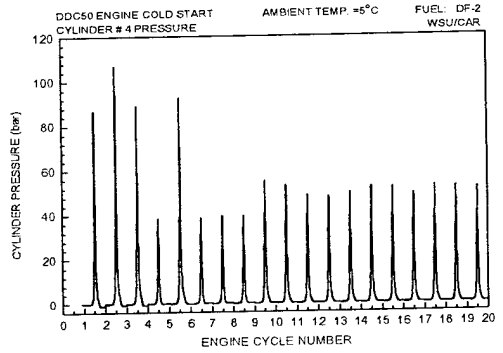

Figure 7. Cylinder # 4 pressure trace at 5 °C

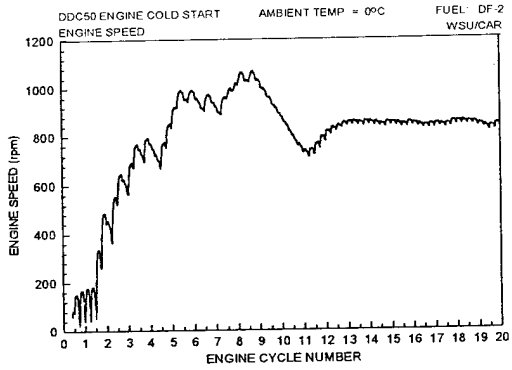

Figure 8. Instantaneous engine speed at 0 °C

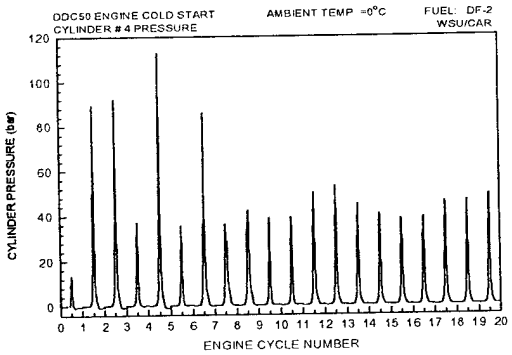

Figure 9. Cylinder # 4 pressure trace at 0 °C

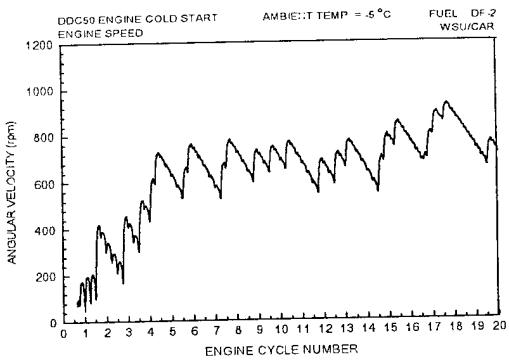

Figure 10. Instantaneous engine speed at -5 °C

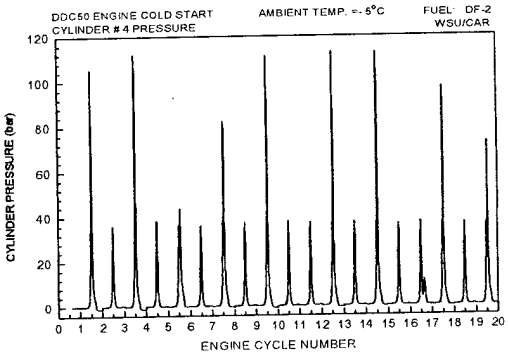

Figure 11. Cylinder # 4 pressure trace at -5 °C

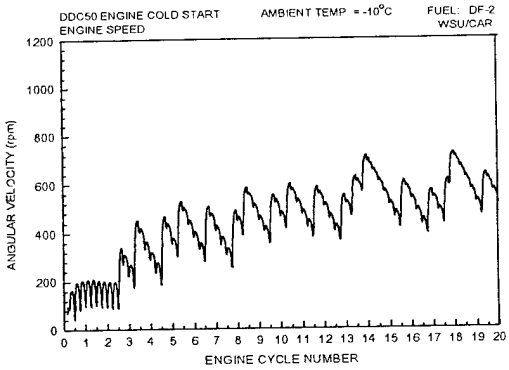

Figure 12. Instantaneous engine speed at -10 °C

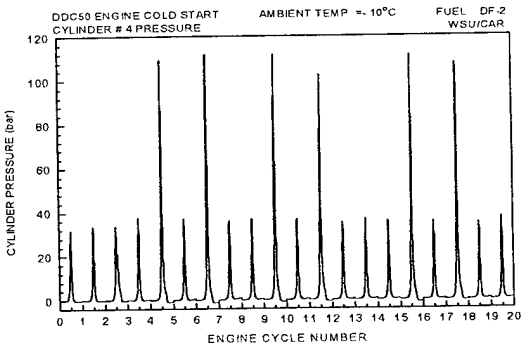

Figure 13. Cylinder # 4 pressure trace at -10 °C

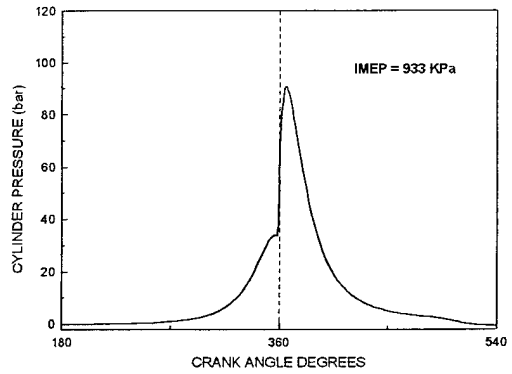

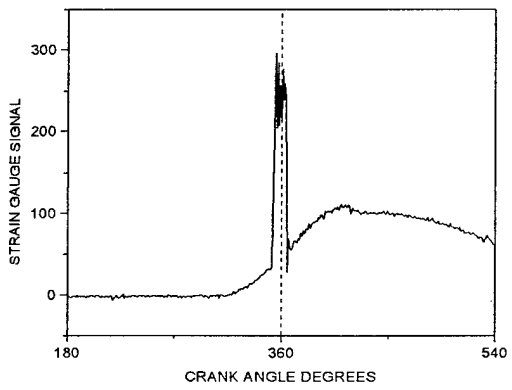

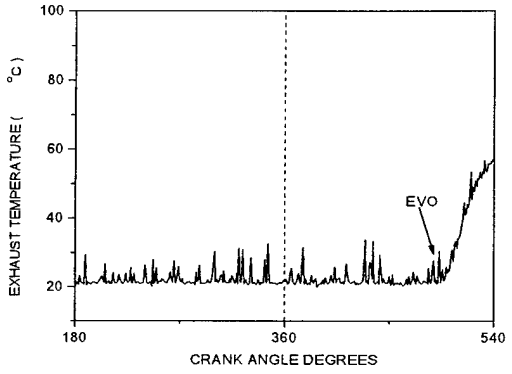

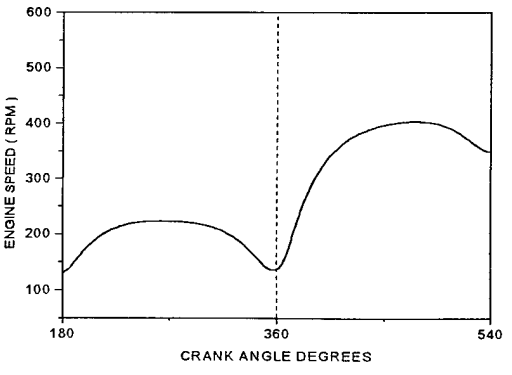

Figure 14. A firing cycle with single injection, sample from 21 ° C test.

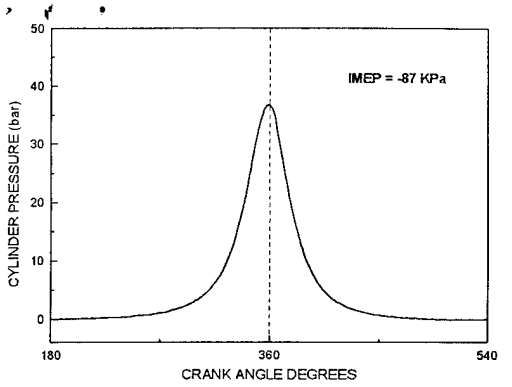

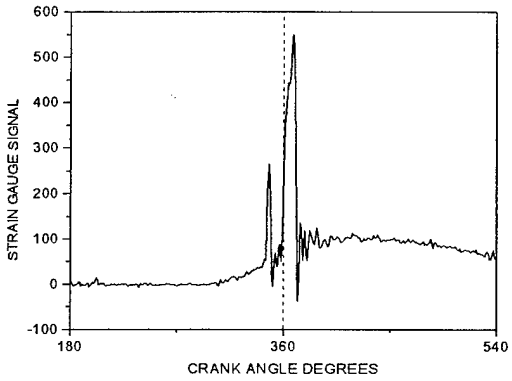

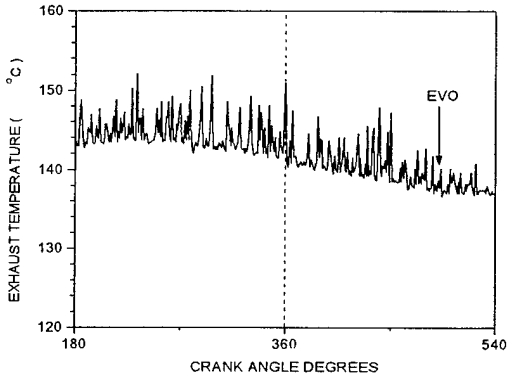

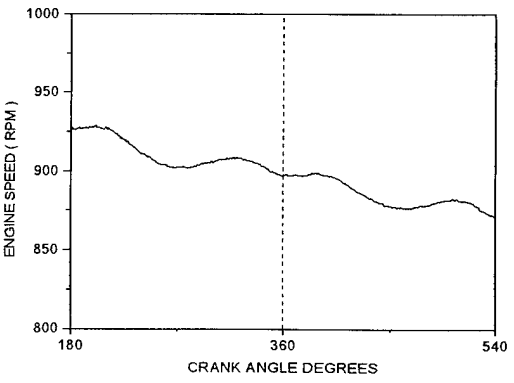

Figure 15. A misfiring cycle with pilot-main injection, sample from 21 ° C test.

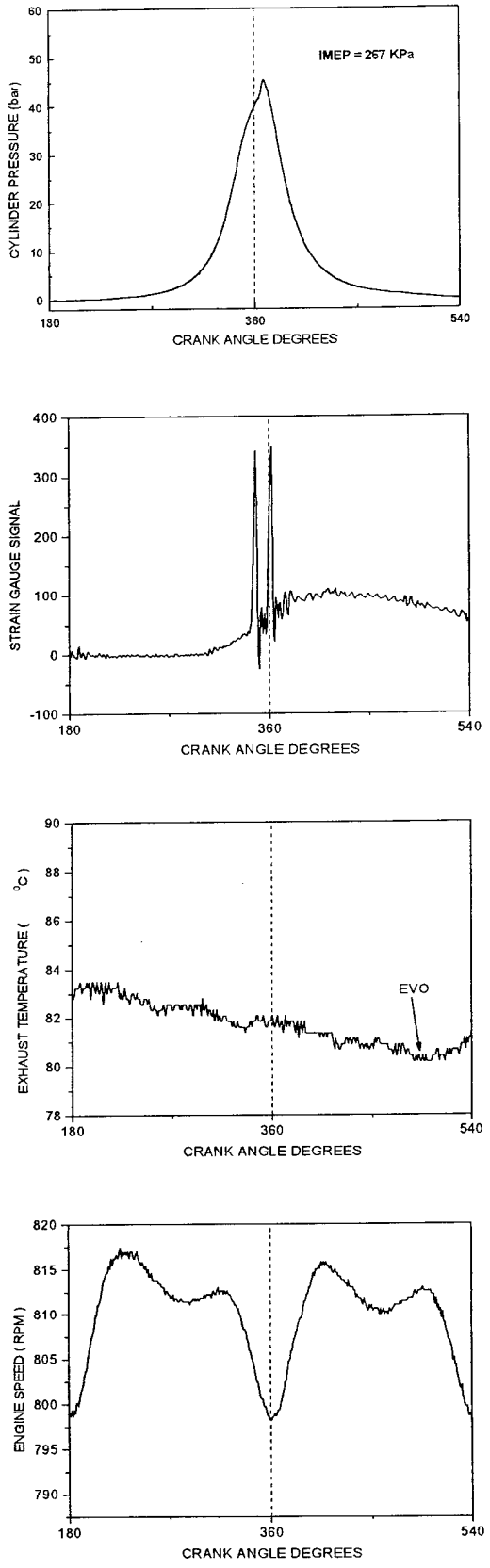

Figure 16. A firing cycle with pilot-main injection, sample from 21 ° C test.

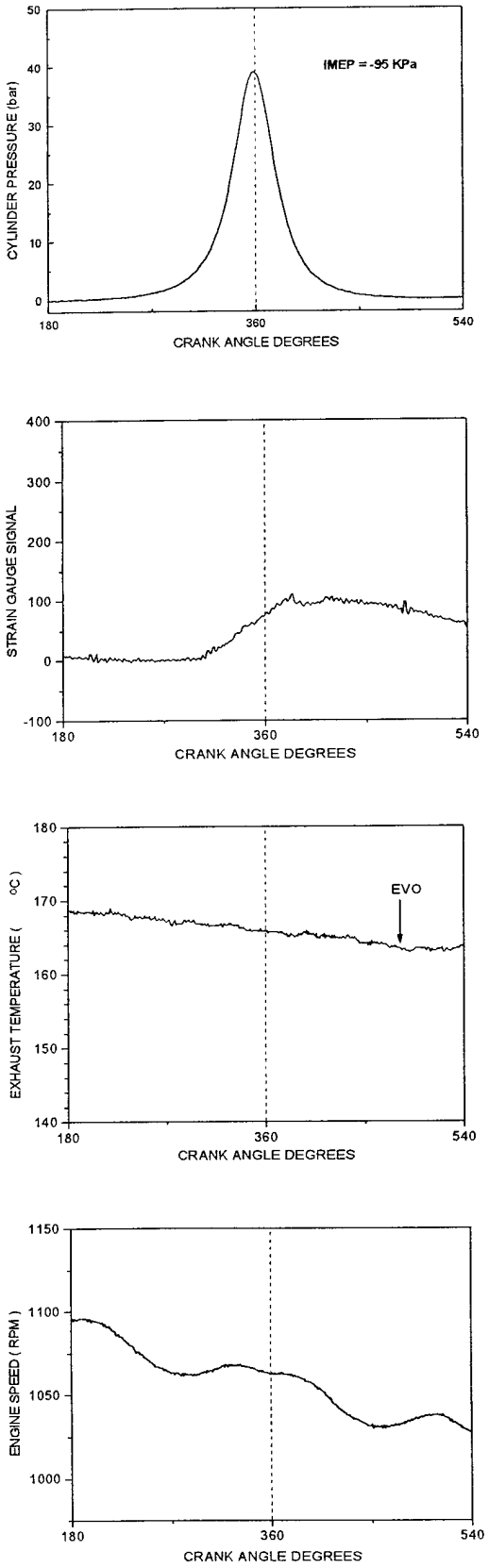

Figure 17. A cycle without injection, sample from 5 ° C test.

Figure 18. A misfiring cycle of single injection, sample from -5 ° C test.

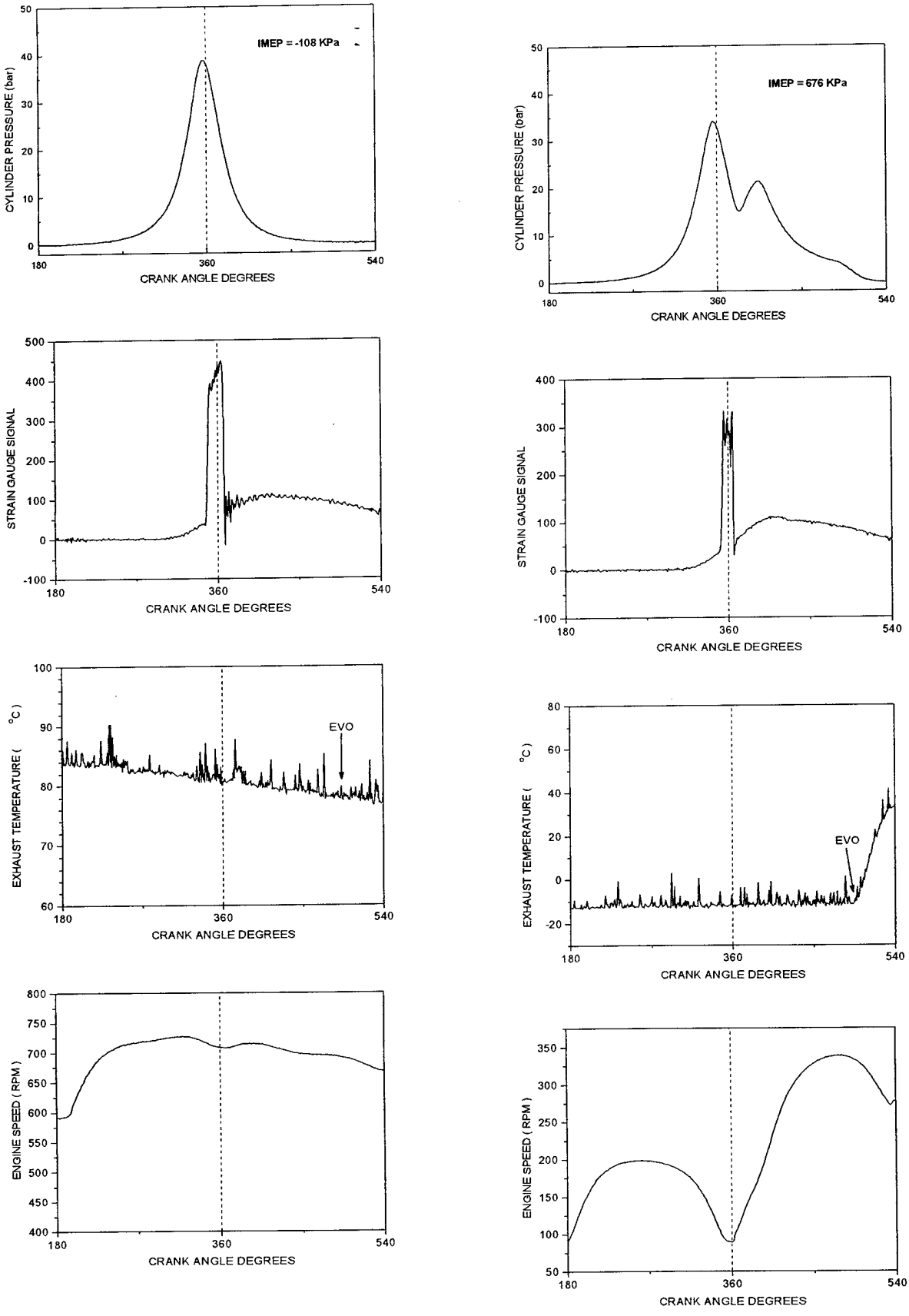

Figure 19. A later combustion cycle, sample from -10 ° C test.

Figure 20 is a composite of the traces for the transient engine speed at the five ambient temperatures. Looking at the general speed trend at different ambient temperatures, the slope of the average engine speed becomes smaller and smaller as the ambient temperature gets lower and lower. It is also seen that the slope is dominated by the firing cycles. The average speed of these firing cycles increased gradually and eventually brought the engine to an idling speed. While for the misfired cycles, since fuel was injected, it became the sheer source of white smoke emissions.

The analysis of the experimental data pointed out toward the role of the injection process in misfiring. Two injection parameters are examined. The first is injection timing, and the second is pilot injection. The injection timing during successive cycles is determined and plotted versus engine speed during the cycle. The speed for each cycle is an average calculated around TDC of the cycle. The negative value of timing indicates that injection starts before

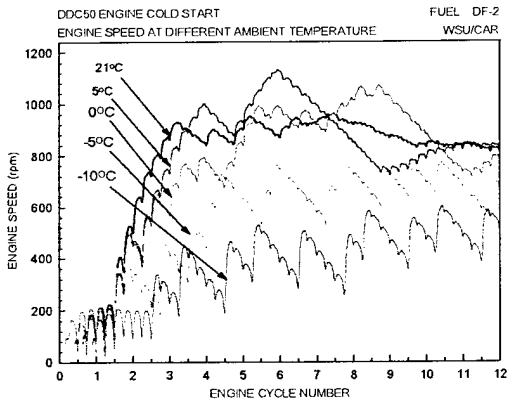

Figure 20. Instantaneous engine speed comparison

TDC. The injection timing is the dynamic timing for the fuel delivery in the combustion chamber. This is determined from the signal of the strain gauge on the rocker arm of each cylinder. The dynamic timing is different from the command signal timing. The difference is in the time taken by the solenoid to act on its valve and the time for the fuel pressure to build up to the opening pressure of the needle. Figure 21 is a speed-injection timing map for engine as it started at an ambient temperature of 21° C. The arrows in the figure indicate the sequential order of successive cycles for cylinder #4. The cycle marked with number 1 is the first cycle in the starting process. Figure 21 shows that the injection timing was at 5° bTDC, while the average engine speed during this cycle was 160 rpm.

The engine accelerated and continued to fire for another 6 cycles, while the injection timing was advanced to 10. 5° bTDC as the speed reached 860 rpm. The successful firing in the seventh cycle caused the engine to accelerate to 925 rpm. In the eighths cycle, injection was retarded to 2° aTDC and the engine misfired. However the speed dropped slightly and the engine misfired in the ninth and tenth cycles causing the engine to slow down to 820 rpm. In the eleventh cycle, the injection timing was advanced to 12.7 ° bTDC.

A misfiring cycle is the result of a failed ignition. The ignition delay in diesel engine is by definition a time interval between the start of fuel injection and the start of combustion. Once fuel is injected, the ignition process becomes uncontrollable. Hence, the fuel injection timing is one of the key parameters to affect the ID and hence the successfulness of autoignition.

During cold starting transient period, engine speed changes drastically. The typical speed pattern is firing - acceleration - misfiring - deceleration. To find out how the dynamic speed change affects the ignition delay, the cycles with sequential order starting from first firing cycle are plotted on the injection timing - engine speed plane to see the dynamic behavior. The speed for each cycle is an average calculated at around TDC of each cycle. The negative value of timing indicates injection start before TDC. The injection timings used for the plots are called effective timings, which means the physical start point of fuel delivery. If the engine control is in pilot - main injection mode and the pilot injection fails to deliver fuel, the timing used will be from the main injection. Figure 21 is the plot for the test at 21 °C ambient temperatures. The arrows in the figure indicate the sequential order of successive cycles.

In figure 21, the first firing cycle marked with '1' is cylinder number 4. The engine continued to fire for another 6 cycles when it misfired for 3 cycles before it started firing again. Recalling that the firing order of 1-3-4-2, the first misfired cycle is cylinder number 3. For cylinder number 3, it fired in first cycle and then misfired in the second one. Also noticed is the big shift of injection timing for the misfired cycles. Figure 22 is an expanded view of fuel injector rocker arm strain gauge signal for the two consecutive cycles of cylinder number 3. The misfired cycle was in pilot-main injection mode, and the pilot injection failed to deliver fuel because the needle did not reach the open pressure. The timing plotted is actually the main injection timing. In the following discussion, to avoid the confusion, the term "engine cycle number" refers to cycles aligned with cylinder number 4, and the "cylinder cycle number" or in short the "cycle number" for an individual cylinder refers to the cycle sequence in that specific cylinder.

The term "failed injection" should be understood as very little fuel delivered in order to represent a general case where too little of fuel has substantially no effect on ignition. The failed pilot injection, should it succeeded, would be about 12.5 degrees before TDC as can be predicted by its rocker arm strain gauge signal rising edge. The injection timing of the main injection was after TDC. In this test, all the cycles with failed pilot injection misfired.

In figure 21, the injection timing, after first firing cycle, decreased during the following two cycles. In general, it is expected that the injection timing should be increased according to the increase in engine speed. The retarded timing could be contributed to the insufficient response of the control module to the fast changing engine speed.

The injection timing-engine speed trace at other ambient temperature tests are shown in figures 23 – 26

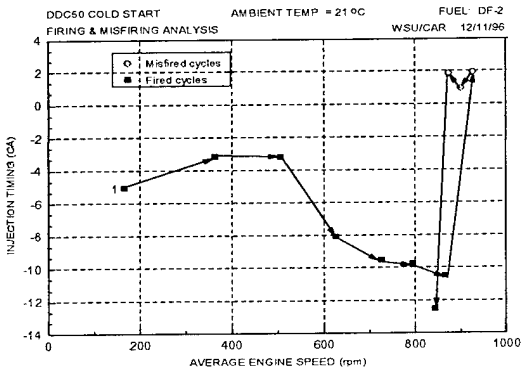

Figure 21. Transient engine speed and injection timing trace at 21 °C ambient temperature

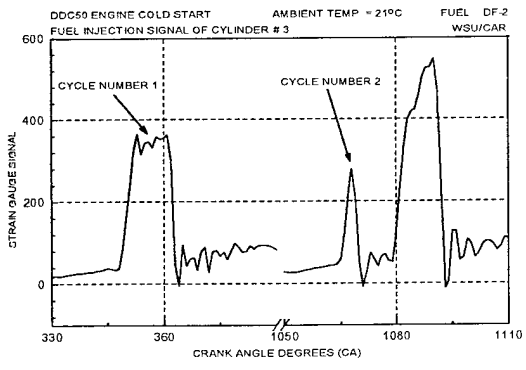

Figure 22. Fuel injection signal comparison between the fired and misfired cycle

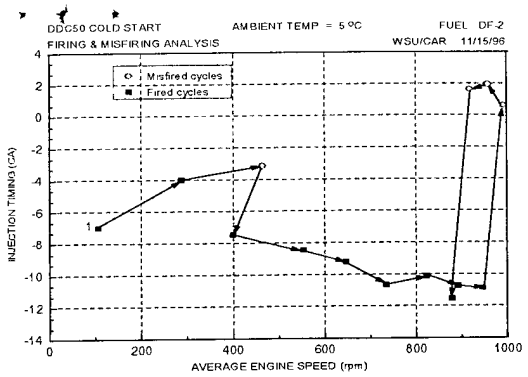

Figure 23. Transient engine speed and injection timing trace at 5 °C ambient temperature

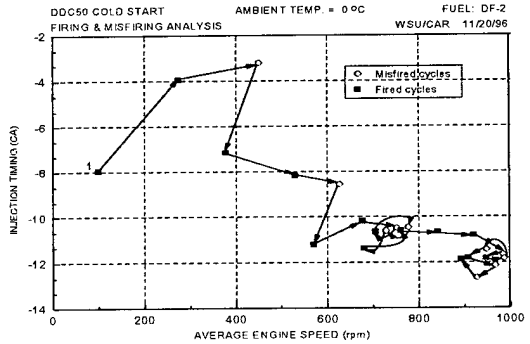

Figure 24. Transient engine speed and injection timing trace at 0 °C ambient temperature

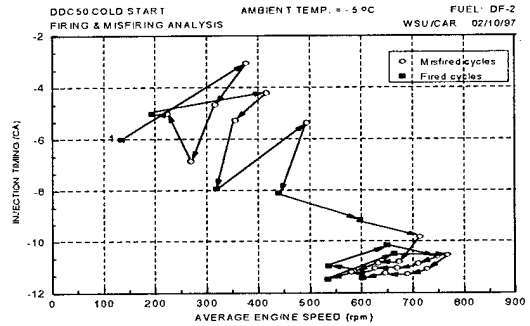

Figure 25. Transient engine speed and injection timing trace at -5 °C ambient temperature

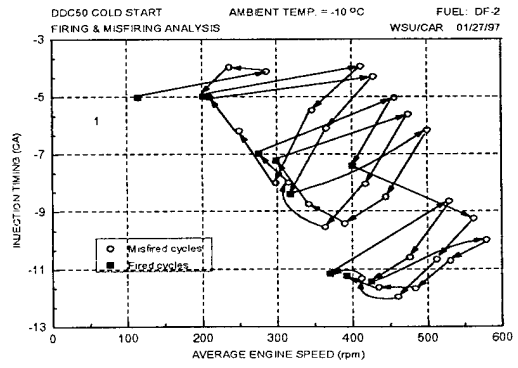

Figure 26. Transient engine speed and injection timing trace at -10 °C ambient temperature

. Figure 22 is an expanded view of strain gauge signal of the rocker arm of cylinder number 1. It is noticed that cycle 1 had the main injection timed to start before TDC. In the following cycle, the injection shifted from one main injection to pilot and main injection. The needle failed to open and deliver the pilot injected fuel. Figure 22 shows that the fuel pressure did not reach the needle opening pressure. It is noticed that, for the four cylinders, misfiring occurred in the cycles in which the injection shifted from main to main-pilot injection after engine acceleration.
The injection timing-engine speed maps at the lower ambient temperatures are given in figure 23 - 26. At 21° C test, the engine started misfiring after it exceeded 800 rpm. When the ambient temperature was decreased, misfiring cycle started early and the number of misfiring cycles increased. This fact can be seen from speed traces at different ambient temperatures and cylinder pressure traces in figure 7,9,11 and 13. Also, in figure 20 through 25, a trend of distribution of the fired cycles in the timing-engine speed plane can be seen.

A PREDICTIVE MODEL FOR ENGINE MISFIRING

To better understand the causes of misfiring and to predict the misfiring, equation (3) was used for ignition delay analysis. Figures 27 - 28 are the calculated results at 20 ° C case, where figure 27 is ignition delay in crank angle degrees, while 28 in time.

1. Effect of injection timing:

The ID at different injection timing is calculated from Eq. (3) and plotted versus injection timing in crank angle degrees and in milliseconds, in figures 27 and 28 consecutively. The ambient temperature is 20 ° C. Very early injection produces long ID because both the air pressure and temperature are fairly low. As injection is retarded toward TDC, higher temperatures and pressures are achieved and ID is reduced. ID reaches a minimum a few degrees before TDC. Retarding the timing any further causes ID to increase. If part of the ID occurs during the expansion stroke, ID increases at a faster rate. This is evident from equation (3). The computations were extended to injection starting after TDC. It is noticed that ID increases at a fast rate as injection occurs in the expansion stroke. There is a limit beyond which ignition would not occur resulting in misfiring.

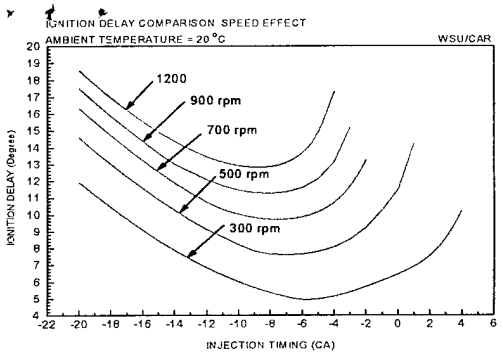

Figure 27 Engine speed effect on ID at 20 ° C

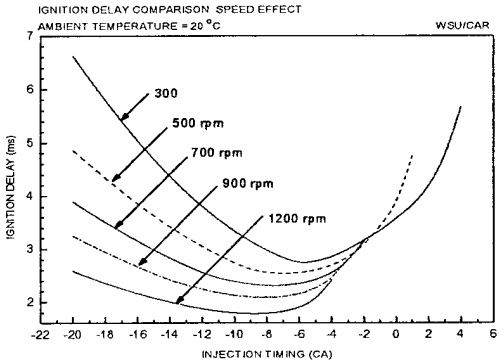

Figure 28 Engine speed effect on ID at 20 ° C

2. Effect of engine speed:

Figure 27 shows that at higher engine speeds ID takes more crank angle degrees. The minimum ID delay points, as well as the misfiring limit, shift slightly toward early injection timing. The reason is that at higher engine speeds the time available for the mixture to react at the high temperature and pressure around TDC becomes shorter. For the same reason, the minimum ignition delay point occurs at an earlier injection timing.

Figure (29) shows the misfiring limit at different speeds. Fuel injection timing below the borderline between the firing and misfiring zones would result in misfiring. The misfiring limit shifts to the earlier injection timing direction at higher engine speeds. As the engine speed decreases the misfiring limit first reach the most retarded timing and then starts shifting back toward the early injection timing. Eventually, the curve would end at a speed at which ignition is impossible at any injection timings because of the severe blow-by and heat losses.
The whole picture of the firing-misfiring boundary line would have the shape shown by figure 30, where an arbitrary scale is used.

3. Effect of Ambient Temperature:

Figures 31 and 32 show the ID at different speeds and an ambient temperature of 10 ° C. Comparing the figures for ambient temperatures of 10 ° C and 20 ° C

injection timing range for firing becomes narrower. This explains why more misfiring occur under lower ambient temperatures. Figure 33 compares the boundary of the firing zone for the two ambient temperatures. The misfiring zone extends toward early injection timing at the lower ambient temperature. The firing-misfiring boundary lines are calculated for DF2, at different temperatures and given in Fig. 34. The area above each of the lines is the misfiring zone at that specific ambient temperature. The strong effect of the ambient temperature on the firing-misfiring boundary lines can be seen. At the lower ambient temperatures, the firing zone becomes smaller and smaller, and the injection timing has to be advanced as the engine gains speed. Consider for example, the starting transient of the multi-cylinder engine used in this study, at an ambient temperature of –10 ° C. Reference is made to Fig. 9 to look at the change in speed during the transient. Notice the engine was cranked for 4 revolutions before it fired, so each cylinder had two injections accumulated in the combustion chamber. The engine speed when the first cylinder fired is 200 rpm and the corresponding injection timing from Fig 34 can be as late as 0.5 degree after TDC. Once the first cylinder fired, the engine accelerated and reached 340 rpm. According to Fig. 34, the injection timing for the second-cylinder-to-fire should be advanced to more than 4 degrees before TDC. This cylinder and the next cylinder misfired and the engine decelerated to 200 rpm again where one cylinder fired. This fluctuation in speed continued for some time. Notice that the minimum speed at which the cylinders fired kept increasing as the engine got warmed up. With very early injection timing, the engine may also experience autoignition failure for another cause. Injecting fuel too early into cylinder under very low air pressure and temperature may cause the liquid fuel to be deposited on the cool walls and hinder fuel evaporation and mixing with the air.

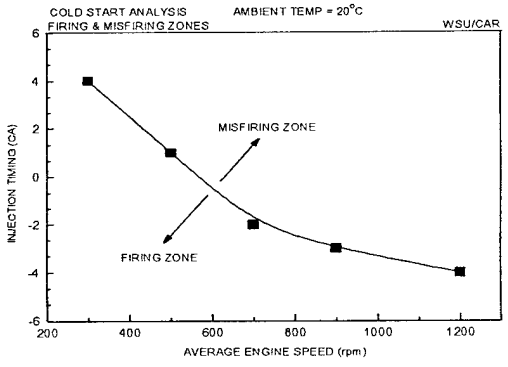

Figure 29. Firing/misfiring boundary line

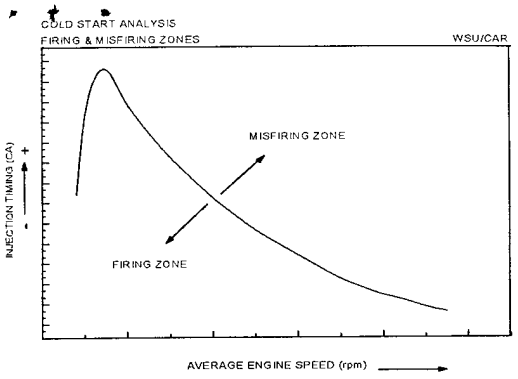

Figure 30. General shape of firing/misfiring boundary line

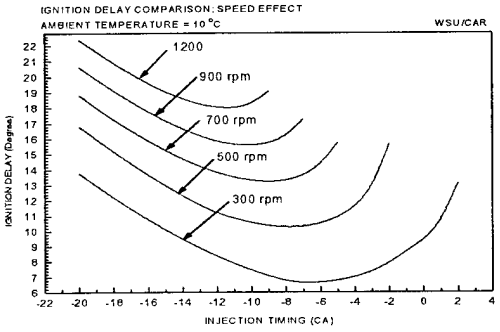

Figure 31. Engine speed effect on ID at 10 °C

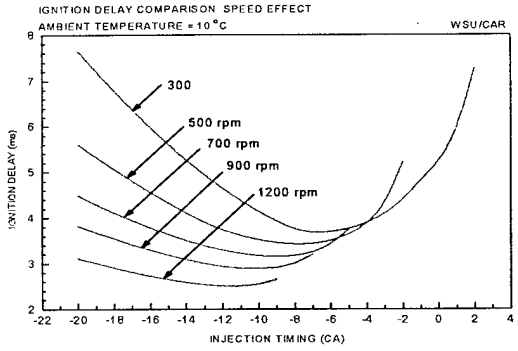

Figure 32. Engine speed effect on ID at 10 °C

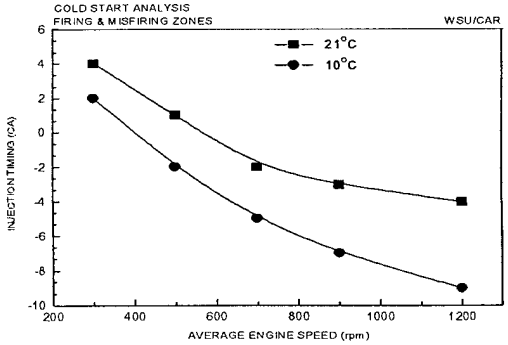

Figure 33. Ambient temperature effect on misfiring boundary

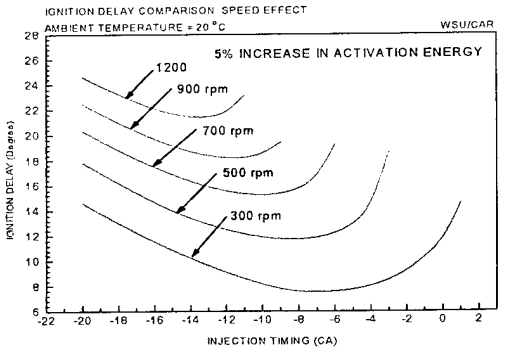

Figure 34. Fuel cetane number effect on ID

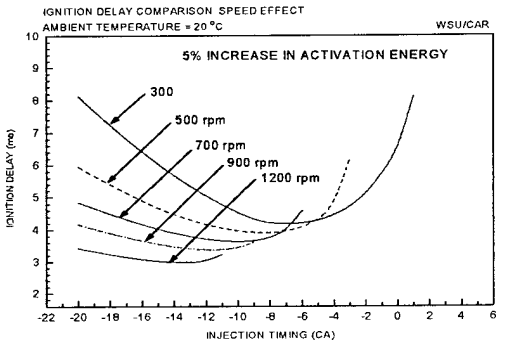

Figure 35. Fuel cetane number effect on ID

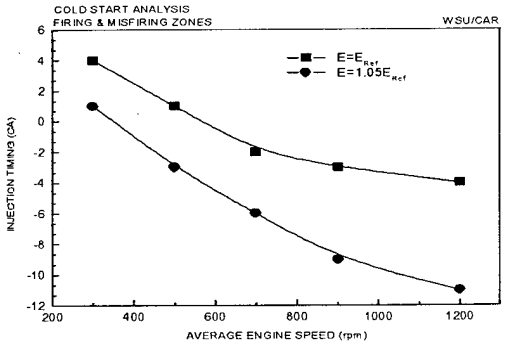

Figure 36. Fuel cetane number effect on misfiring boundary

4. Effect of Cetane Number:

The effect of fuel cetane number on ID is evaluated by changing the apparent activation energy in the ID equation. In general, higher cetane number fuels have lower activation energies. Figures 34 and 35 show the computed ID for a fuel having activation energy 5 % higher than the fuel of figures 27 and 28. The 5% increase in activation energy caused a big shift of the misfiring boundary line. This means that low cetane fuels require earlier injection timing in order to avoid misfiring.

COLD START FIRING and MISFIRING ZONES

From above discussion, it can be concluded that whether a cycle will misfire or not depends on which zone it is located in. Figures 33 and 36 show the boundary between the firing and misfiring zones as a single line. This is not the case in multi-cylinder engines due to the synergistic effect of cylinders, particularly during the cold starting transient. The conditions at the start of injection differ from one cylinder to the other. Consider for example the engine speed and its effect on the compression pressure and temperature. The engine speed when the first cylinder fires is the cranking speed. The second cylinder to fire will have a higher pressure and temperature in the compression stroke, because of the higher engine speed. This means that the last cylinder to fire will have the highest compression pressure and temperature. Accordingly, the ignition delay will vary from one cylinder to the other during the cold start transient. Similarly, during deceleration, the conditions will vary from one cylinder-to cylinder and from cycle-to-cycle. As a result of this variation, the boundary between the firing and misfiring zones will be in a form of a band rather than a single line.

Under cold start conditions, figure 34 shows that for specific injection timing, there exists a maximum speed limit at a given ambient temperature. The lower the ambient temperature, the lower the speed limit will be. To increase the speed limit, the injection timing has to be advanced further. But the injection timing can not be advanced without limit. If the ambient temperature is low enough, the speed limit can become lower than the stable idling speed. Under such low ambient temperature condition, one measure is to use a starting aid.
The behavior of the engine under the cold starting at ambient temperatures of 21 °C, 5 °C, 0 °C and -5 °C can be explained by considering the misfiring zone at each temperature. In this paper we will discuss the cold starting transient at -10 °C. The misfiring boundary at -10 °C is calculated and superimposed on the speed-injection-timing map (figure 6), as shown in figure 38. The figure clearly shows that the engine moved from the firing zone into the misfiring zone many times.

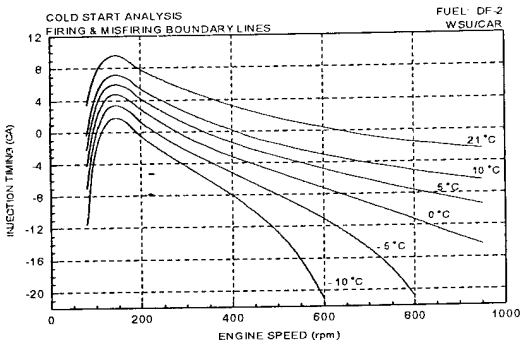

Figure 37. Firing-misfiring boundary lines

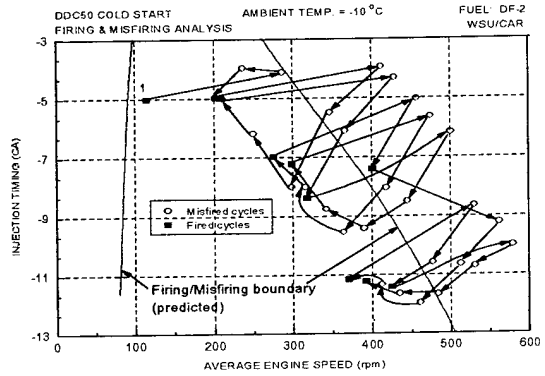

Figure 38. Transient timing - speed trace at -10 °C

COMBUSTION INSTABILITY AND COLD START CONTROL STRATEGY

Many factors contribute to combustion instability, most important of which are the ambient temperature and injection timing. The above analysis indicates that combustion instability during cold starting is not a random phenomenon, but it can be explained by considering the engine-injection timing map at different temperatures and cranking speeds. Combustion instability can be reduced or eliminated if correct measures are taken.

Based on the ID equation (3), in order to have stable combustion during cold starting depends not only on the compressed air temperature and pressure, but also on injection timing. Injection timing need to be advanced at higher engine speeds, and stay in the misfiring zone explained earlier. In multi-cylinder engines, during the cold start transient, each of the cylinders starts firing at a higher speed than the previous firing cylinder. Ideally, injection timing should be adjusted to suit the conditions in each cylinder. This requires fast response injection controls. The input to the controls would be an indicator of the engine acceleration during the expansion stroke of the previous firing cylinder.

In some engines, the strategy is to shift from a single injection to pilot and/or split injection once the engine accelerates beyond a certain speed limit. This requires a different injection timing than that for one single main injection. In many cases the engine might overshoot in speed during the cold start transient and temporarily reach this limit. If injection timing is corrected to suit this high speed, misfiring might occur.

The existence of firing-misfiring boundary on the timing-speed plane means that misfiring during cold start is not random, but predictable, or preventable if correct measures can be taken.

Based on the ID equation (3), to have successful autoignition, not only the temperature and pressure levels should be high enough above certain level, but should be kept for long enough time period. If the instantaneous engine speed at around the TDC is low, there will be good chance for the autoignition to occur. For the two speed profiles in figure 39, the profile 1 would be more favorable to ignition, since it has fast compression to reduce the heat transfer and blow-by losses, and slow speed at around TDC where peak pressure and temperature can stay longer. This means that, if the cranking speed is too high, engine will not have successful ignition.

The traditional strategy of cold start is to dump large amount of fuel during cranking period, and then reduce the fueling when engine reaches preset idling speed. The over fueling has been thought to have more chances to start the engine quickly.

When engine starts firing, with large amount of fuel dumped into the combustion chamber, the engine speed will be accelerated up high above the idling speed, then the governor kicks in and reduce the fuel delivery and eventually stabilizes the engine at idling speed. This type of speed history pattern can be called overshooting.

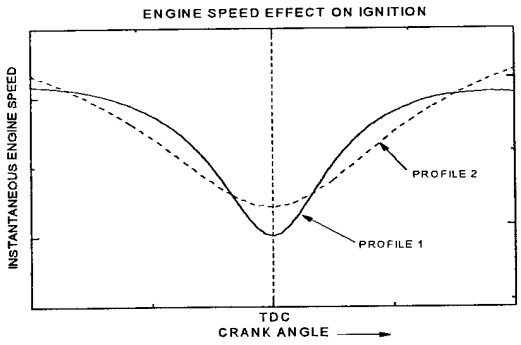

Figure 39. Instantaneous engine speed profile effect

The fast acceleration of engine speed during this overshooting period may easily cause the engine to run into the misfiring zone at low ambient temperatures. Under low ambient temperatures, the up speed limit the engine can run without suffering misfiring is restricted by the firing-misfiring boundary lines, and the up speed limit gets lower and lower as ambient temperature gets lower. The high acceleration of speed will certainly be frustrated by

unstable combustion: misfiring and white smoke emissions.

Under very low or marginal ambient temperatures, the firing zone is very small regarding to both available injection timing and engine speed range. The firing zone will only cover an area of a low speed range requiring very early injection timings. In such a situation, a slow initial acceleration of engine speed by the firing cycles would provide more chance for engine to stay in firing zone longer, then more firing cycles would be possible, this in turn will warm up the combustion chamber walls and expand the firing zone for subsequent cycles. Overall, this start strategy may start the engine successfully in a shorter time, meanwhile reduce or eliminate the misfiring and white smoke.

In general, the cold start strategy should include the overall reduction of fueling during cranking period to reduce speed acceleration. Some kind of devices which can "hold" the engine in firing zone longer will be very helpful. The control algorithm should also reach the level of cycle-by-cycle basis regarding to fueling and injection timings until idling speed is reached. The speed is low during cold start period in general, and this makes the control to reach cycle-by-cycle level possible from both hardware and software aspects.

CONCLUSIONS

1. Both analytical and experimental results showed that the diesel engine cold start combustion instability can be well explained with the firing-misfiring zones on the injection timing - engine speed plane.

2. The misfiring zone expands while firing zone shrinks as ambient temperature decreases, or fuel cetane number decreases.

3. Under low ambient temperatures, over fueling during cold start period often make the engine to run into misfiring zone once engine starts firing.

4. To start the diesel engine under very low ambient temperatures, the engine should be controlled in such a way that, the engine speed is accelerated slowly to avoid over shooting, and to let the firing zone to be expanded by firing cycles gradually.

5. The fueling and timing control should reach the cycle-by-cycle level during cold start transient.

ACKNOWLEDGMENT

The authors greatly acknowledge the financial support to this study by the U. S. Army Tank Automotive Research and Development Engineering Center and ARO. The authors are grateful for the technical support by Dr. Nabil Hakim, Mr. Leland Haines, Dr. He Jiang from Detroit Diesel Corporation, and the donation of a turbocharger speed sensor by Dynamic Control and air mass flow sensor by Bosch North America. The help in engine instrumentation work from Ms. Nedeltcheva Lidia, Mr. Alexander Lasky, Machine Shop, and Electric Shop of Wayne State University are greatly appreciated.

REFERENCES

1. Naeim A. Henein, Akram R. Zahdeh, Mahmoud K. Yassine, Walter Bryzik, " Diesel Engine Cold Starting: Combustion Instability ", SAE paper No. 920005, 1992.
2. Akram Zahdeh, Naeim Henein, Walter Bryzik, " Diesel Cold Starting: Actual Cycle Analysis Under Border-Line Condition ", SAE paper No. 900441, 1990.
3. Walter Bryzik, Naeim Henein, "Fundamental cold start phenomena within advanced military diesel engines", Army Science Conference Proceedings vol.III, pp1091-1099, 1994.
4. Mahmoud K. Yassine, "Combustion instability and white smoke emissions under cold starting of diesel engines", Ph. D. Dissertation, Wayne State University, 1995
5. A. E. W. Austen, W.-T. Lyn, " Some investigations on cold-starting phenomena in diesel engines ", Proc. Instn. Mech. Engrs. No. 5, 1959-60
6. W. T. Lyn, E. Valdmanis, "The effects of physical factors on ignition delay", SAE paper 680102.
7. T. W. Biddulph, W. T. Lyn, "Unaided starting of diesel engines", SAE paper 680103.
8. T. C. Yu, O. A. Uyehara, P. S. Myers, R. N. Collins, K. Mahadevan, "Physical and Chemical Ignition Delay in an Operating Diesel Engine Using the Hot-Motored Technique", SAE Transactions, Vol. 68(1960), paper 125-U
9. A.Andree, S. J. Pachernegg, "Ignition Conditions in Diesel Engines", SAE paper 690253
10. A. Kobayashi, T. Suzuki, M. Nakajima, "Combustion analysis of the high speed diesel engine in cold starting condition via high speed photography", ASME paper, n80-DGP-7 for meet. Feb. 3-7, 1980 P
11. H. Kanesaka, H. Sakai, "A new cold starting system for diesel engines", 14th international congress on combustion engines, Helsinki, 1981
12. Ramkrishna Phatak, Tadao Nakamura, "Cold startability of Open-Chamber Direct-Injection Diesel Engines- Part I: Measurement Technique and Compression Ratio", SAE paper 831335
13. Ramkrishna Phatak, Tadao Nakamura, "Cold startability of Open-Chamber Direct-Injection Diesel Engines- Part II: Combustion Chamber Design and Fuel Spray Geometry and Additional Air and Glow Plug as a Starting Aid", SAE paper 831396

14. Akio Kobayashi, Akira Kurashima, Shin Endo, "Analysis of cold start combustion in a direct injection diesel engine", SAE paper 840106
15. Naeim A. Henein, "Starting of diesel engines: Uncontrolled fuel injection problems", SAE paper 860253
16. N. A. Henein, Chiu-Shan Lee, "Autoignition and combustion of fuels in diesel engines under low ambient temperatures", SAE paper 861230
17. Steven G. Fritz, Duane L. Abata, "A photographic study of cold start characteristics of a spark assisted diesel engine operating on broad cut diesel fuels", SAE paper 871674
18. M. A. Gonzalez D, G. L. Borman, R. D. Reitz, "A study of diesel cold starting using both cycle analysis and multidimensional calculations", SAE paper 910180
19. Yasuhiko Itoh, "The characteristics of diesel combustion and the mechanisms of misfiring under low ambient temperature", MS thesis, Wayne State University, Detroit, Michigan, 1992
20. Y. Asou, H. Fujimoto, J. Senda, K. Tsurutani, M. Nagae, "Combustion in a small DI diesel engine at starting", SAE paper 920697
21. I. Osuka, M. Nishimura, Y. Tanaka, M. Miyaki, "Benefits of new fuel injection system technology on cold startability of diesel engines - Improvement of cold startability and white smoke reduction by means of multi injection with common rail fuel system (ECU-U2)", SAE paper 940586
22. Soon-Ik Kwon, Masataka Arai, Hiroyuki Hiroyasu, "Ignition delay of a diesel spray injected into a residual gas mixture", SAE paper 911841
23. John F. Roesler, Richard A. Yetter, Frederick L. Dryer, "Kinetic interactions of CO, No_x, and HCI emissions in postcombustion gases", Combustion and flame, 100: 495-504, 1995
24. C. Arcoumanis, C. Bae, A. Nagwaney, J. H. Whitelaw, "Effect of EGR on combustion development in a 1.9L DI diesel optical engine", SAE paper 950850
25. Z. Liu, G. A. Karim, "An Examination of the role of residual gases in the combustion processes of motored engines fueled with gaseous fuels", SAE paper 961081
26. Zhiping Han, Naeim A. Henein, Walter Bryzik, "A New Ignition Delay Formulation Applied to Predict Misfiring During Cold Starting of Diesel Engines", SAE paper 2000-01-1184

APPENDIX

The installation of the strain gauge has been shown before. Figure 1 is the schematic view of the strain gauge signal. The signal includes two humps, one high and one low. The high hump is the fuel injection signal, while the low hump is generated by compressing the plunger spring. For the EUI, after the issuing of the injection command, there is a response time to reach the point where the poppet control valve closes. The pressure inside the plunger cell starts rising following the closure of the poppet valve indicated by the number '1' in the figure. Actually, the pressure starts increasing slightly before the poppet valve is completely closed because of the throttling effect. The fuel injection starts when the fuel pressure reaches the nozzle's needle open pressure, and this point is called actual BOI (Begin Of Injection). The BOI is marked with '2' in the figure. The point when the poppet valve closes is called electrical BOI. The injection stops when the poppet valve is opened, and is marked with '3'.

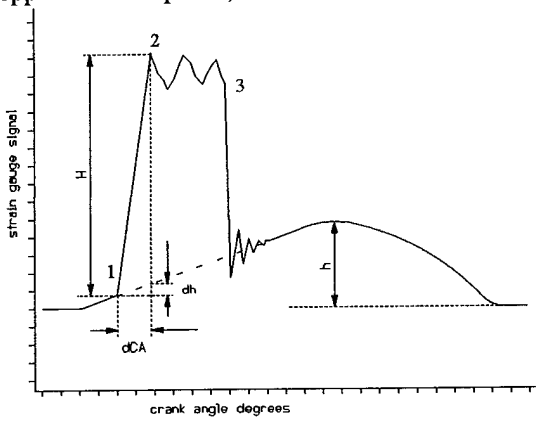

Figure 1. A schematic view of rocker arm strain gauge signal

If the poppet valve keeps open during compression stroke of plunger, no fuel will be injected, and the steep signal section represented by 1-2-3 will be replaced by the dashed line. A critical case where no fuel is injected is when the two points marked by '2' and '3' in the figure meet. This is a case where BOI also is the end of injection. The pulse width at this case is called minimum pulse width. Any pulse width value less than the minimum pulse width will not deliver any fuel. The minimum pulse width was used to determine the needle open pressure from a special built fuel injection test bench. The needle open pressure is determined through the following procedure.

There are two humps in the figure. The lower one, connected with the dashed line, is the profile produced by the plunger restoring spring. The high one is produced by the fuel injection process. When the poppet control valve is closed, the pressure of the plunger cell starts to build up, the output of the signal deviates from the dashed line, and rises sharply until it reaches the needle open pressure point. This is represented by the signal increment 'H' in the figure. By the time the pressure reaches needle open value, the plunger restoring spring is also compressed by a value of 'dh'. The engine crank angle elapsed during this time is 'dCA', which can also be called 'pressure rising time'. The peak value of the lower hump is given by 'h'. The plunger stroke is 'S_p'. The constant of the restoring spring is 'K_R'. The force corresponding to the peak value 'h' can be calculated as F_h:

$$F_h = K_R * S_p$$

or:

$$F_h = C_p * h$$

where C_p is the calibration constant, and

$$C_p = (K_R * S_p) / h \qquad (1)$$

The force corresponding to the needle open pressure can be calculated as F_{open}:

$$F_{open} = C_p * (H - dh) \qquad (2)$$

If the designed plunger velocity is V_p, applying the force balance will give:

$$dh = \frac{V_p * dCA * K_R}{C_p} \qquad (3)$$

If the plunger cross section area is given as 'A_p', the needle open pressure P_{open} will be:

$$P_{open} = F_{open} / A_p \qquad (4)$$

It is possible that the plunger cell pressure may continue to rise after the needle is opened. In another word, the 'H' value should be well determined to give correct needle open pressure. This was done in fuel injection bench by fine adjust the pulse width to the minimum value when the fuel is visually observed to just start of injection. After the "H" in equation (2) is obtained the calibration constant C_p can be calculated via equation (1). The needle open pressure can then be determined.

The needle open point determined in this way may change from measurement to measurement. The effect was investigated and it was found that the variation of pressure alone the rising edge is about 142 psi per 0.1 CA. If the calibration error of the injector is ± 5 per cent, the needle open point error will be ± 0.18 CA. Throughout the investigation, the constant needle open pressure was used based on the assumption that needle open pressure depends only on the preset restoring spring force of the needle. The needle open point located through the open pressure method on the signal trace was used as the injection start point, or actual injection timing.

The dynamic effect to the strain gauge signal output by the inertia forces of plunger and rocker arm at different speed was also investigated and was found negligible.